

Invited lectures presented at the Joint ICTP-IAEA  
Advanced Workshop on Model Codes for Spallation Reactions,  
February 4–8, 2008, ICTP, Trieste, Italy  
(LANL Report LA-UR-08-2931)

## CEM03.03 and LAQGSM03.03 Event Generators for the MCNP6, MCNPX, and MARS15 Transport Codes

S. G. Mashnik<sup>1</sup>, K. K. Gudima<sup>2</sup>, R. E. Prael<sup>1</sup>,  
A. J. Sierk<sup>1</sup>, M. I. Baznat<sup>2</sup>, and N. V. Mokhov<sup>3</sup>

<sup>1</sup>*Los Alamos National Laboratory, Los Alamos, NM 87545, USA*

<sup>2</sup>*Institute of Applied Physics, Academy of Science of Moldova, Chişinău, Moldova*

<sup>3</sup>*Fermi National Accelerator Laboratory, Batavia, IL, USA*

### Abstract

A description of the IntraNuclear Cascade (INC), preequilibrium, evaporation, fission, coalescence, and Fermi breakup models used by the latest versions of our CEM03.03 and LAQGSM03.03 event generators is presented, with a focus on our most recent developments of these models. The recently developed “S” and “G” versions of our codes, that consider multi-fragmentation of nuclei formed after the preequilibrium stage of reactions when their excitation energy is above 2A MeV using the Statistical Multifragmentation Model (SMM) code by Botvina *et al.* (“S” stands for SMM) and the fission-like binary-decay model GEMINI by Charity (“G” stands for GEMINI), respectively, are briefly described as well. Examples of benchmarking our models against a large variety of experimental data on particle-particle, particle-nucleus, and nucleus-nucleus reactions are presented. Open questions on reaction mechanisms and future necessary work are outlined.

April 2008

## Contents

<b>1. Introduction</b>	2
<b>2. A Brief Survey of CEM and LAQGSM Physics</b>	3
<b>3. The Intranuclear Cascade Mechanism</b>	4
<i>3.1. The INC of CEM03.03</i>	8
<i>3.2. The INC of LAQGSM03.03</i>	22
<b>4. The Coalescence Model</b>	28
<b>5. Preequilibrium Reactions</b>	29
<b>6. Evaporation</b>	43
<b>7. Fission</b>	53
<i>7.1. Fission Probability</i>	53
<i>7.2. Mass Distribution</i>	56
7.2.a. Asymmetric fission	56
7.2.b. Symmetric fission	56
<i>7.3. Charge Distribution</i>	57
<i>7.4. Kinetic Energy Distribution</i>	57
<i>7.5. Modifications to GEM2 in CEM03.01 and LAQGSM03.01</i>	58
<b>8. The Fermi Breakup Model</b>	62
<b>9. Reactions Involving Pions and Photons; Excitation Functions</b>	67
<b>10. CEM03.S1, CEM03.G1, LAQGSM03.S1, and LAQGSM03.G1</b>	70
<b>Acknowledgments</b>	83
<b>References</b>	84

# 1. Introduction

Following an increased interest in intermediate- and high-energy nuclear data in relation to such projects as the Accelerator Transmutation of nuclear Wastes (ATW), Accelerator Production of Tritium (APT), Spallation Neutron Source (SNS), Rare Isotope Accelerator (RIA), Proton Radiography (PRAD) as a radiographic probe for the Advanced Hydro-test Facility, NASA needs, and others, the US Department of Energy has supported during the last decade our work on the development of improved versions of the Cascade-Exciton Model (CEM) and of the Los Alamos version of the Quark Gluon String Model (LAQGSM) which has led to our intermediate- and high-energy event generators CEM03.03 and LAQGSM03.03, respectively, and their modifications described below.

The main focus of our workshop is nucleon-induced reactions for Accelerator Driven Systems (ADS) and spallation neutron sources (up to 2–3 GeV), usually described well enough by our intermediate-energy code CEM03.03 without a need to use our high-energy code LAQGSM03.03. This is why we focus below mostly on CEM03.03 and its modifications. However, as discussed below in Section 3.1, CEM does not consider the so-called “trawling” effect (depletion of target nucleons during a cascade), therefore does not describe well reactions on very light nuclei like C at incident energies above about 1 GeV. Therefore, in transport codes that use both CEM and our high-energy code LAQGSM as event generators, we recommend simulating nuclear reactions with CEM at incident energies up to about 1 GeV for light nuclei like C and up to about 5 GeV for actinide nuclei, and to switch to simulations by LAQGSM, which does consider the “trawling” effect, at higher energies of transported particles. This is the reason we have included in the present lectures a brief description of LAQGSM as well. Even at energies of ADS applications below about 3 GeV, we recommend using LAQGSM instead of CEM in the case of light target nuclei.

The Cascade-Exciton Model (CEM) of nuclear reactions was proposed almost 30 years ago at the Bogoliubov Laboratory of Theoretical Physics, Joint Institute for Nuclear Research, Dubna, USSR by Gudima, Mashnik, and Toneev [1, 2]. It is based on the standard (non time-dependent) Dubna IntraNuclear Cascade (INC) [3, 4] and the Modified Exciton Model (MEM) [5, 6]. CEM was extended later to consider photonuclear reactions [7] and to describe fission cross sections using different options for nuclear masses, fission barriers, and level densities [8] and its 1995 version, CEM95, was released to the public via NEA/OECD, Paris as the code IAEA1247, and via the Radiation Safety Information Computational Center (RSICC) at Oak Ridge, USA, as the RSICC code package PSR-357 [9].

The *International Code Comparison for Intermediate Energy Nuclear Data* [10, 11] organized during 1993–1994 at NEA/OECD in Paris to address the subject of codes and models used to calculate nuclear reactions from 20 to 1600 MeV showed that CEM95 (more exactly, CEM92m, which is almost identical in its physics content to the publicly released CEM95 version) had one of the best predictive powers to describe nucleon-induced reactions at energies above about 150 MeV when compared to other models and codes available at that time.

The code LAQGSM03.03 described briefly below is the latest modification [12] of LAQGSM [13], which in its turn is an improvement of the Quark-Gluon String Model (QGSM) [14]. It describes reactions induced by both particles and nuclei at incident energies up to about 1 TeV/nucleon, generally, as a three-stage process: IntraNuclear Cascade (INC), followed by preequilibrium emission of particles during the equilibration of the excited residual nuclei formed after the INC, followed by evaporation of particles from and/or fission of the compound nuclei.

CEM95 and/or its predecessors and successors like CEM97 [15, 16], CEM2k [17], CEM2k+GEM2 [18]–[20], CEM03 [21, 22], including the latest version available to the public from RSICC and NEA OECD, CEM03.01 [23], as well as different versions of LAQGSM and its predecessor QGSM are used as stand-alone codes to study different nuclear reactions for applications and fundamental nuclear physics (see, *e.g.*, [25]–[42] and references therein). Parts of different versions of the CEM, LAQGSM, or QGSM codes are used in many other stand-alone codes, like **PICA95** [43], **PICA3** [44], **CASCADE** [45], **CAMO** [46], **MCFX** [47], **ECM** [48], and **NUCLEUS** [49]. Different versions of CEM and LAQGSM, or of the older QGSM, are incorporated wholly, or in part in many transport codes used in a variety of applications, like **CASCADE** [50], **MARS** [51], **MCNPX** [52], **GEANT4** [53, 54], **SHIELD** [55], **RTS&T** [56], **SONET** [57], **CALOR** [58], **HETC-3STEP** [59], **CASCADE/INPE** [60], **HADRON** [61], **CASCADE-2004** [62], and others.

In these lectures, we present a brief description of all models, approximations, and systematics used in the latest versions of our CEM and LAQGSM event generators.

## 2. A Brief Survey of CEM and LAQGSM Physics

The basic version of both our CEM and LAQGSM event generators is the so-called “03.01” version, namely CEM03.01 [23] and LAQGSM03.01 [24]. The CEM03.01 code calculates nuclear reactions induced by nucleons, pions, and photons. It assumes that the reactions occur generally in three stages. The first stage is the IntraNuclear Cascade (INC), in which primary particles can be re-scattered and produce secondary particles several times prior to absorption by, or escape from the nucleus. When the cascade stage of a reaction is completed, CEM03.01 uses the coalescence model to “create” high-energy d, t,  $^3\text{He}$ , and  $^4\text{He}$  by final-state interactions among emitted cascade nucleons, already outside of the target. The emission of the cascade particles determines the particle-hole configuration,  $Z$ ,  $A$ , and the excitation energy that is the starting point for the second, preequilibrium stage of the reaction. The subsequent relaxation of the nuclear excitation is treated in terms of an improved version of the modified exciton model of preequilibrium decay followed by the equilibrium evaporation/fission stage of the reaction. Generally, all four components may contribute to experimentally measured particle spectra and other distributions. But if the residual nuclei after the INC have atomic numbers with  $A \leq 12$ , CEM03.01 uses the Fermi breakup model to calculate their further disintegration instead of using the preequilibrium and evaporation models. Fermi breakup is much faster to calculate and gives results very similar to the continuation of the more detailed models to much lighter nuclei. As already mentioned in the Introduction, LAQGSM03.01 also describes nuclear reactions, generally, as a three-stage process: IntraNuclear Cascade (INC), followed by preequilibrium emission of particles during the equilibration of the excited residual nuclei formed after the INC, followed by evaporation of particles from or fission of the compound nuclei. LAQGSM was developed with a primary focus on describing reactions induced by nuclei, as well as induced by most elementary particles, at high energies, up to about 1 TeV/nucleon. The INC of LAQGSM is completely different from the one in CEM. LAQGSM03.01 also considers Fermi breakup of nuclei with  $A \leq 12$  produced after the cascade, and the coalescence model to “produce” high-energy d, t,  $^3\text{He}$ , and  $^4\text{He}$  from nucleons emitted during the INC.

The main difference of the following, so-called “03.02” versions of CEM and LAQGSM from the basic “03.01” versions is that the latter use the Fermi breakup model to calculate the disintegration of light nuclei instead of using the preequilibrium and evaporation models only after the INC, when the excited nuclei after the INC have a mass number  $A \leq 12$ , but do not

use the Fermi breakup model at the preequilibrium, evaporation, and fission stages, when, due to emission of preequilibrium particles or due to evaporation or to a very asymmetric fission, we get an excited nucleus or a fission fragment with  $A \leq 12$ . This problem was solved in the 03.02 versions of CEM and LAQGSM, where the Fermi breakup model is used at any stage of a reaction, when we get an excited nucleus with  $A \leq 12$ .

In addition, the routines that describe the Fermi breakup model in the basic 03.01 version of our codes were written some twenty years ago in the group of Prof. Barashenkov at JINR, Dubna, Russia, and are far from being perfect, though they are quite reliable and are still used currently without any changes in some transport codes. First, these routines allow in rare cases production of some light unstable fragments like  $^5\text{He}$ ,  $^5\text{Li}$ ,  $^8\text{Be}$ ,  $^9\text{B}$ , etc., as a result of a breakup of some light excited nuclei. Second, these routines allowed in some very rare cases even production of “neutron stars” (or “proton stars”), i.e., residual “nuclei” produced via Fermi breakup that consist of only neutrons (or only protons). Lastly, in some very rare cases, these routines could even crash the code, due to cases of 0/0. All these problems of the Fermi breakup model routines are addressed and solved in the 03.02 version of our codes [63]. Several bugs are also fixed in 03.02 in comparison with its predecessor. On the whole, the 03.02 versions describe nuclear reactions on intermediate and light nuclei, and production of fragments heavier than  $^4\text{He}$  from heavy targets much better than their predecessors, almost do not produce any unstable unphysical final products, and are free of the fixed bugs.

However, even after solving these problems and after implementing the improved Fermi breakup model into CEM03.02 and LAQGSM03.02 [63], in some very rare cases, our event generators still could produce some unstable products via very asymmetric fission, when the excitation energy of such fragments was below 3 MeV and they were not checked and not disintegrated with the Fermi breakup model (see details in [12]). This problem was addressed in the 03.03 versions of our codes, where we force such unstable products to disintegrate via Fermi breakup independently of their excitation energy. Several more bugs were fixed on the 03.03 version as well. A schematic outline of a nuclear reaction calculation by CEM03.03 or LAQGSM03.03 is shown in Fig. 1. We emphasize that the occurrence of these problems even in the 03.01 versions is quite rare, allowing stand-alone calculations of many nuclear reactions to proceed without problems, but are unacceptable when the event generators are used inside transport codes doing large-scale simulations.

In the following Sections, we highlight the main assumptions of the models contained in CEM and LAQGSM.

### 3. The Intranuclear Cascade Mechanism

The inelastic interaction of a high-energy particle with a nucleus, and even more the collisions of two nuclei, is a very complex and multi-faceted phenomenon whose analytical description encounters considerable difficulties [3, 4]. In recent years calculations of such interactions have been carried out by statistical simulations using the Monte-Carlo method.

The INC approach was apparently first developed by Goldberger [64], who in turn based his work on the ideas of Heisenberg and Serber [65], who regarded intranuclear cascades as a series of successive quasi-free collisions of the fast primary particle with the individual nucleons of the nucleus.

Let us recall here the main basic assumptions of the INC, following [3, 4]. The main condition for the applicability of the intranuclear-cascade model is that the DeBroglie wavelength  $\lambda$  of the particles participating in the interaction be sufficiently small: It is necessary that for

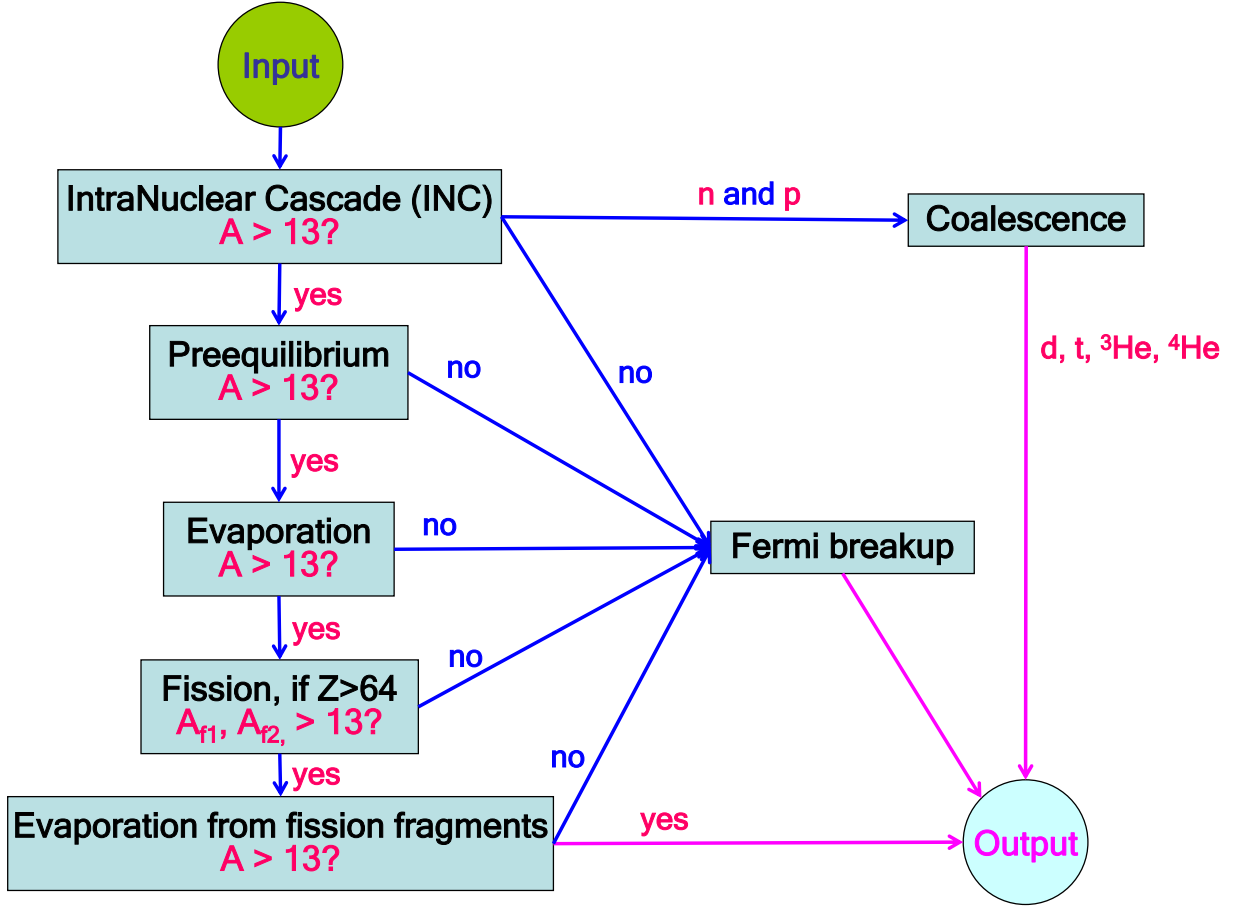


Figure 1: Flow chart of nuclear-reaction calculations by CEM03.03 and LAQGSM03.03.

most of these particles  $\lambda$  be less than the average distance between the intranuclear nucleons  $\Delta \sim 10^{-13}$  cm. Only in this case does the particle acquire quasi-classical features and can we speak approximately of particle trajectory and two-particle collisions inside the nucleus. It is clear that for this to be the case the primary particle kinetic energy  $T$  must be greater than several tens of MeV.

Another important condition for applicability of the INC is the requirement that the time in which an individual two-particle intranuclear collision occurs on the average,  $\tau \sim 10^{-23}$  sec, be less than the time interval between two such consecutive interactions

$$\Delta t = l/c \gtrsim 4\pi R^3/3A\sigma c \gtrsim 3 \cdot 10^{-22}/\sigma \text{ (mb) sec},$$

where  $l$  is the mean range of the cascade particle before the interaction,  $c$  is the velocity of light,  $R = r_0 A^{1/3}$  is the mean radius of the nucleus, and  $\sigma$  is the cross section for interaction with an intranuclear nucleon. This permits the interaction of the incident particle with the nucleus to be reduced to a set of individual statistically independent intranuclear collisions.

The requirement  $\tau < \Delta t$  is equivalent to the requirement that the intranuclear interaction cross section be sufficient small:  $\sigma \lesssim 100\xi$  mb, where the coefficient  $\xi \sim 1$ .

Since the energy of the particles participating in the cascade is rather large—as a rule significantly greater than the binding energy of the intranuclear nucleons—the same characteristics can be used for interaction of cascade particles inside the nucleus as for the interaction of free particles. The effect of other intranuclear nucleons is taken into account by introduction of some average potential  $V$ , and also by the action of the Pauli principle.<sup>1</sup>

We can say that a high-energy particle which has entered the nucleus passes through a gas of free nucleons, producing a cascade (avalanche) of secondary particles. A fraction of these secondary particles leaves the nucleus, and the remaining fraction is absorbed, exciting the nucleus to some energy  $E^*$ .

Following [3, 4], after the choice of a nuclear model and an algorithm for determination of the elementary particles involved in the INC with the intranuclear nucleons (for this purpose it is necessary to store in the computer memory also the values of the integrated cross sections for elastic and inelastic interactions  $\sigma_{el}(T)$  and  $\sigma_{in}(T)$ ), calculation of the intranuclear cascade is carried out according to the scheme shown in Fig. 2. The turquoise boxes 1, 2, 4, 5, 8–10, 12, and 14 in the diagram denote operations which are definite logically closed parts of the INC program. The yellow boxes 3, 6, 7, 11, and 13 denote logical operations which control the various branchings of the program (transfer conditions).

Box 1 takes into account the change in primary-particle momentum due to the effect of the intranuclear potential and to refraction and reflection of the DeBroglie wave of the particle at the nuclear boundary.

In box 2 is chosen the momentum and isospin (proton or neutron) of the intranuclear nucleon with which the interaction occurs (for brevity we will call this nucleon the partner), and from the given elementary cross section  $\sigma_{tot}(t) = \sigma_{el}(t) + \sigma_{in}(t)$  (where  $t$  is the relative energy of the primary particle and the partner taking part in the intranuclear motion) the mean free path of the particle in nuclear matter  $L = L(\sigma_{tot})$  is calculated and the point of interaction is determined.

Box 3 tests whether this point of interaction is inside the nucleus. If it is not, then the particle is assumed to have passed through the nucleus without interaction. The ratio of the number of such particles to the total number of interactions considered with the nucleus  $N_{tot}$  obviously characterizes the reaction cross section  $\sigma_{in}(t)$ .

If the point of interaction is inside the nucleus, then the type of interaction: elastic or inelastic, is determined from the known cross sections  $\sigma_{el}(t)$  and  $\sigma_{in}(t)$  in box 4.

In box 5 the secondary-particle characteristics are determined in accordance with the type of interaction selected (the nature, number, energy, and the emission angle).

Box 6 is a test of whether the Pauli principle is satisfied. Interactions which do not satisfy this principle are considered forbidden and the particle trajectory is followed beyond the point of the forbidden interaction.

In box 7 the particle energy  $T$  is compared with some initially specified cutoff energy  $T_{cut}$  which determinates whether this particle is sufficiently energetic ( $T > T_{cut}$ ) to take further part in development of the intranuclear cascade or whether its energy is so small ( $T \leq T_{cut}$ ) that the particle is simply absorbed by the nucleus. In the first case the particle is followed further as was described above. (For this the parameters of all cascade particles with energy  $T > T_{cut}$  are stored in the memory in box 8 and later the cascade calculation is repeated for each of them

---

<sup>1</sup>The nucleus is considered to be a degenerate Fermi gas of nucleons enclosed in the nuclear volume. According to the Pauli principle the nucleons, after an intranuclear collision, must have energy above the Fermi energy; otherwise such an interaction is forbidden. The action of the Pauli principle leads in effect to an increase of the mean free path of fast particles inside the nucleus.

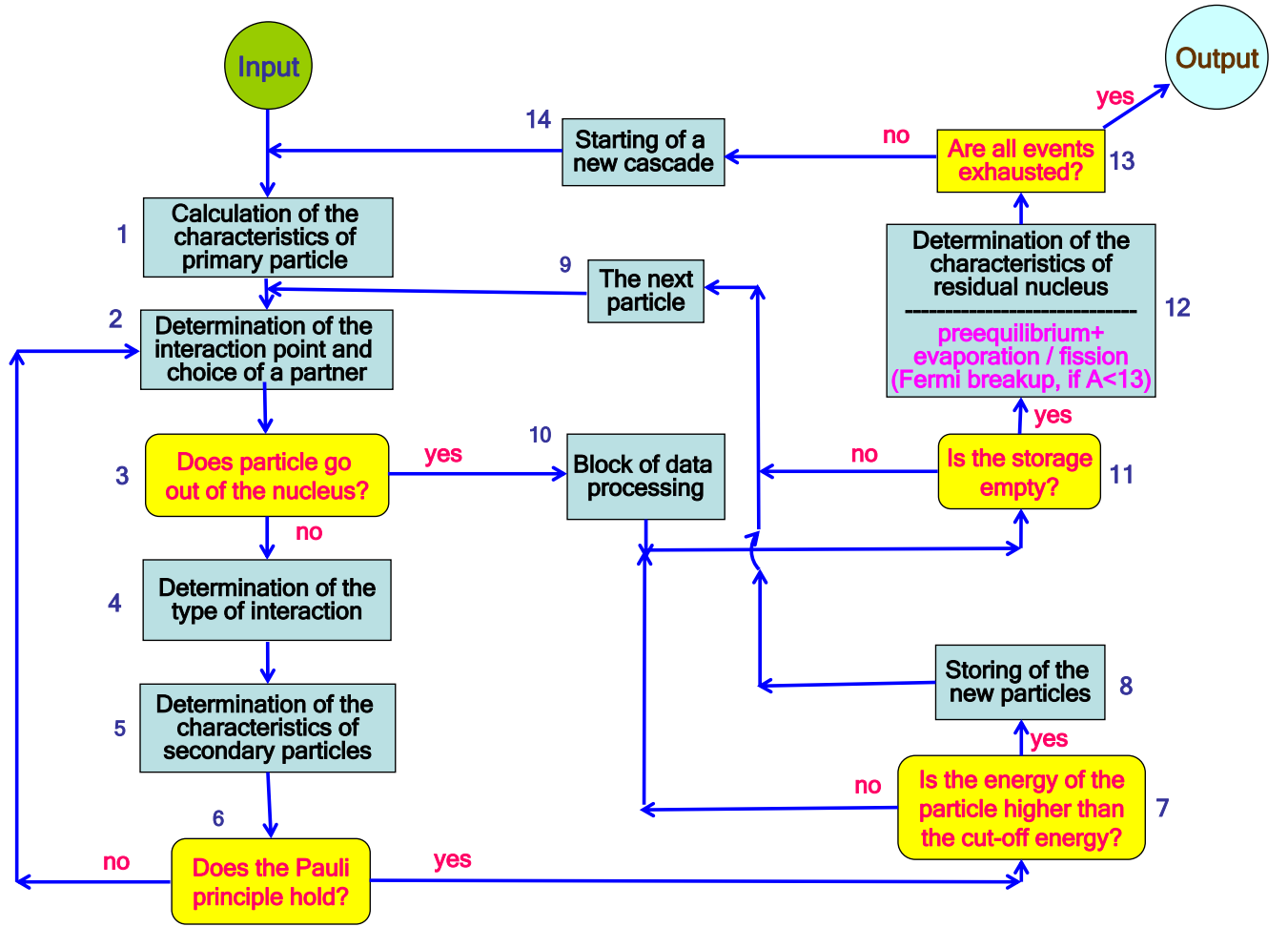


Figure 2: Flow chart for the intranuclear cascade calculation.

in turn by going to boxes 9 and 2.) In the second case the INC treatment of this particle is terminated; if this particle is a nucleon, in box 10 it contributes to the energy of the residual nucleus and become an exciton to be further treated by the Modified-Exciton Model in box 12.

The calculation is carried out until all particles are absorbed or leave the nucleus. The operations in boxes 8, 9, and 11 are responsible for this. If the history of one particle which entered the nucleus had been completed (*i.e.*, if the computer memory is empty; see box 11), a possible preequilibrium, followed by evaporation/fission, or/and Fermi breakup stage of this event is simulated in box 12 until the excitation energy of the residual nucleus is below the binding energy of a neutron or other particles that could be emitted from this nucleus, then, the history of the next particle (*i.e.*, next “event”) is simulated (boxes 13 and 14), and so forth, until all events are simulated and we get the needed statistics.

Any cascade calculation at not very high energies where it is still possible to neglect many-particle interactions and the change in density of the intranuclear nucleons can be fitted into the general scheme shown in Fig. 2. The specific form of the box operations and their complexity are determined by the choice of the nuclear model and by the number and variety of elementary processes which it is considered necessary to take into account in a given calculation. The

individual boxes can be studied in more detail in Refs. [66, 67], as well as in the quite old, but still one of the best monographs on the INC and other nuclear reaction models we highly recommend to readers interested in details of high-energy nuclear reactions [3]. Some specific details on the INC of CEM and LAQGSM are provided in the following Sections 3.1 and 3.2.

### 3.1. The INC of CEM03.03

The intranuclear cascade model in CEM03.03 is based on the standard (non-time-dependent) version of the Dubna cascade model [3, 4, 66, 67]. All the cascade calculations are carried out in a three-dimensional geometry. The nuclear matter density  $\rho(r)$  is described by a Fermi distribution with two parameters taken from the analysis of electron-nucleus scattering, namely

$$\rho(r) = \rho_p(r) + \rho_n(r) = \rho_0 \{1 + \exp[(r - c)/a]\}^{-1}, \quad (1)$$

where  $c = 1.07A^{1/3}$  fm,  $A$  is the mass number of the target, and  $a = 0.545$  fm. For simplicity, the target nucleus is divided by concentric spheres into seven zones in which the nuclear density is considered to be constant. The energy spectrum of the target nucleons is estimated in the perfect Fermi-gas approximation with the local Fermi energy  $T_F(r) = \hbar^2[3\pi^2\rho(r)]^{2/3}/(2m_N)$ , where  $m_N$  is the nucleon mass. An example of the nucleon density and the Fermi energy used by CEM03.01 to calculate nuclear reactions on  $^{208}\text{Pb}$  is shown in Fig. 3.

The influence of intranuclear nucleons on the incoming projectile is taken into account by adding to its laboratory kinetic energy an effective real potential  $V$ , as well as by considering the Pauli principle which forbids a number of intranuclear collisions and effectively increases the mean free path of cascade particles inside the target. For incident nucleons  $V \equiv V_N(r) = T_F(r) + \epsilon$ , where  $T_F(r)$  is the corresponding Fermi energy and  $\epsilon$  is the binding energy of the nucleons. For pions, CEM03.01 uses a square-well nuclear potential with the depth  $V_\pi \simeq 25$  MeV, independently of the nucleus and pion energy, as was done in the initial Dubna INC [3, 4].

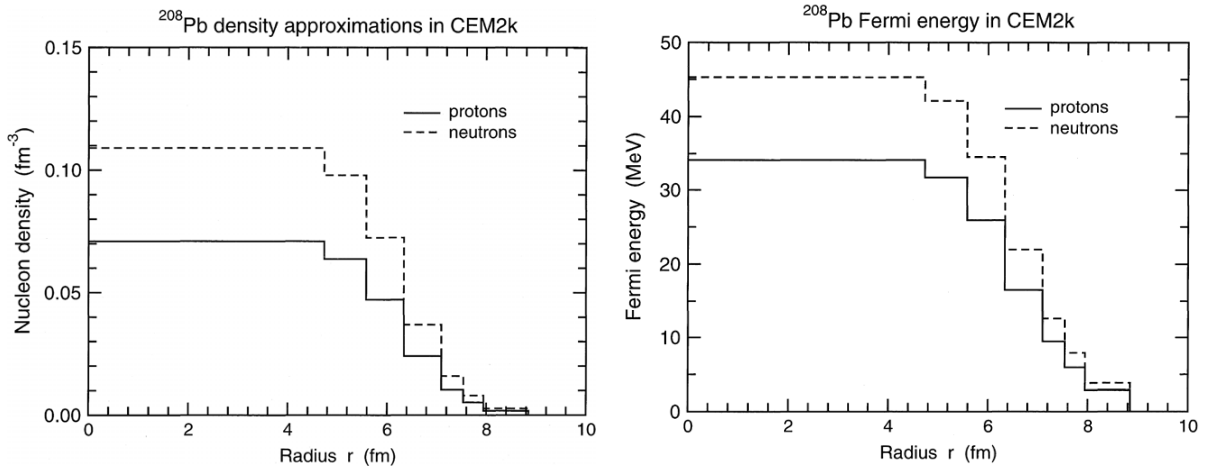


Figure 3: Examples of the nucleon density and the Fermi energy used by CEM03.01 to calculate nuclear reactions on  $^{208}\text{Pb}$ .

The interaction of the incident particle with the nucleus is approximated as a series of successive quasi-free collisions of the fast cascade particles ( $N$ ,  $\pi$ , or  $\gamma$ ) with intranuclear nucleons:

$$NN \rightarrow NN, \quad NN \rightarrow \pi NN, \quad NN \rightarrow \pi_1, \dots, \pi_i NN, \quad (2)$$

$$\pi N \rightarrow \pi N, \quad \pi N \rightarrow \pi_1, \dots, \pi_i N \quad (i \geq 2). \quad (3)$$

In the case of pions, besides the elementary processes (3), CEM03.01 also takes into account pion absorption on nucleon pairs

$$\pi NN \rightarrow NN. \quad (4)$$

The momenta of the two nucleons participating in the absorption are chosen randomly from the Fermi distribution, and the pion energy is distributed equally between these nucleons in the center-of-mass system of the three particles participating in the absorption. The direction of motion of the resultant nucleons in this system is taken as isotropically distributed in space. The effective cross section for absorption is related (but not equal) to the experimental cross sections for pion absorption by deuterons.

In the case of photonuclear reactions [22], CEM03.01 follows the ideas of the photonuclear version of the Dubna INC proposed initially 35 years ago by one of us (KKG) in collaboration with Iljinov and Toneev [68] to describe photonuclear reactions at energies above the Giant Dipole Resonance (GDR) region [69]. [At photon energies  $T_\gamma = 10\text{--}40$  MeV, the DeBroglie wavelength  $\lambda$  is of the order of 20–5 fm, greater than the average inter-nucleonic distance in the nucleus; the photons interact with the nuclear dipole resonance as a whole, thus the INC is not applicable.] Below the pion-production threshold, the Dubna INC considers absorption of photons on only “quasi-deuteron” pairs according to the Levinger model [70]:

$$\sigma_{\gamma A} = L \frac{Z(A-Z)}{A} \sigma_{\gamma d}, \quad (5)$$

where  $A$  and  $Z$  are the mass and charge numbers of the nucleus,  $L \approx 10$ , and  $\sigma_{\gamma d}$  is the total photo-absorption cross section on deuterons as defined from experimental data.

At photon energies above the pion-production threshold, the Dubna INC considers production of one or two pions; the specific mode of the reaction is chosen by the Monte-Carlo method according to the partial cross sections (defined from available experimental data):

$$\gamma + p \rightarrow p + \pi^0, \quad (6)$$

$$\rightarrow n + \pi^+, \quad (7)$$

$$\rightarrow p + \pi^+ + \pi^-, \quad (8)$$

$$\rightarrow p + \pi^0 + \pi^0, \quad (9)$$

$$\rightarrow n + \pi^+ + \pi^0. \quad (10)$$

The cross sections of  $\gamma + n$  interactions are derived from consideration of isotopic invariance, *i.e.* it is assumed that  $\sigma(\gamma + n) = \sigma(\gamma + p)$ . The Compton effect on intranuclear nucleons is neglected, as its cross section is less than  $\approx 2\%$  of other reaction modes (see, *e.g.* Fig. 6.13 in Ref. [71]). The Dubna INC does not consider processes involving production of three and more pions; this limits the model’s applicability to photon energies  $T_\gamma \lesssim 1.5$  GeV [for  $T_\gamma$  higher than the threshold for three-pion production, the sum of the cross sections (8)–(10) is assumed to be equal to the difference between the total inelastic  $\gamma + p$  cross section and the sum of the cross sections of the two-body reactions (6)–(7)].

The integral cross sections for the free  $NN$ ,  $\pi N$ , and  $\gamma N$  interactions (2)–(10) are approximated in the Dubna INC model [3] used in CEM95 [9] and its predecessors using a special algorithm of interpolation/extrapolation through a number of picked points, mapping as well as possible the experimental data. This was done very accurately by the group of Prof. Barashenkov using all experimental data available at that time, about 35 years ago. Currently the experimental data on cross sections is much more complete than at that time; therefore we have

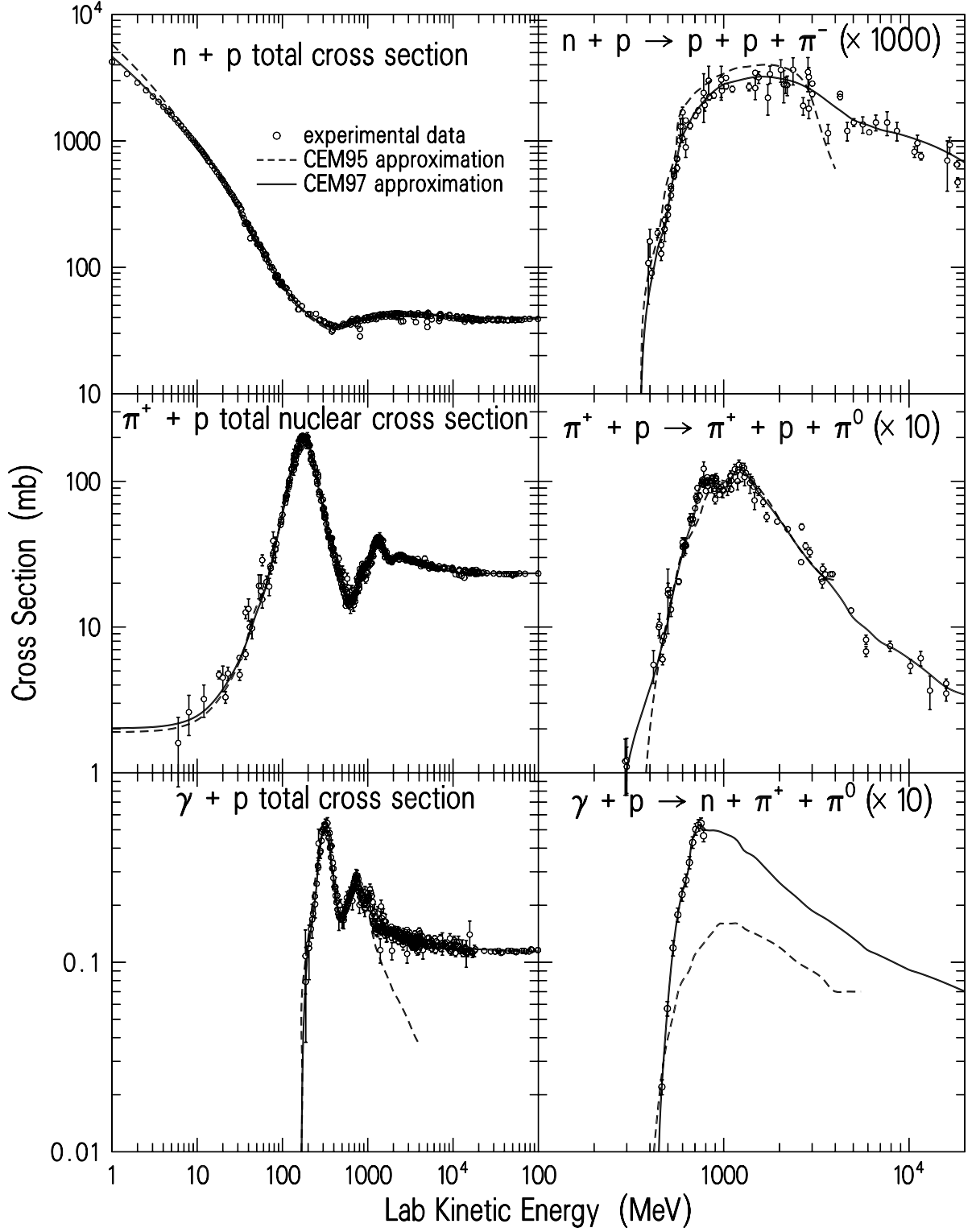


Figure 4: Energy dependence of the  $np$ ,  $\pi^+p$ , and  $\gamma p$  total cross sections and of the  $np \rightarrow pp\pi^-$ ,  $\pi^+p \rightarrow \pi^+p\pi^0$ , and  $\gamma p \rightarrow n\pi^+\pi^0$  ones. Experimental points are from our compilation [15]. Solid lines are results using our new approximations; dashed lines show the standard Dubna INC approximations [3] used in CEM95 [9].

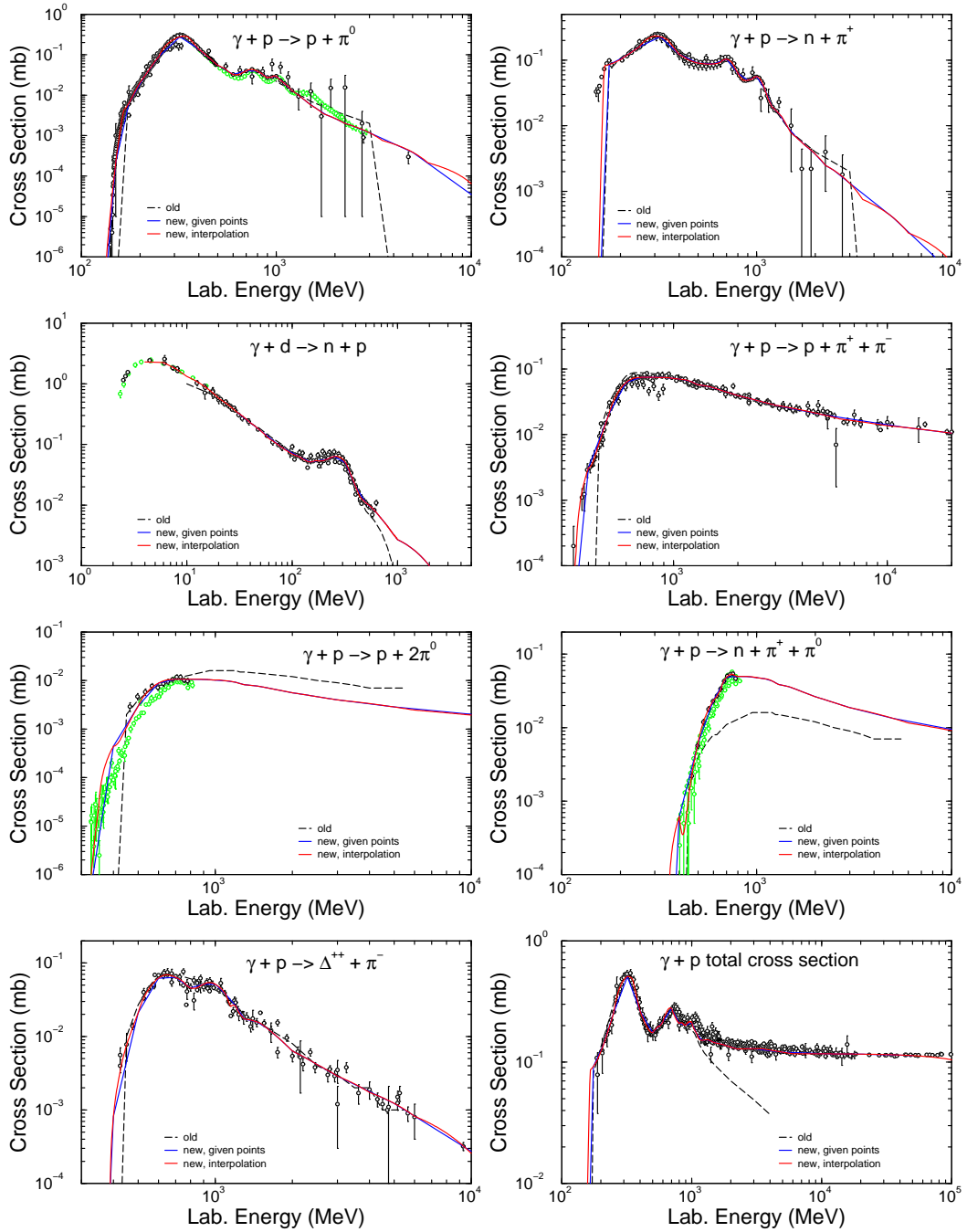


Figure 5: Comparison of eight experimental total  $\gamma + p(d)$  cross sections with the old approximations used in the Dubna INC [3] and with our approximations incorporated into the CEM03.01 and LAQGSM03.01 codes. The red curve gives the code results using parabolic interpolation, while the blue solid curve uses linear interpolation between our tabulated points. Where no blue curve is visible, it is coincident with the red curve. References to experimental data shown by black and green circles may be found in our recent paper [22]. The green circles show recent experimental data that became available to us after we completed our fit; Although these recent data agree reasonably well with our approximations, a refitting would slightly improve the agreement.

revised the approximations of all the integral elementary cross sections used in CEM95 [9] and its predecessors. We started by collecting all published experimental data from all available sources. Then we developed an improved, as compared with the standard Dubna INC [3], algorithm for approximation of cross sections and developed simple and fast approximations for elementary cross sections which fit very well presently available experimental data not only to 5 GeV, the upper recommended energy for the present version of the CEM, but up to 50–100 GeV and higher, depending on availability of data (see details in [15, 22]). So far, we have in CEM03.01 new approximations for 34 different types of elementary cross sections induced by nucleons, pions, and gammas. Integral cross sections for other types of interactions taken into account in CEM03.01 are calculated from isospin considerations using the former as input.

Examples of several compiled experimental cross sections together with our new approximations and the old approximations from CEM95 [9] are shown in Figs. 4 and 5. We see that our new approximations describe indeed very well all data. Although presently we have much more data than 35 years ago when Barashenkov’s group produced their approximations used in CEM95, for a number of interaction modes like the total cross sections shown in the left panel of Fig. 4, the original approximations also agree very well with presently available data, in the energy region where the Dubna INC was developed to work. This is a partial explanation of why the old Dubna INC [3] and the younger CEM95 [9] work so well for the majority of characteristics of nuclear reactions. On the other hand, for some modes of elementary interactions like the ones shown in the right panel of Fig. 4, the old approximations differ significantly from the present data, demonstrating the need for our recent improvements for a better description of all modes of nuclear reactions.

The kinematics of two-body elementary interactions and absorption of photons and pions by a pair of nucleons is completely defined by a given direction of emission of one of the secondary particles. The cosine of the angle of emission of secondary particles in the c.m. system is calculated by the Dubna INC [3] as a function of a random number  $\xi$ , distributed uniformly in the interval  $[0,1]$  as

$$\cos \Theta = 2\xi^{1/2} \left[ \sum_{n=0}^N a_n \xi^n + \left(1 - \sum_{n=0}^N a_n\right) \xi^{N+1} \right] - 1, \quad (11)$$

where  $N = M = 3$ ,

$$a_n = \sum_{k=0}^M a_{nk} T_i^k. \quad (12)$$

The coefficients  $a_{nk}$  were fitted to the then available experimental data at a number of incident kinetic energies  $T_i$ , then interpolated and extrapolated to other energies (see details in [3, 68, 69] and references therein). The distribution of secondary particles over the azimuthal angle  $\varphi$  is assumed isotropic. For elementary interactions with more than two particles in the final state, the Dubna INC uses the statistical model to simulate the angles and energies of products (see details in [3]).

For the improved version of the INC in CEM03.01, we use currently available experimental data and recently published systematics proposed by other authors and have developed new approximations for angular and energy distributions of particles produced in nucleon-nucleon and photon-proton interactions. So, for  $pp$ ,  $np$ , and  $nn$  interactions at energies up to 2 GeV, we did not have to develop our own approximations analogous to the ones described by Eqs. (11) and (12), since reliable systematics have been developed recently by Cugnon *et al.* for

the Liege INC [72], then improved still further by Duarte for the BRIC code [73]; we simply incorporate into CEM03.01 the systematics by Duarte [73].

Examples of angular distributions of secondary particles from  $np$  reactions at several energies are shown in Fig. 6. The new approximations reproduce the experimental data much better than the old Dubna INC used in our previous code versions (and in several other codes developed from the Dubna INC).

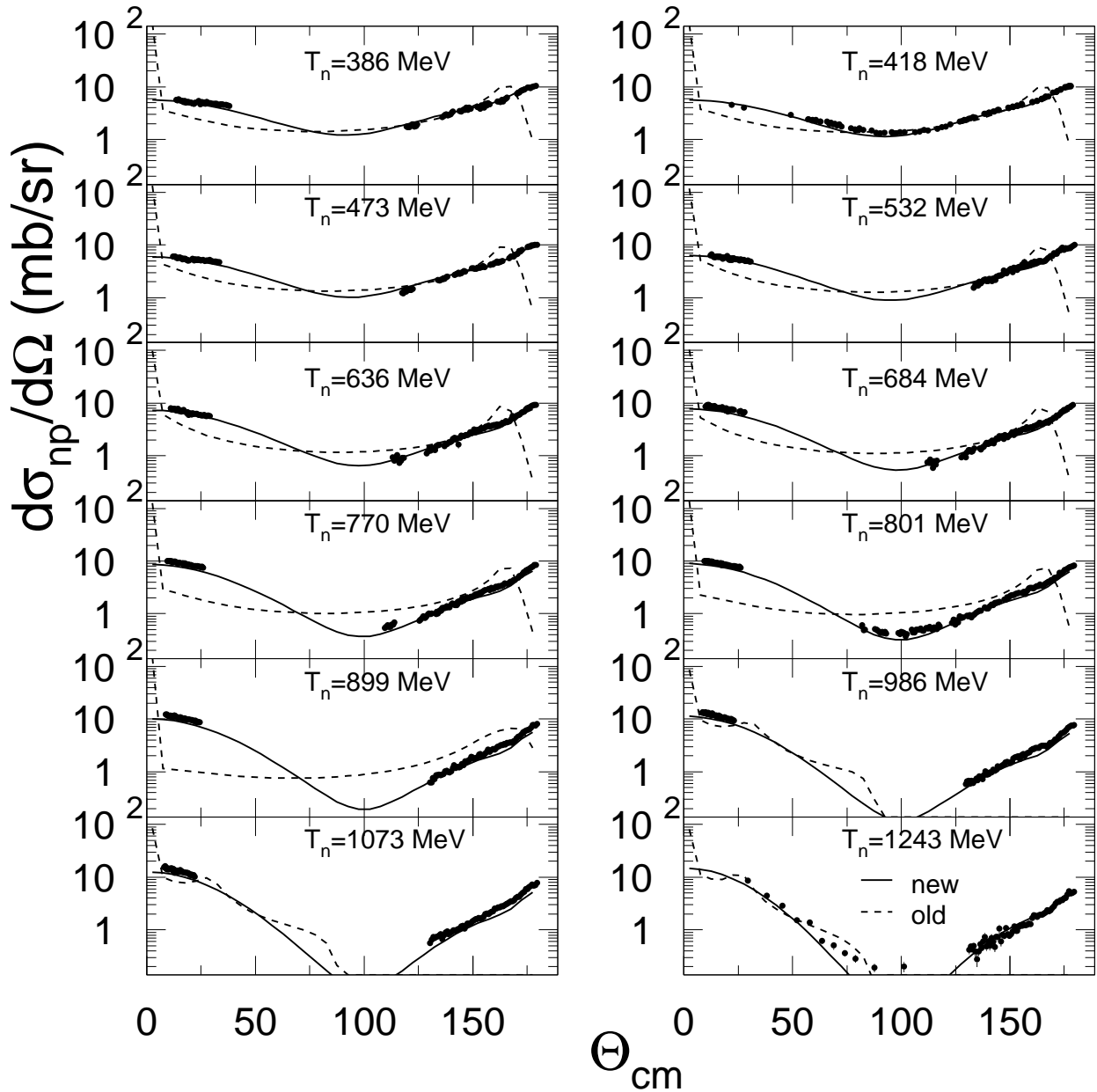


Figure 6: Example of twelve angular distributions of  $n$  from  $np$  elastic interactions as functions of  $\Theta_{c.m.}^n$  at  $T_n$  from 386 to 1243 MeV. The dashed lines show the old approximations from the Dubna INC while the solid lines are the new approximations incorporated into CEM03 and LAQGSM03. References to experimental data shown here by black circles may be found in our paper [21].

In the case of  $\gamma p$  reactions (6) and (7), we chose another way: Instead of fitting the param-

eters  $a_n$  from Eq. (11) at different  $E_\gamma$  we found data (see, *e.g.*, Fig. 7) and finding the energy dependence of parameters  $a_{nk}$  in Eq. (12) using the values obtained for  $a_n$ , we took advantage of the event generator for  $\gamma p$  and  $\gamma n$  reactions from the Moscow INC [74] kindly sent us by Dr. Igor Pshenichnov. That event generator includes a data file with smooth approximations through presently available experimental data at 50 different gamma energies from 117.65 to 6054 MeV (in the system where the  $p$  or  $n$  interacting with  $\gamma$  is at rest) for the c.m. angular distributions  $d\sigma/d\Omega$  of secondary particles as functions of  $\Theta$  tabulated for values of  $\Theta$  from 0 to 180 deg., with the step  $\Delta\Theta = 10$  deg., for 60 different channels of  $\gamma p$  and  $\gamma n$  reactions considered by the Moscow INC (see details in [74]). We use part of that data file with data for reactions (6) and (7), and have written an algorithm to simulate unambiguously  $d\sigma/d\Omega$  and to choose the corresponding value of  $\Theta$  for any  $E_\gamma$ , using a single random number  $\xi$  uniformly distributed in the interval  $[0,1]$ . This is straightforward due to the fact that the function  $\xi(\cos\Theta)$

$$\xi(\cos\Theta) = \frac{\int_{-1}^{\cos\Theta} d\sigma/d\Omega d\cos\Theta}{\int_{-1}^1 d\sigma/d\Omega d\cos\Theta}$$

is a smooth monotonic function increasing from 0 to 1 as  $\cos\Theta$  varies from -1 to 1. Naturally, when  $E_\gamma$  differs from the values tabulated in the data file, we perform first the needed interpolation in energy. We use this procedure to describe in CEM03.01 angular distributions of secondary particles from reactions (6) and (7), as well as for isotopically symmetric reactions  $\gamma + n \rightarrow n + \pi^0$  and  $\gamma + n \rightarrow p + \pi^-$ .

Examples of eight angular distributions of  $\pi^+$  from  $\gamma p \rightarrow \pi^+ n$  as functions of  $\Theta_{c.m.s}^\pi$  are presented in Fig. 7. We see that the approximations developed in CEM03.01 (solid histograms) agree much better with the available experimental data than the old Dubna INC approximations (11)–(12) used in all predecessors of CEM03 (dashed histograms).

The analysis of experimental data has shown that the channel (8) of two-pion photoproduction proceeds mainly through the decay of the  $\Delta^{++}$  isobar listed in the last Review of Particle Physics by the Particle Data Group as having the mass  $M = 1232$  MeV

$$\begin{aligned} \gamma + p &\rightarrow \Delta^{++} + \pi^- , \\ \Delta^{++} &\rightarrow p + \pi^+ , \end{aligned} \tag{13}$$

whereas the production cross section of other isobar components  $(\frac{3}{2}, \frac{3}{2})$  are small and can be neglected. The Dubna INC uses the Lindenbaum-Sternheimer resonance model [75] to simulate the reaction (13). In this model, the mass of the isobar  $M$  is determined from the distribution

$$\frac{dW}{dM} \sim F(E, M)\sigma(M) , \tag{14}$$

where  $E$  is the total energy of the system,  $F$  is the two-body phase space of the isobar and  $\pi^-$  meson, and  $\sigma$  is the isobar production cross section which is assumed to be equal to the cross section for elastic  $\pi^+ p$  scattering.

The c.m. emission angle of the isobar is approximated using Eqs. (11) and (12) with the coefficients  $a_{nk}$  listed in Tab. 3 of Ref. [69]; isotropy of the decay of the isobar in its c.m. system is assumed.

In order to calculate the kinematics of the non-resonant part of the reaction (8) and the two remaining three-body channels (9) and (10), the Dubna INC uses the statistical model.

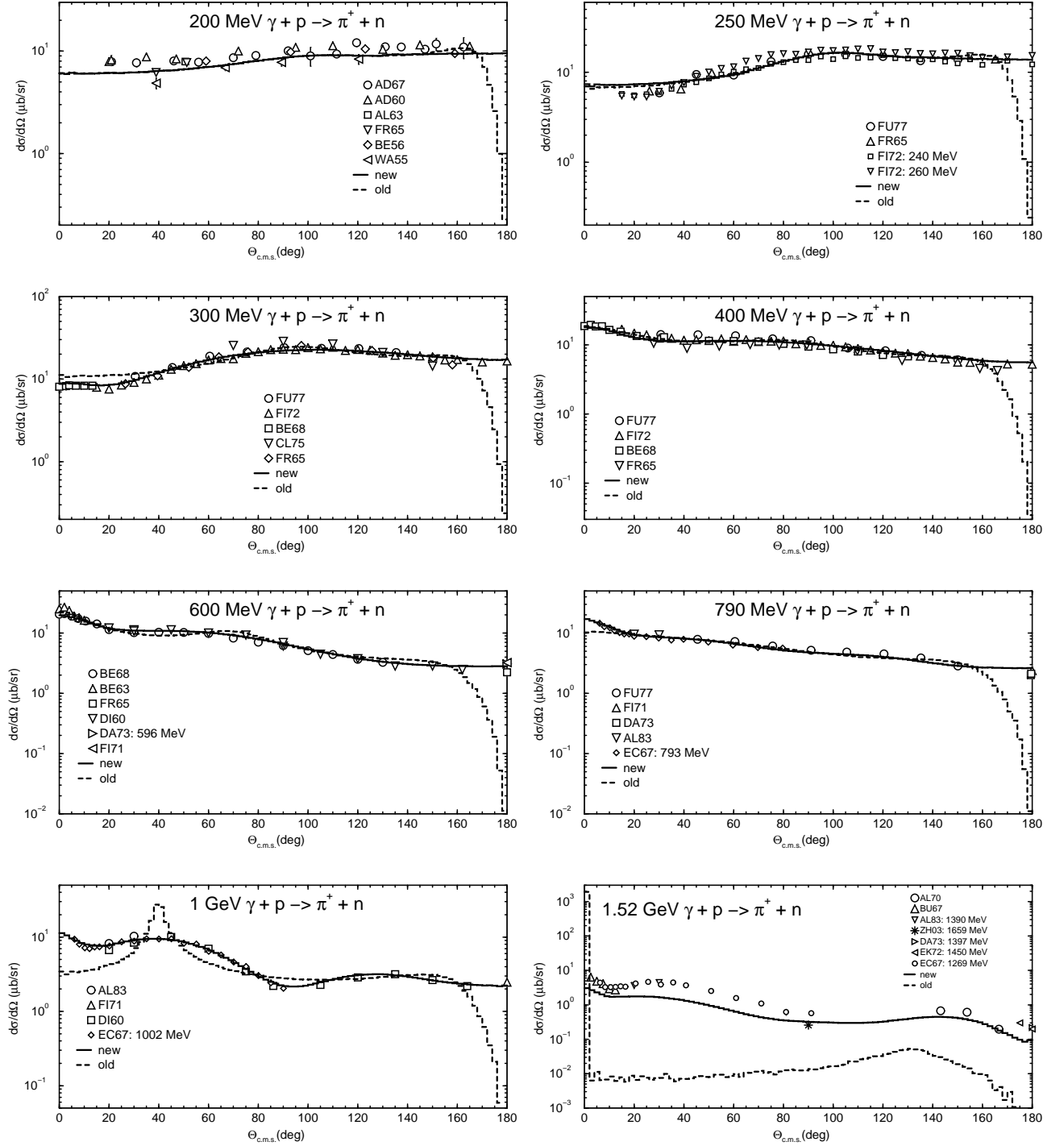


Figure 7: Example of eight angular distributions of  $\pi^+$  from  $\gamma p \rightarrow \pi^+ n$  as functions of  $\Theta_{c.m.s.}^\pi$  at photon energies from 200 MeV to 1.52 GeV. The dashed lines show the old approximations used in the Dubna INC PRM while the solid lines are our new approximations incorporated into the CEM03 and LAQGSM03 codes. References to experimental data shown by symbols may be found in our recent paper [22].

The total energies of the two particles (pions) in the c.m. system are determined from the

distribution

$$\frac{dW}{dE_{\pi_1}dE_{\pi_2}} \sim (E - E_{\pi_1} - E_{\pi_2})E_{\pi_1}E_{\pi_2}/E, \quad (15)$$

and that of the third particle (nucleon,  $N$ ) from conservation of energy. The actual simulation of such reactions is done as follows: Using a random number  $\xi$ , we simulate in the beginning the energy of the first pion using

$$E_{\pi_1} = m_{\pi_1} + \xi(E_{\pi_1}^{max} - m_{\pi_1}),$$

where

$$E_{\pi_1}^{max} = [E^2 + m_{\pi_1}^2 - (m_{\pi_2} + m_N)^2]/2E.$$

Then, we simulate the energy of the second pion  $E_{\pi_2}$  according to Eq. (15) using the Monte-Carlo rejection method. The energy of the nucleon is calculated as  $E_N = E - E_{\pi_1} - E_{\pi_2}$ , following which we check that the “triangle law” for momenta

$$|p_{\pi_1} - p_{\pi_2}| \leq p_N \leq |p_{\pi_1} + p_{\pi_2}|$$

is fulfilled, otherwise this sampling is rejected and the procedure is repeated. The angles  $\Theta$  and  $\varphi$  of the pions are sampled assuming an isotropic distribution of particles in the c.m. system,

$$\cos \Theta_{\pi_1} = 2\xi_1 - 1, \quad \cos \Theta_{\pi_2} = 2\xi_2 - 1, \quad \varphi_{\pi_1} = 2\pi\xi_3, \quad \varphi_{\pi_2} = 2\pi\xi_4,$$

and the angles of the nucleon are defined from momentum conservation,  $\vec{p}_N = -(\vec{p}_{\pi_1} + \vec{p}_{\pi_2})$ . More details on our new approximations for differential elementary cross sections may be found in [21, 22].

The Pauli exclusion principle at the cascade stage of the reaction is handled by assuming that nucleons of the target occupy all the energy levels up to the Fermi energy. Each simulated elastic or inelastic interaction of the projectile (or of a cascade particle) with a nucleon of the target is considered forbidden if the “secondary” nucleons have energies smaller than the Fermi energy. If they do, the trajectory of the particle is traced further from the forbidden point and a new interaction point, a new partner and a new interaction mode are simulated for the traced particle, *etc.*, until the Pauli principle is satisfied or the particle leaves the nucleus.

In this version of the INC, the kinetic energy of the cascade particles is increased or decreased as they move from one of the seven potential regions (zones) to another, but their directions remain unchanged. That is, in our calculations, refraction or reflection of cascade nucleons at potential boundaries is neglected. CEM03.01 allows us to take into account refractions and reflections of cascade nucleons at potential boundaries; for this, one needs to change the value of the parameter **irefrac** from 0 to 1 in the subroutine **initial**. But this option provides somewhat worse overall agreement of calculations with some experimental data, therefore the option of no refractions/reflections was chosen as the default in CEM03.01.

The INC in CEM does not take into account the so-called “trawling” effect [3]. That is, in the beginning of the simulation of each event, the nuclear density distributions for the protons and neutrons of the target are calculated according to Eq. (1) and a subsequent decrease of the nuclear density with the emission of cascade particles is not taken into account. Our detailed analysis of different characteristics of nucleon- and pion-induced reactions for targets from C to Am has shown that this effect may be neglected at incident energies below about 5 GeV in the case of heavy targets like actinides and below about 1 GeV for light targets like carbon. At higher incident energies the progressive decrease of nuclear density with the development of

the intranuclear cascade has a strong influence on the calculated characteristics and this effect has to be taken into account [3]. Therefore, in transport codes that use as event generators both CEM03.01 [23] and our high-energy code LAQGSM03.01 [24], we recommend simulating nuclear reactions with CEM03.01 at incident energies up to about 1 GeV for light nuclei like C and up to about 5 GeV for actinide nuclei, and to switch to simulations using LAQGSM03.01, which considers the “trawling” effect, at higher energies of transported particles.

An important ingredient of the CEM is the criterion for transition from the intranuclear cascade to the preequilibrium model. In conventional cascade-evaporation models (like the Bertini INC used in MCNPX [52]), fast particles are traced down to some minimal energy, the cutoff energy  $T_{cut}$  (or one compares the duration of the cascade stage of a reaction with a cutoff time, in “time-like” INC models, such as the Liege INC [72]). This cutoff is usually less than  $\simeq 10$  MeV above the Fermi energy, below which particles are considered to be absorbed by the nucleus. The CEM uses a different criterion to decide when a primary particle is considered to have left the cascade.

An effective local optical absorptive potential  $W_{opt. mod.}(r)$  is defined from the local interaction cross section of the particle, including Pauli-blocking effects. This imaginary potential is compared to one defined by a phenomenological global optical model  $W_{opt. exp.}(r)$ . We characterize the degree of similarity or difference of these imaginary potentials by the parameter

$$\mathcal{P} = | (W_{opt. mod.} - W_{opt. exp.}) / W_{opt. exp.} | . \quad (16)$$

When  $\mathcal{P}$  increases above an empirically chosen value, the particle leaves the cascade, and is then considered to be an exciton. From a physical point of view, such a smooth transition from the cascade stage of the reaction seems to be more attractive than the “sharp cut-off” method. In addition, as was shown in Ref. [2], this improves the agreement between the calculated and experimental spectra of secondary nucleons, especially at low incident energies and backward angles of the detected nucleons (see *e.g.*, Figs. 3 and 11 of Ref. [2]). More details about this can be found in [2, 17, 76].

CEM03.01 uses a fixed value  $\mathcal{P} = 0.3$  (at incident energies below 100 MeV), just as all its predecessors did. With this value, we find that the cascade stage of the CEM is generally shorter than that in other cascade models. This fact leads to an overestimation of preequilibrium particle emission at incident energies above about 150 MeV, and correspondingly to an underestimation of neutron production from such reactions, as was established in Ref. [17]. In Ref. [17], this problem was solved temporarily in a very rough way by using the transition from the INC to the preequilibrium stage according to Eq. (16) when the incident energy of the projectile is below 150 MeV, and by using the “sharp cut-off” method with a cutoff energy  $T_{cut} = 1$  MeV for higher incident energies. This “ad hoc” rough criterion solved the problem of underestimating neutron production at high energies, providing meanwhile a reasonably good description of reactions below 150 MeV. But it provides an unphysical discontinuity in some observables calculated by MCNPX using CEM2k [17] as an event generator, observed but not understood by Broeders and Konobeev [77]. In CEM03.01, this problem is solved by using a smooth transition from the first criterion to the second one in the energy interval from 75 to 225 MeV, so that no discontinuities are produced in results from CEM03.01.

Beside the changes to the Dubna INC mentioned above, we also made in the INC a number of other improvements and refinements, such as imposing momentum-energy conservation for each simulated event (the Monte-Carlo algorithm previously used in the CEM provided momentum-energy conservation only statistically, on the average, but not exactly for each simulated event) and using real binding energies for nucleons in the cascade instead of the approximation of

a constant separation energy of 7 MeV used in previous versions of the CEM. We have also improved many algorithms used in the Monte-Carlo simulations in many subroutines, decreasing the computing time by up to a factor of 6 for heavy targets, which is very important when performing practical simulations with transport codes like MCNPX or MARS.

Let us mention that in the CEM the initial configuration for the preequilibrium decay (number of excited particles and holes, *i.e.* excitons  $n_0 = p_0 + h_0$ , excitation energy  $E_0^*$ , linear momentum  $\mathbf{P}_0$ , and angular momentum  $\mathbf{L}_0$  of the nucleus) differs significantly from that usually postulated in exciton models. Our calculations [2, 78, 79] have shown that the distributions of residual nuclei remaining after the cascade stage of the reaction, *i.e.* before the preequilibrium emission, with respect to  $n_0$ ,  $p_0$ ,  $h_0$ ,  $E_0^*$ ,  $\mathbf{P}_0$ , and  $\mathbf{L}_0$  are rather broad.<sup>2</sup>

CEM03.01 (just like LAQGSM03.01 and many other INC-based models) calculates the total reaction cross section,  $\sigma_{in}$ , by the Monte-Carlo method using the geometrical cross section,  $\sigma_{geom}$ , and the number of inelastic,  $N_{in}$ , and elastic,  $N_{el}$ , simulated events, namely:  $\sigma_{in} = \sigma_{geom} N_{in} / (N_{in} + N_{el})$ . The value of the total reaction cross section calculated this way is printed in the beginning of the CEM03.01 output labeled as *Monte Carlo inelastic cross section*. This approach provides a good agreement with available data for reactions induced by nucleons, pions, and photons at incident energies above about 100 MeV, but is not reliable enough at energies below 100 MeV (see, *e.g.*, Figs. 8 and 9 below).

To address this problem, we have incorporated [19] into CEM03.01 the NASA systematics by Tripathi *et al.* [80] for all incident protons and for neutrons with energies above the maximum in the NASA reaction cross sections, and the Kalbach systematics [81] for neutrons of lower energy. For reactions induced by monochromatic and bremsstrahlung photons, we incorporate [22] into CEM03.01 the recent systematics by Kossov [82]. Details on these systematics together with examples of several total inelastic cross sections calculated with them compared with available experimental data may be found in [19, 22]. Our analysis of many different reactions has shown that at incident energies below about 100 MeV these systematics generally describe the total inelastic cross sections better than the Monte-Carlo method does, and no worse than the Monte-Carlo method at higher energies. Therefore we choose these systematics as the default for normalization of all CEM03.01 results. The total reaction cross sections calculated by these systematics are printed in the CEM03.01 output labeled as *Inelastic cross section used here*. (Of course, users may re-normalize all the CEM03.01 results to the Monte-Carlo total reaction cross sections by making a small change to the code in the subroutine **typeout**).

Let us note, however, that in applications, when CEM03.01 and LAQGSM03.01, or any other codes, are used as event generators in transport codes, it does not matter how they calculate the total reaction cross sections (normalization): All transport codes use their own routines or systematics to calculate the total elastic and inelastic cross sections of the projectiles, before starting to simulate with an event generator an inelastic interaction of the traced projectile with a nucleus of the thick target.

To summarize this Section, in comparison with the initial version of the Dubna INC [3, 4]

---

<sup>2</sup>Unfortunately, this fact was misunderstood by the authors of the code HETC-3STEP [59]. In spite of the fact that it has been stressed explicitly, and figures with distributions of excited nuclei after the cascade stage of a reaction with respect to the number of excitons and other characteristics were shown in a number of publications (see, *e.g.*, Fig. 5 in Ref. [2], Fig. 1 in Ref. [79], p. 109 in Ref. [78], and p. 706 in Ref. [26]), the authors of Ref. [59] misstated this fact as “*Gudima et al. assumed the state of two particles and one hole at the beginning ... Hence, their assumption is not valid for the wide range of incident energy*”, claiming this as a weakness of the CEM and a priority of the code HETC-3STEP, where smooth distributions of excited nuclei after the cascade stage of reactions with respect to  $n_0$  are used. This had already been done in the CEM [1, 2].

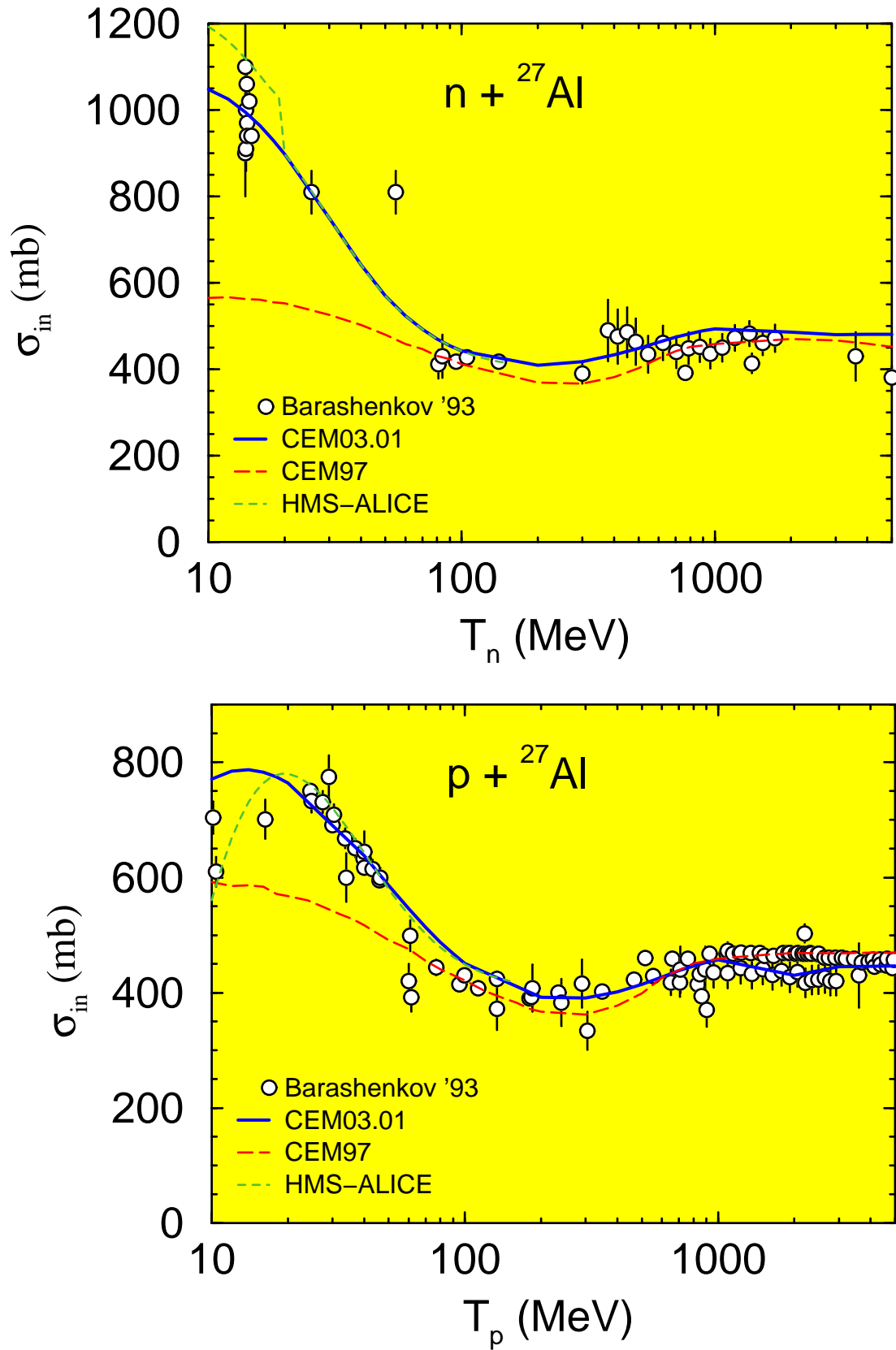


Figure 8: Total reaction cross sections for  $n$ - and  $p$ -induced reactions on Al calculated by CEM03.01 and its predecessor CEM97 with experimental data compiled by Barashenkov [83] and calculations from the HMS-ALICE code [84].

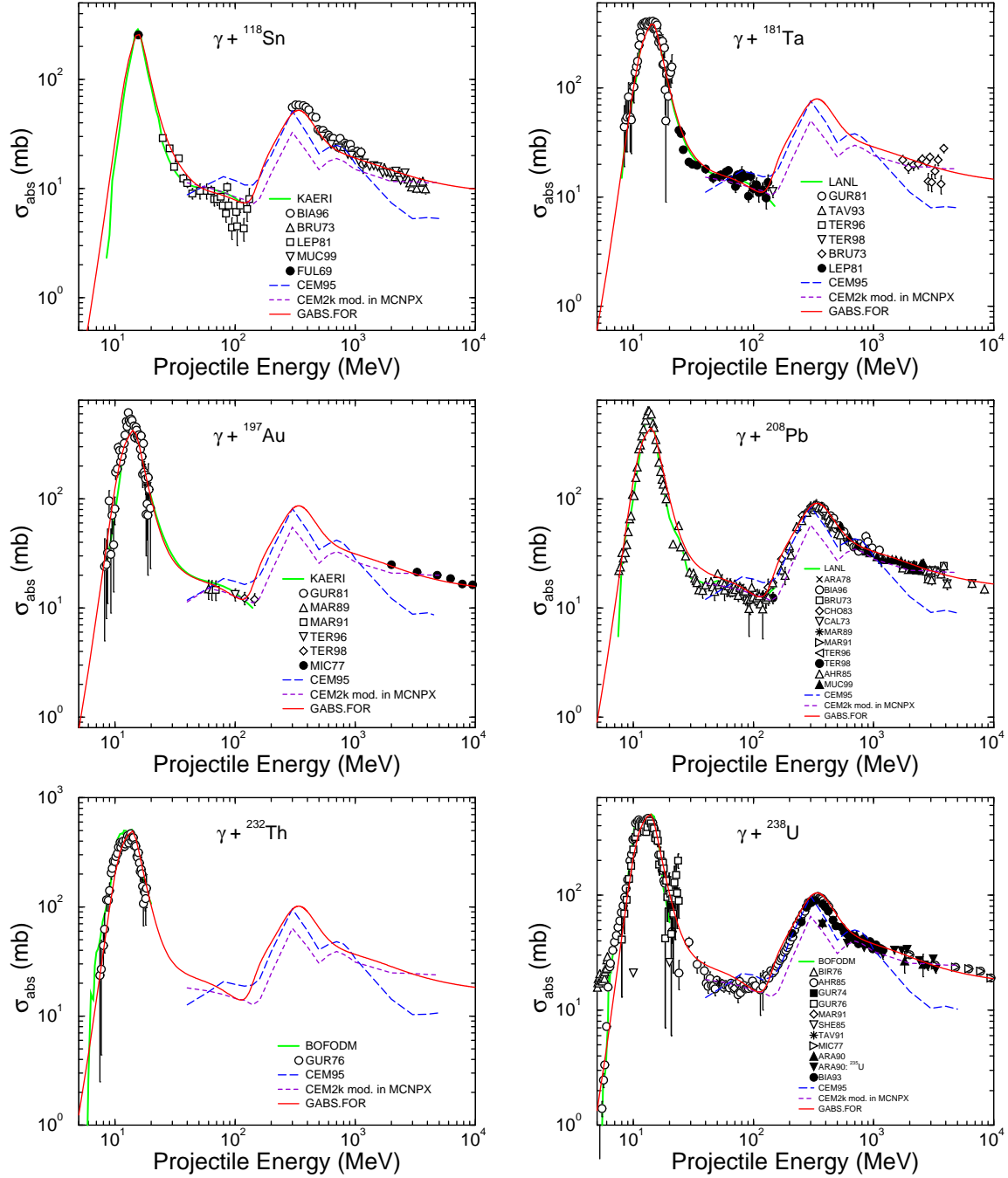


Figure 9: Examples of total photoabsorption cross sections for  $^{118}\text{Sn}$ ,  $^{181}\text{Ta}$ ,  $^{197}\text{Au}$ ,  $^{208}\text{Pb}$ ,  $^{232}\text{Th}$ , and  $^{238}\text{U}$  as functions of photon energy. The red lines marked as “GABS.FOR” are results by a CEM03.01 subroutine written to reproduce Kossov’s [82] systematics, as described in [22]. The green line marked as “LANL”, “KAERI”, or “BOFODM” show the evaluations by LANL, KAERI, or by a collaboration between IPPE/Obninsk and CDFE/Moscow (the BOFOD(MOD) Library) from the IAEA Photonuclear Data Library [85]. Results from the photonuclear version of CEM95 [7] and from CEM2k as modified for MCNPX by Gallmeier [86] are shown by the blue and brown dashed lines, respectively. References to experimental data shown by different symbols may be found in our recent paper [22].

used in CEM95 [9], for CEM03.03 we have:

- 1) developed better approximations for the total elementary cross sections;
- 2) developed new approximations to describe more accurately experimental elementary energy and angular distributions of secondary particles from hadron-hadron and photon-hadron interactions;
- 3) normalized the photonuclear reactions to detailed systematics developed by M. Kossov and the nucleon-induced reactions, to NASA and Kalbach systematics;
- 4) changed the condition for transition from the INC stage of a reaction to preequilibrium; on the whole, the INC stage in CEM03.01 is longer while the preequilibrium stage is shorter in comparison with previous versions;
- 5) incorporated real binding energies for nucleons in the cascade instead of the approximation of a constant separation energy of 7 MeV used in the initial versions of the CEM;
- 6) imposed momentum-energy conservation for each simulated event (provided only “on the average” by the initial versions);
- 7) changed and improved the algorithms of many INC routines and almost all INC routines were rewritten, which speeded up the code significantly;
- 8) fixed some preexisting bugs.

On the whole, the INC of CEM03.01 describes nuclear reactions better and much faster than the the initial version of the Dubna INC [3, 4] used in CEM95 [9]. One example of results by the INC from our CEM03.01 is shown in Fig. 10, namely,  $\pi^0$  spectra from 500 MeV  $\pi^- + \text{Cu}$ .

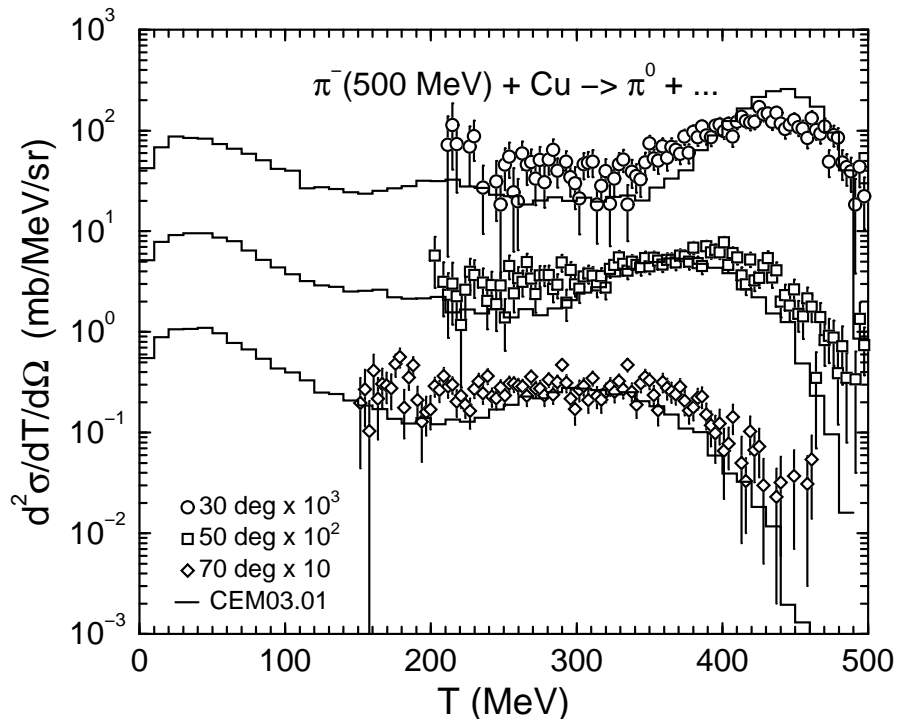


Figure 10: Experimental  $\pi^0$  spectra from 500 MeV  $\pi^- + \text{Cu}$  [27, 87] compared with CEM03.01 results. Let us recall here that as pions are produced by CEM03.01 only at the INC stage of reactions, calculated pion spectra do not depend at all on how other reaction mechanisms like coalescence, evaporation, fission, or Fermi breakup are calculated.

### 3.2. The INC of LAQGSM03.03

The INC of LAQGSM03.03 is described with a recently improved version [12, 24, 88] of the time-dependent intranuclear cascade model developed initially at JINR in Dubna, often referred to in the literature as the Dubna intranuclear Cascade Model, DCM (see [89] and references therein). The DCM models interactions of fast cascade particles (“participants”) with nucleon spectators of both the target and projectile nuclei and includes as well interactions of two participants (cascade particles). It uses experimental cross sections at energies below 4.5 GeV/nucleon, or those calculated by the Quark-Gluon String Model [90]–[96] at higher energies to simulate angular and energy distributions of cascade particles, and also considers the Pauli exclusion principle.

In contrast to the CEM03.01 version of the INC described above, DCM uses a continuous nuclear density distribution (instead of the approximation of several concentric zones, where inside each the nuclear density is considered to be constant); therefore, it does not need to consider refraction and reflection of cascade particles inside or on the border of a nucleus. It also keeps track of the time of an intranuclear collision and of the depletion of the nuclear density during the development of the cascade (the so-called “trawling effect” mentioned above) and takes into account the hadron formation time (see Fig. 11).

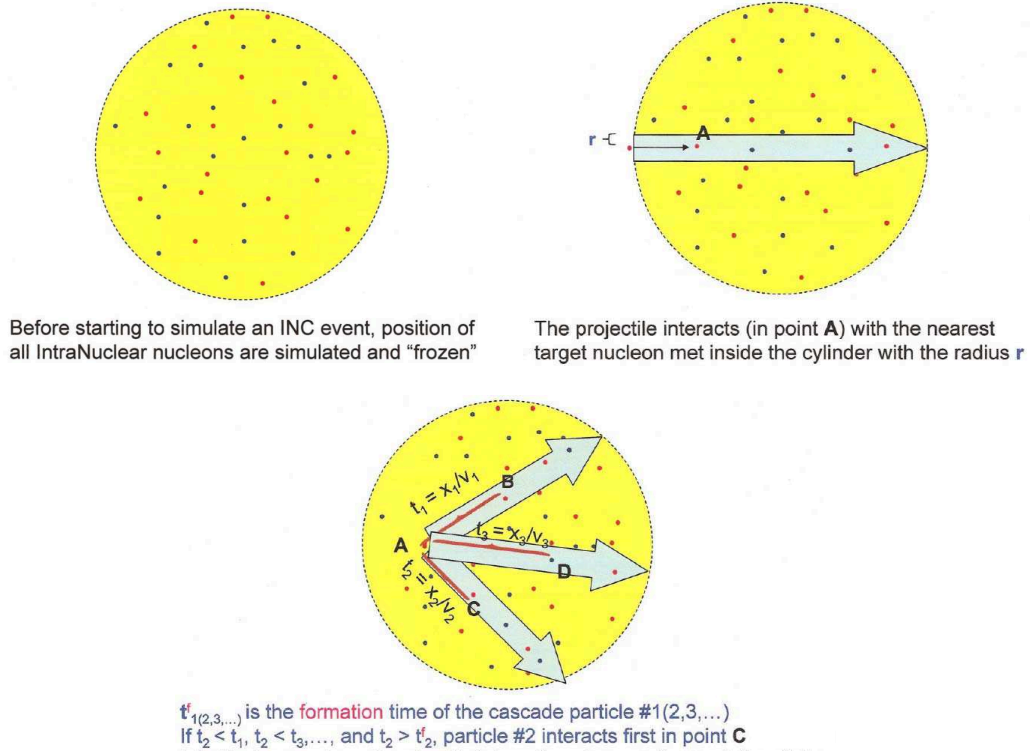


Figure 11: An illustrative scheme of a target nucleus, of interaction points of cascade particles (participants) with intranuclear nucleons (spectators), and of selection of the corresponding time of such interactions, as performed in the INC used in LAQGSM.

In the INC used in LAQGSM, all the new approximations developed recently for the INC of CEM03.01 to describe total cross sections and elementary energy and angular distributions of secondary particles from hadron-hadron interactions have been incorporated [24]. Then, a new high-energy photonuclear reaction model based on the of the event generators for  $\gamma p$  and

$\gamma n$  reactions from the Moscow INC [74] kindly provided us by Dr. Igor Pshenichnov, and on the latest photonuclear version of CEM [22] was developed and incorporated [88] into the INC of LAQGSM, which allows us to calculate reactions induced by photons with energies of up to tens of GeV. Finally, the algorithms of many LAQGSM INC routines were changed and some INC routines were rewritten, which speeded up the code significantly; some preexisting bugs in the DCM were fixed; many useful comments were added [12].

In the latest version of LAQGSM, LAQGSM03.03 [12], the INC was modified for a better description of nuclear reactions at very high energies (above 20 GeV/nucleon), namely:

1) The latest fits to currently available evaluated experimental databases for the total and elastic  $\pi^+p$ ,  $\pi^-p$ ,  $pp$ , and  $pn$  cross sections (see Chapter 40 in the last Review of Particle Physics [98] and references therein) have been incorporated into LAQGSM. LAQGSM03.03 uses now these approximations at energies above 20–30 GeV, and its own approximations developed for CEM03.01 [23] at lower energies.

2) Previously, LAQGSM was used only at energies below 800 GeV. In [12], the possibility of using LAQGSM03.03 at ultra-relativistic energies, above 1 TeV was studied. It was found that to describe ultra-high energy reactions, the value of the parameter  $\sigma_\perp = 0.51$  GeV/c in the transverse momentum distribution of the constituent quarks of QGSM (see Eq. (12) in [13] or Eq. (10) in Ref. [93]) has to be increased from 0.51 GeV/c at  $T_p \leq 200$  GeV [13] to  $\approx 2$  GeV/c at  $T_p \simeq 21$  TeV.

More details on the INC and other nuclear reaction models considered by different versions of LAQGSM may be found in Refs. [12, 13, 24, 88, 97]. Several examples of recent results by LAQGSM are shown in Figs. 12–16.

Fig. 12 shows a test of LAQGSM03.03 on inclusive pion production spectra in proton-beryllium collisions at 6.4, 12.3, and 17.5 GeV/c obtained from data taken by the already quite old E910 measurements at Brookhaven National Laboratory, but analyzed and published only several months ago [99]. Let us recall again that pions are produced only at the INC stage of reactions, without any contributions from other reaction mechanisms, so that such results test just the INC part of any model. We see that LAQGSM03.03 describes these pion spectra quite well, just as we obtained and published with previous versions of LAQGSM for other spectra of different particles measured by the E910 experiment.

Fig. 13 presents part of the recent extensive experimental data on fragmentation cross sections of  $^{28}\text{Si}$  on H, C, Al, Cu, Sn, and Pb at energies from 290 to 1200 MeV/nucleon [100]. Such measurements are of interest for NASA to plan long-duration space-flights and to test the models used to evaluate radiation exposure in flight, and were performed at many incident energies in this energy range at the Heavy Ion Medical Accelerator in Chiba (HIMAC) and at Brookhaven National Laboratory (see details in [100] and references therein). We calculate in our model practically all these data, but here limit ourselves to examples of results for only three energies, for each measured target. For comparison, we present in Fig. 13 results from both LAQGSM03.03 (solid lines) and its predecessor LAQGSM03.02 (dashed lines). In general, LAQGSM03.03 describes these new data slightly better than LAQGSM03.02 [63], although this is not obvious on the scale of the figure. The agreement of our calculations with these data is excellent, especially considering that the results presented in this figure, just as all our other results shown in these lectures, are obtained without fitting any parameters in our codes;

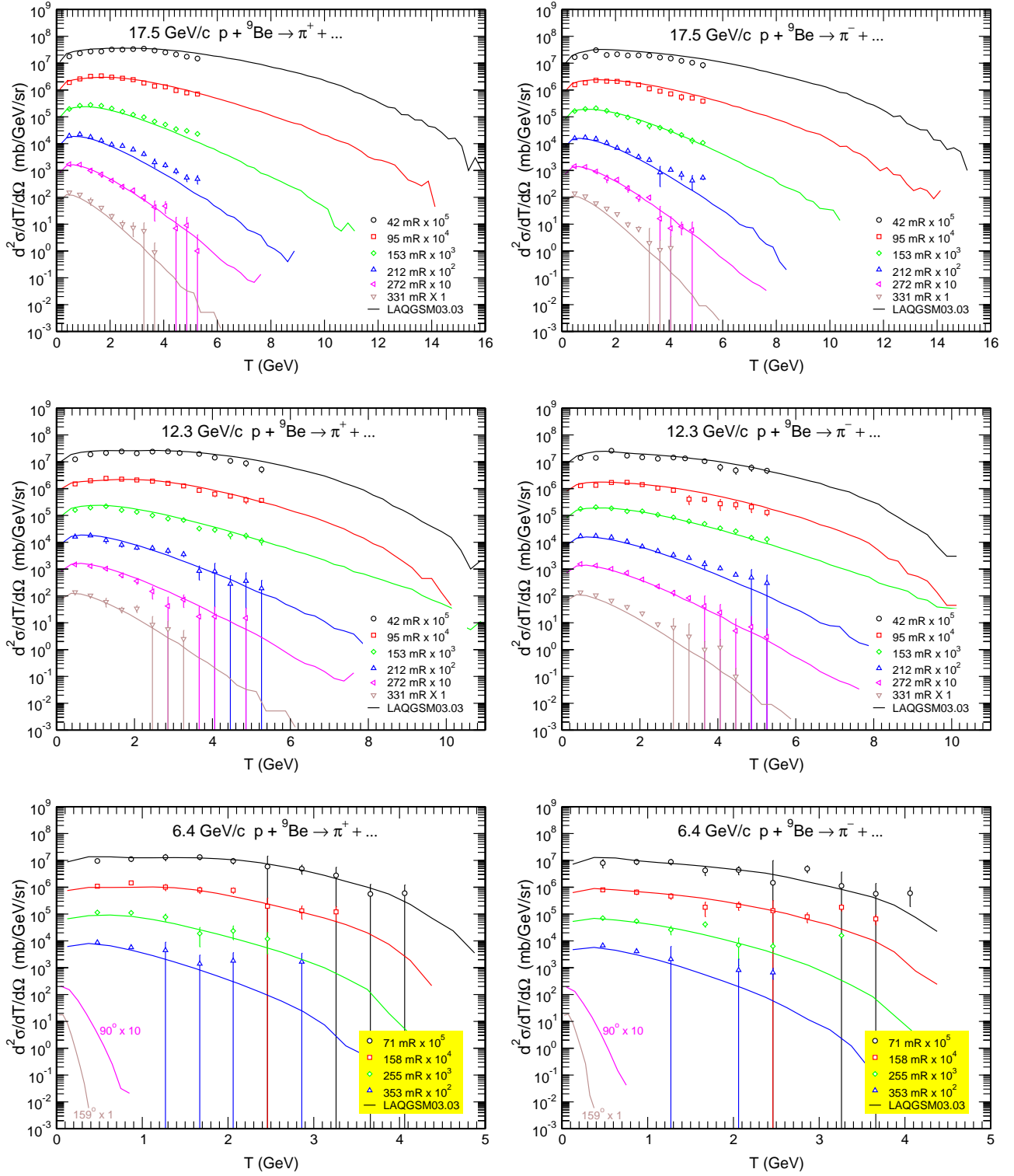


Figure 12: Measured inclusive forward  $\pi^+$  and  $\pi^-$  spectra from 6.4, 12.3, and 17.5 GeV/c  $p + {}^9\text{Be}$  [99] compared with LAQGSM03.03 results at angles of detection as indicated in the plots. For reactions induced by 6.4 GeV/c protons, we also show LAQGSM03.03 predictions [12] for unmeasured spectra at 90 and 159 degrees.

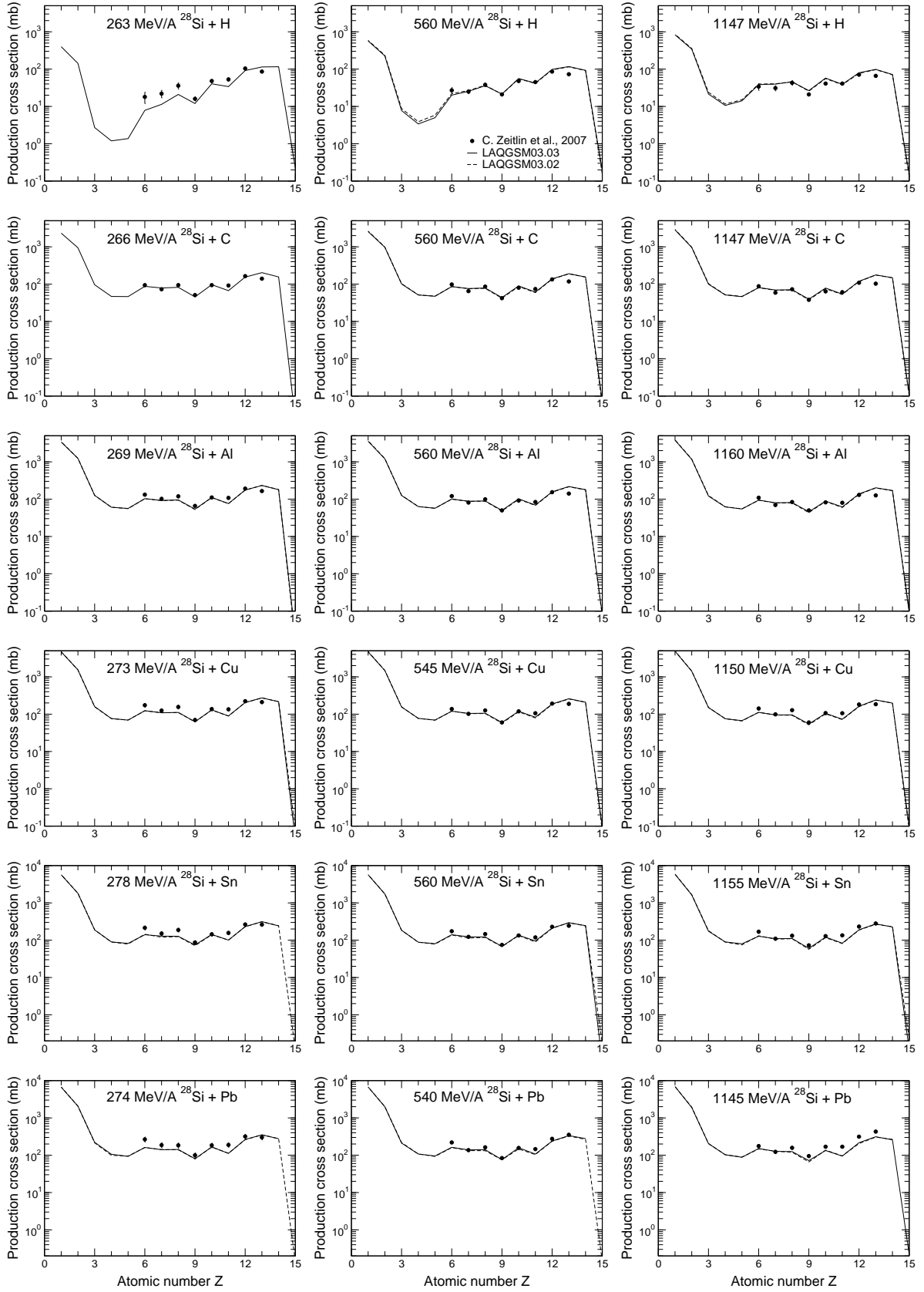


Figure 13: Atomic-number dependence of the fragment-production cross sections from the interactions of  $^{28}\text{Si}$  of about 270, 560, and 1150 MeV/nucleon with H, C, Al, Cu, Sn, and Pb, as indicated. Filled circles are measurements by Zeitlin *et al.* [100]; solid lines are results from LAQGSM03.03 [12], while dashed lines are results from LAQGSM03.02 [63].

we simply input  $A$  and  $Z$  of the projectile and target and the energy of the projectile, then calculate without changing or fitting anything.

Fig. 14. shows proton spectra spectra at 30, 60, 90, 120 and 150 degrees from interaction of bremsstrahlung  $\gamma$  quanta of maximum energy 4.5 GeV with  $^{12}\text{C}$ ,  $^{27}\text{Al}$ ,  $^{63}\text{Cu}$ , and  $^{208}\text{Pb}$ . Experimental data shown by symbols in the figures are quite old, measured about 30 years ago by Alanakyan *et al.* [101, 102], however, to the best of our knowledge, we have described with LAQGSM03.01 these data for the first time: We do not know of any publications or oral presentations where these measurements were reproduced by a theoretical model, event generator, or transport code.

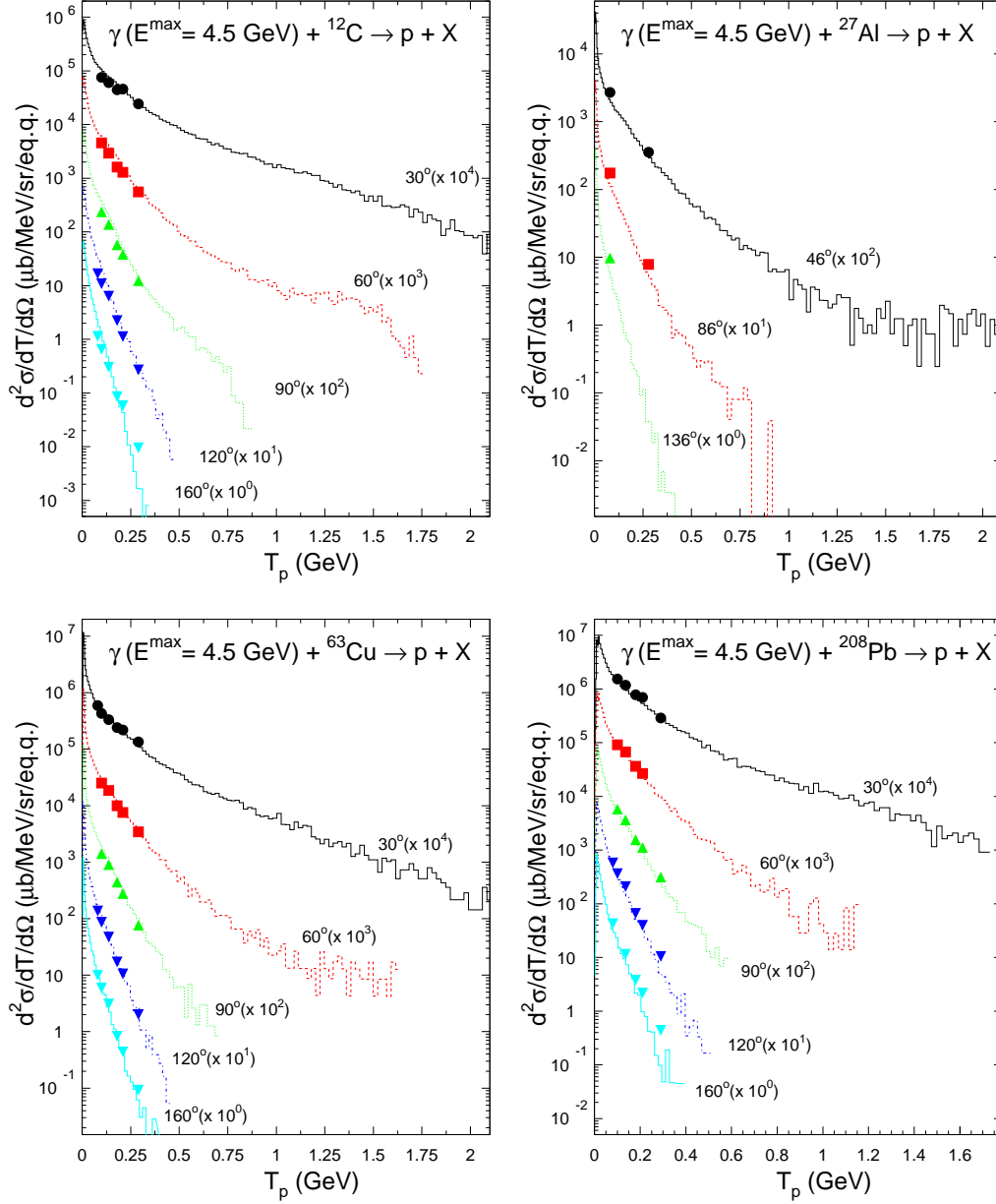


Figure 14: Proton spectra at 30, 60, 90, 120 and 150 degrees from interaction of bremsstrahlung  $\gamma$  quanta of maximum energy 4.5 GeV with  $^{12}\text{C}$ ,  $^{27}\text{Al}$ ,  $^{63}\text{Cu}$ , and  $^{208}\text{Pb}$ . Experimental values shown by symbols are from [101, 102] while histograms show results from LAQGSM03.01.

Fig. 15. shows an example of neutron spectra from intermediate-energy nucleus-nucleus interactions studied lately by many authors because of a great interest in such reactions for radiotherapy and because such processes contribute substantially to the dose and dose equivalent in space-flight. Namely, in Fig. 15, we compare results from LAQGSM03.01 for neutron spectra at 5, 10, 20, 30, 40, 60, and 80 degrees from interactions of 600 MeV/nucleon  $^{20}\text{Ne}$ , on  $^{12}\text{C}$ ,  $^{27}\text{Al}$ ,  $^{64}\text{Cu}$ , and  $^{208}\text{Pb}$  with measurements by Iwata *et al.* [103] and calculations by JQMD [104] and HIC [105]. We see that LAQGSM describes these data reasonably well, generally as well as or better than do JQMD or HIC.

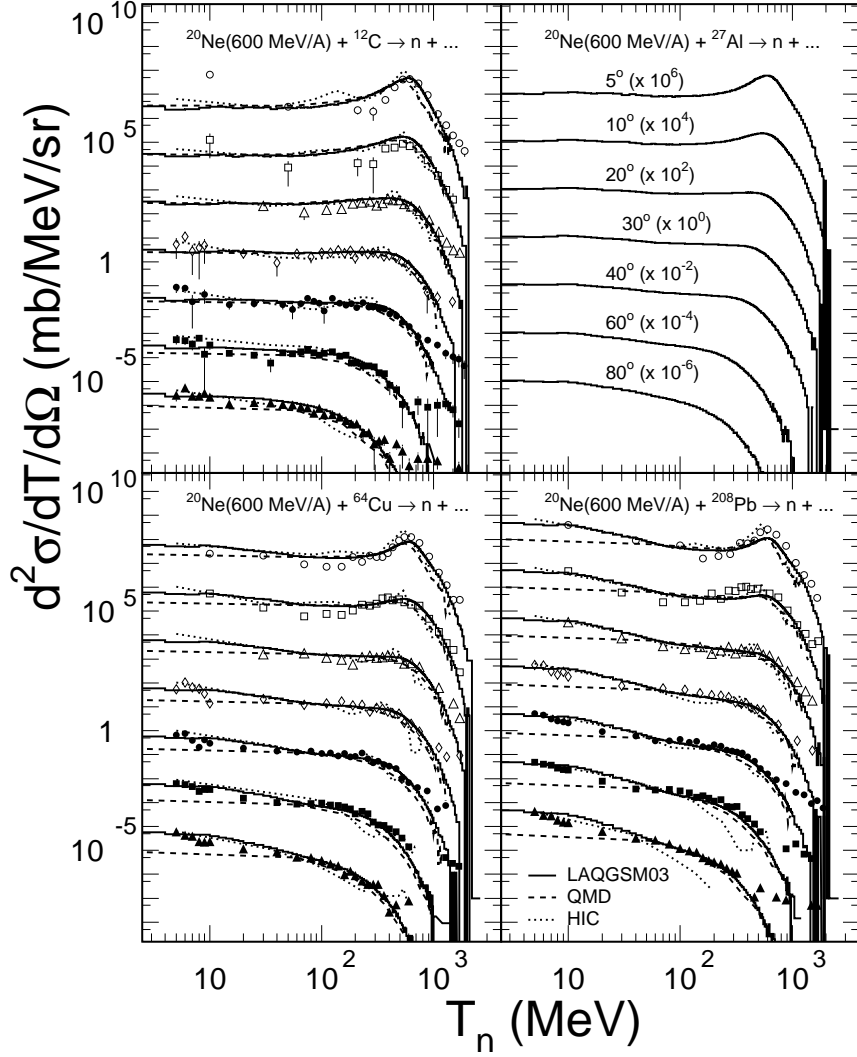


Figure 15: Comparison of measured [103] double differential cross sections of neutrons from 600 MeV/nucleon  $^{20}\text{Ne}$ , on  $^{12}\text{C}$ ,  $^{27}\text{Al}$ ,  $^{64}\text{Cu}$ , and  $^{208}\text{Pb}$  with our LAQGSM03.01 results and calculations by JQMD [104] and HIC [105]. Experimental data for these reactions on Al are not yet available so we present here [106] only our predictions from LAQGSM03.01.

Finally, Fig. 16 shows an example of product mass yields measured recently at GSI in inverse kinematics [107, 108], namely, product yields of 9 isotopes from Zn to Hg produced from interactions of a  $^{238}\text{U}$  beam with a liquid-hydrogen target as calculated by LAQGSM03.01 as a stand-alone code and by the transport code MARS15 [51] using LAQGSM03.01 as its event generator [109]. The results from MARS15 using LAQGSM03.01 agree very well with

the results from LAQGSM03.01 as a stand-alone code and with experimental data.

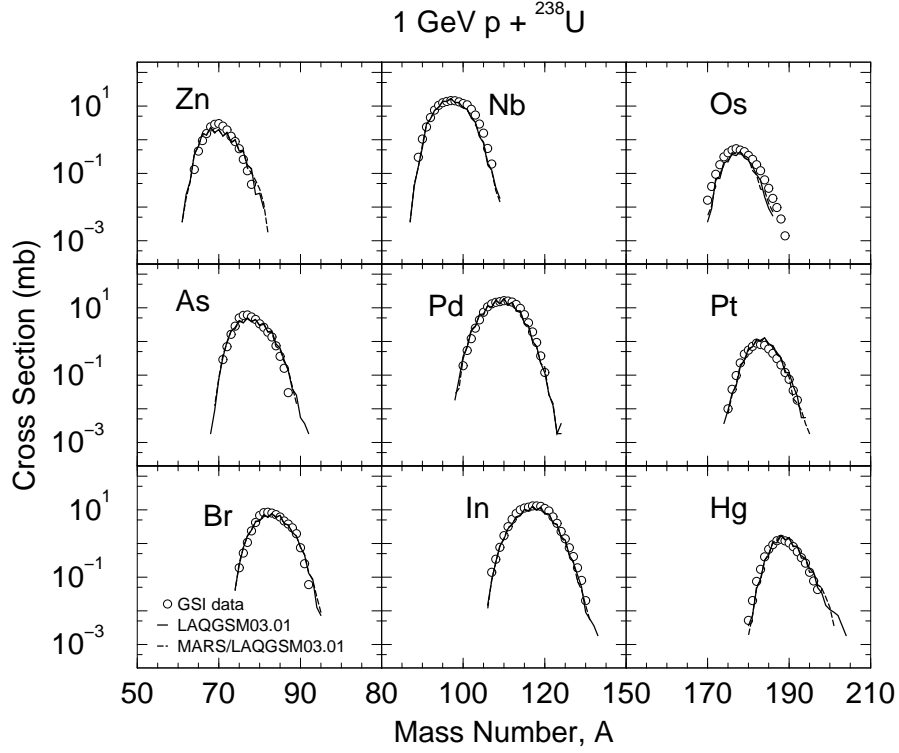


Figure 16: Experimental mass yield in 1 GeV p +  $^{238}\text{U}$  measured in inverse kinematics at GSI [107, 108] compared with results by MARS15 using LAQGSM03.01 as its event generator (dashed lines) and by LAQGSM03.01 as a stand-alone code (solid lines).

#### 4. The Coalescence Model

When the cascade stage of a reaction is completed, CEM03.0x and LAQGSM03.0x use the coalescence model described in Refs. [89, 110] to “create” high-energy  $d$ ,  $t$ ,  $^3\text{He}$ , and  $^4\text{He}$  by final-state interactions among emitted cascade nucleons, already outside of the target nucleus. In contrast to most other coalescence models for heavy-ion-induced reactions, where complex-particle spectra are estimated simply by convolving the measured or calculated inclusive spectra of nucleons with corresponding fitted coefficients (see, *e.g.*, [111] and references therein), CEM03.0x and LAQGSM03.0x use in their simulations of particle coalescence real information about all emitted cascade nucleons and do not use integrated spectra. We assume that all the cascade nucleons having differences in their momenta smaller than  $p_c$  and the correct isotopic content form an appropriate composite particle. This means that the formation probability for, *e.g.* a deuteron is

$$W_d(\vec{p}, b) = \int \int d\vec{p}_p d\vec{p}_n \rho^C(\vec{p}_p, b) \rho^C(\vec{p}_n, b) \delta(\vec{p}_p + \vec{p}_n - \vec{p}) \Theta(p_c - |\vec{p}_p - \vec{p}_n|), \quad (17)$$

where the particle density in momentum space is related to the one-particle distribution function  $f$  by

$$\rho^C(\vec{p}, b) = \int d\vec{r} f^C(\vec{r}, \vec{p}, b). \quad (18)$$

Here,  $b$  is the impact parameter for the projectile interacting with the target nucleus and the superscript index  $C$  shows that only cascade nucleons are taken into account for the coalescence process. The coalescence radii  $p_c$  were fitted for each composite particle in Ref. [89] to describe available data for the reaction Ne+U at 1.04 GeV/nucleon, but the fitted values turned out to be quite universal and were subsequently found to satisfactorily describe high-energy complex-particle production for a variety of reactions induced both by particles and nuclei at incident energies up to about 200 GeV/nucleon, when describing nuclear reactions with different versions of LAQGSM [12, 63, 13] or with its predecessor, the Quark-Gluon String Model (QGSM) [90]. These parameters are:

$$p_c(d) = 90 \text{ MeV/c}; \quad p_c(t) = p_c(^3\text{He}) = 108 \text{ MeV/c}; \quad p_c(^4\text{He}) = 115 \text{ MeV/c} . \quad (19)$$

As the INC of CEM03.0x is different from those of LAQGSM or QGSM, it is natural to expect different best values for  $p_c$  as well. Our recent studies show that the values of parameters  $p_c$  defined by Eq. (19) are also good for CEM03.01 for projectile particles with kinetic energies  $T_0$  lower than 300 MeV and equal to or above 1 GeV. For incident energies in the interval  $300 \text{ MeV} < T_0 \leq 1 \text{ GeV}$ , a better overall agreement with the available experimental data is obtained by using values of  $p_c$  equal to 150, 175, and 175 MeV/c for  $d$ ,  $t(^3\text{He})$ , and  $^4\text{He}$ , respectively. These values of  $p_c$  are fixed as defaults in CEM03.01. If several cascade nucleons are chosen to coalesce into composite particles, they are removed from the distributions of nucleons and do not contribute further to such nucleon characteristics as spectra, multiplicities, *etc.*

In comparison with the initial version [89, 110], in CEM03.0x and LAQGSM03.0x, several coalescence routines have been changed/deleted and have been tested against a large variety of measured data on nucleon- and nucleus-induced reactions at different incident energies.

Two examples of results from the coalescence model are shown in Figs. 17 and 18. We see that for a reaction between an intermediate-energy neutron and a medium-mass nucleus (Fig. 17; 96 MeV  $n + \text{Fe}$ ), where the mean multiplicity of the secondary nucleons is small, the contribution from coalescence to the total angle-integrated energy spectra of complex particles is very low, less than a few percent. On the other hand, in the case of interaction of a high-energy proton with a heavy nucleus (Fig. 18, 70 GeV  $p + \text{Pb}$ ), very energetic secondary complex particles produced at forward angles: deuterons with 14 GeV/c and tritons with 19 GeV/c were measured [113] at 160 mrad. Probably all such extremely energetic  $d$  and  $t$  at forward angles are produced only via coalescence of complex particles from energetic nucleons emitted during the INC stage of the reaction: We do not know any other interaction mechanisms that would produce  $d$  and  $t$  of such high energies from this reaction. The coalescence model in LAQGSM03.0x reproduces these experimental spectra quite well. It is clear that the coalescence mechanism is more important for high-energy heavy-ion reactions, where the multiplicity of secondary INC nucleons is much higher than in the case of nucleon-induced reactions.

## 5. Preequilibrium Reactions

The subsequent preequilibrium interaction stage of nuclear reactions is considered by our current CEM and LAQGSM in the framework of the latest version of the Modified Exciton Model (MEM) [5, 6] as implemented in CEM03.01 [23]. At the preequilibrium stage of a reaction we take into account all possible nuclear transitions changing the number of excitons  $n$  with  $\Delta n = +2, -2$ , and 0, as well as all possible multiple subsequent emissions of  $n$ ,  $p$ ,  $d$ ,  $t$ ,  $^3\text{He}$ , and  $^4\text{He}$ . The corresponding system of master equations describing the behavior of a nucleus at the preequilibrium stage is solved by the Monte-Carlo technique [1, 2].

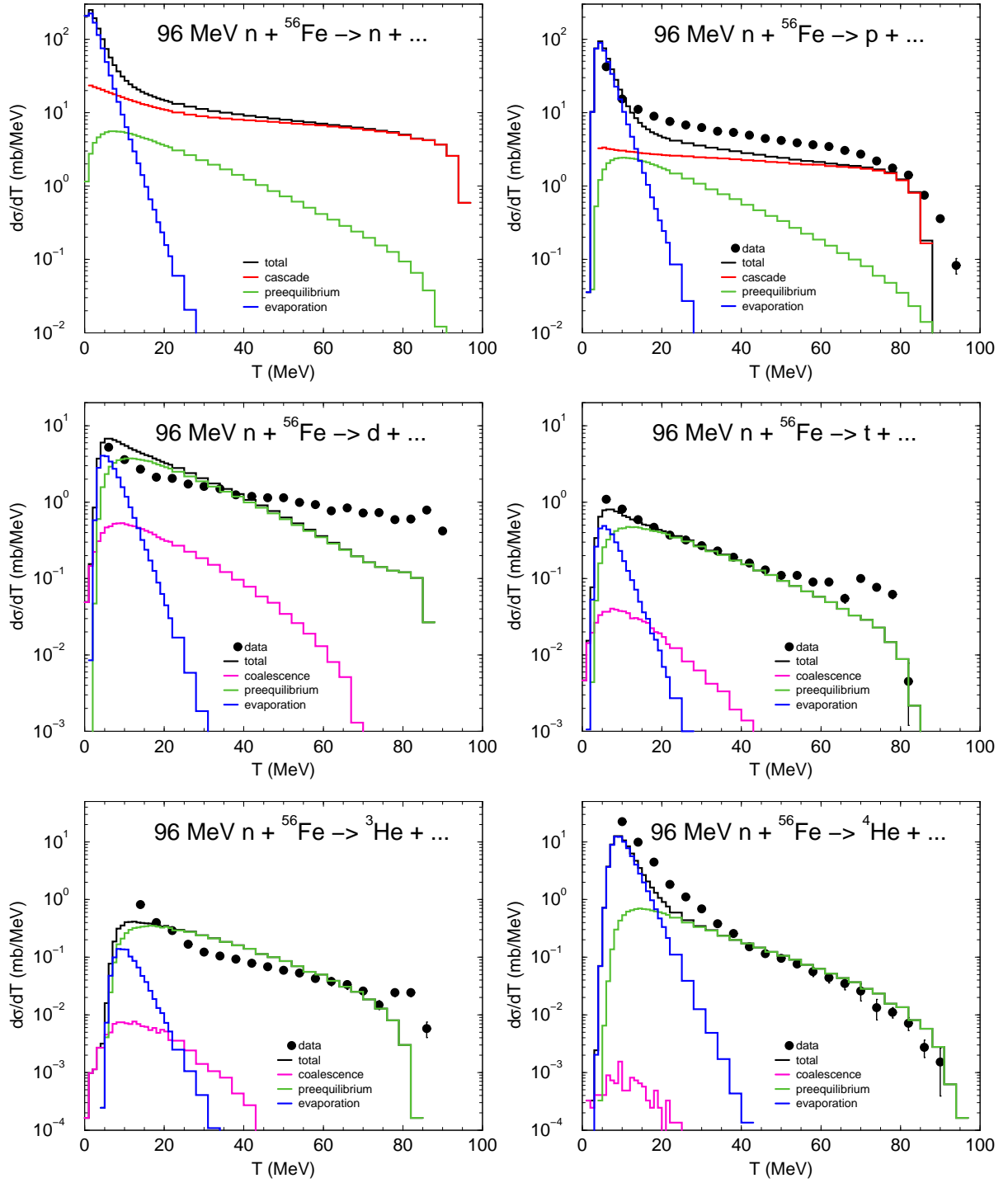


Figure 17: Angle-integrated energy spectra of  $n$ ,  $p$ ,  $d$ ,  $t$ ,  ${}^3\text{He}$ , and  ${}^4\text{He}$  from 96 MeV  $n + {}^{56}\text{Fe}$  calculated by CEM03.01 compared with experimental data by Blideanu *et al.* [112]. The black histograms show the total calculated spectra (all reaction mechanisms considered by CEM03.0x), while the color histograms show separately contributions to the total spectra from INC, coalescence, preequilibrium, and evaporation, respectively, as indicated in the corresponding legends of plots.

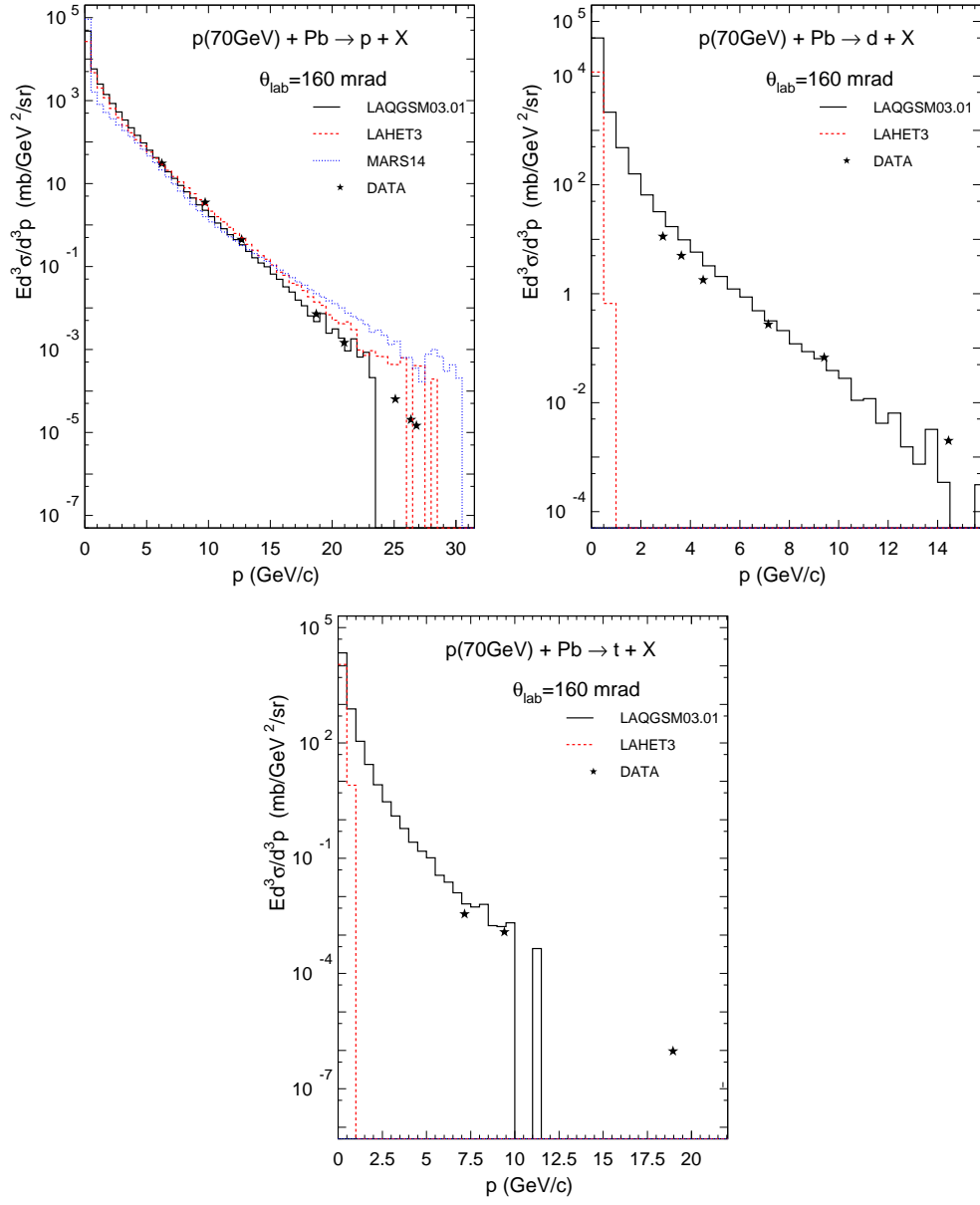


Figure 18: Invariant cross sections  $Ed^3\sigma/d^3p$  for forward production of p, d, and t at 160 mrad (9.17 deg) as functions of particle momentum  $p$  from 70 GeV protons on  $^{208}\text{Pb}$ . Experimental data shown by stars are from Ref. [113], while calculations by LAQGSM03.01, LAHET3 [114], and MARS14 [51] are shown by histograms, as indicated in the legends.

For a preequilibrium nucleus with excitation energy  $E$  and number of excitons  $n = p + h$ , the partial transition probabilities changing the exciton number by  $\Delta n$  are

$$\lambda_{\Delta n}(p, h, E) = \frac{2\pi}{\hbar} |M_{\Delta n}|^2 \omega_{\Delta n}(p, h, E) . \quad (20)$$

The emission rate of a nucleon of type  $j$  into the continuum is estimated according to the detailed balance principle

$$\Gamma_j(p, h, E) = \int_{V_j^c}^{E-B_j} \lambda_c^j(p, h, E, T) dT ,$$

$$\lambda_c^j(p, h, E, T) = \frac{2s_j + 1}{\pi^2 \hbar^3} \mu_j \mathfrak{R}_j(p, h) \frac{\omega(p-1, h, E - B_j - T)}{\omega(p, h, E)} T \sigma_{inv}(T) , \quad (21)$$

where  $s_j$ ,  $B_j$ ,  $V_j^c$ , and  $\mu_j$  are the spin, binding energy, Coulomb barrier, and reduced mass of the emitted particle, respectively. The factor  $\mathfrak{R}_j(p, h)$  ensures the condition for the exciton chosen to be the particle of type  $j$  and can easily be calculated by the Monte-Carlo technique.

Assuming an equidistant level scheme with the single-particle density  $g$ , we have the level density of the  $n$ -exciton state as [115]

$$\omega(p, h, E) = \frac{g(gE)^{p+h-1}}{p!h!(p+h-1)!} . \quad (22)$$

This expression should be substituted into Eq. (21). For the transition rates (20), one needs the number of states taking into account the selection rules for intranuclear exciton-exciton scattering. The appropriate formulae have been derived by Williams [116] and later corrected for the exclusion principle and indistinguishability of identical excitons in Refs. [117, 118]:

$$\begin{aligned} \omega_+(p, h, E) &= \frac{1}{2} g \frac{[gE - \mathcal{A}(p+1, h+1)]^2}{n+1} \left[ \frac{gE - \mathcal{A}(p+1, h+1)}{gE - \mathcal{A}(p, h)} \right]^{n-1} , \\ \omega_0(p, h, E) &= \frac{1}{2} g \frac{[gE - \mathcal{A}(p, h)]}{n} [p(p-1) + 4ph + h(h-1)] , \\ \omega_-(p, h, E) &= \frac{1}{2} g p h (n-2) , \end{aligned} \quad (23)$$

where  $\mathcal{A}(p, h) = (p^2 + h^2 + p - h)/4 - h/2$ . By neglecting the difference of matrix elements with different  $\Delta n$ ,  $M_+ = M_- = M_0 = M$ , we estimate the value of  $M$  for a given nuclear state by associating the  $\lambda_+(p, h, E)$  transition with the probability for quasi-free scattering of a nucleon above the Fermi level on a nucleon of the target nucleus. Therefore, we have

$$\frac{\langle \sigma(v_{rel}) v_{rel} \rangle}{V_{int}} = \frac{\pi}{\hbar} |M|^2 \frac{g[gE - \mathcal{A}(p+1, h+1)]}{n+1} \left[ \frac{gE - \mathcal{A}(p+1, h+1)}{gE - \mathcal{A}(p, h)} \right]^{n-1} . \quad (24)$$

Here,  $V_{int}$  is the interaction volume estimated as  $V_{int} = \frac{4}{3} \pi (2r_c + \lambda/2\pi)^3$ , with the de Broglie wave length  $\lambda/2\pi$  corresponding to the relative velocity  $v_{rel} = \sqrt{2T_{rel}/m_N}$ . A value of the order of the nucleon radius is used for  $r_c$  in the CEM:  $r_c = 0.6$  fm.

The averaging in the left-hand side of Eq. (24) is carried out over all excited states taking into account the Pauli principle in the approximation

$$\langle \sigma(v_{rel}) v_{rel} \rangle \simeq \langle \sigma(v_{rel}) \rangle \langle v_{rel} \rangle . \quad (25)$$

The averaged cross section  $\langle \sigma(v_{rel}) \rangle$  is calculated by the Monte-Carlo simulation method and by introducing a factor  $\eta$  effectively taking into account the Pauli principle exactly as is done in the Fermi-gas model (see, *e.g.*, [119])<sup>3</sup>

$$\sigma(v_{rel}) = \frac{1}{2} [\sigma_{pp}(v_{rel}) + \sigma_{pn}(v_{rel})] \eta(T_F/T) , \text{ where} \quad (26)$$

$$\eta(x) = \begin{cases} 1 - \frac{7}{2}x, & \text{if } x \leq 0.5 , \\ 1 - \frac{7}{5}x + \frac{2}{5}x(2 - \frac{1}{x})^{5/2}, & \text{if } x > 0.5 . \end{cases} \quad (27)$$

---

<sup>3</sup>Unfortunately, formula (27) as presented in Ref. [2] had some misprints; in the prior publication [1], it was correct.

Here,  $v_{rel}$  is the relative velocity of the excited nucleon (exciton) and the target nucleon in units of the speed of light and  $T$  is the kinetic energy of the exciton. The free-particle interaction cross sections  $\sigma_{pp}(v_{rel})$  and  $\sigma_{pn}(v_{rel})$  in Eq. (26) are estimated using the relations suggested by Metropolis *et al.* [120]

$$\begin{aligned}\sigma_{pp}(v_{rel}) &= \frac{10.63}{v_{rel}^2} - \frac{29.92}{v_{rel}} + 42.9 , \\ \sigma_{pn}(v_{rel}) &= \frac{34.10}{v_{rel}^2} - \frac{82.2}{v_{rel}} + 82.2 ,\end{aligned}\tag{28}$$

where the cross sections are given in mb.

The relative kinetic energy of colliding particles necessary to calculate  $\langle v_{rel} \rangle$  and the factor  $\eta$  in Eqs. (26,27) are estimated in the so-called “right-angle-collision” approximation [5], *i.e.* as a sum of the mean kinetic energy of an excited particle (exciton) measured from the bottom of the potential well  $T_p = T_F + E/n$  plus the mean kinetic energy of an intranuclear nucleon partner  $T_N = 3T_F/5$ , that is  $T_{rel} = T_p + T_N = 8T_F/5 + E/n$ .

Combining (20), (22) and (24), we get finally for the transition rates:

$$\begin{aligned}\lambda_+(p, h, E) &= \frac{\langle \sigma(v_{rel})v_{rel} \rangle}{V_{int}} , \\ \lambda_0(p, h, E) &= \frac{\langle \sigma(v_{rel})v_{rel} \rangle}{V_{int}} \frac{n+1}{n} \left[ \frac{gE - \mathcal{A}(p, h)}{gE - \mathcal{A}(p+1, h+1)} \right]^{n+1} \frac{p(p-1) + 4ph + h(h-1)}{gE - \mathcal{A}(p, h)} , \\ \lambda_-(p, h, E) &= \frac{\langle \sigma(v_{rel})v_{rel} \rangle}{V_{int}} \left[ \frac{gE - \mathcal{A}(p, h)}{gE - \mathcal{A}(p+1, h+1)} \right]^{n+1} \frac{ph(n+1)(n-2)}{[gE - \mathcal{A}(p, h)]^2} .\end{aligned}\tag{29}$$

CEM considers the possibility of fast  $d$ ,  $t$ ,  $^3\text{He}$ , and  $^4\text{He}$  emission at the preequilibrium stage of a reaction in addition to the emission of nucleons. We assume that in the course of a reaction  $p_j$  excited nucleons (excitons) are able to condense with probability  $\gamma_j$  forming a complex particle which can be emitted during the preequilibrium state. A modification of Eq. (21) for the complex-particle emission rates is described in detail in Refs. [1, 2]. The “condensation” probability  $\gamma_j$  is estimated in those references as the overlap integral of the wave function of independent nucleons with that of the complex particle (cluster)

$$\gamma_j \simeq p_j^3 (V_j/V)^{p_j-1} = p_j^3 (p_j/A)^{p_j-1} .\tag{30}$$

This is a rather crude estimate. In the usual way the values  $\gamma_j$  are taken from fitting the theoretical preequilibrium spectra to the experimental ones, which gives rise to an additional, as compared to (30), dependence of the factor  $\gamma_j$  on  $p_j$  and excitation energy (see, *e.g.*, Refs. [121, 122]), for each considered reaction.

The single-particle density  $g_j$  for complex-particle states is found in the CEM by assuming the complex particles move freely in a uniform potential well whose depth is equal to the binding energy of this particle in a nucleus [2]

$$g_j(T) = \frac{V(2s_j + 1)(2\mu_j)^{3/2}}{4\pi^2 \hbar^3} (T + B_j)^{1/2} .\tag{31}$$

As we stated previously, this is a crude approximation and it does not provide a good prediction of emission of preequilibrium  $\alpha$  particles (see, *e.g.*, [76] and references therein). In CEM03.0x, to improve the description of preequilibrium complex-particle emission, we estimate

$\gamma_j$  by multiplying the estimate provided by Eq. (30) by an empirical coefficient  $M_j(A, Z, T_0)$  whose values are fitted to available nucleon-induced experimental complex-particle spectra. We fix the fitted values of  $M_j(A, Z, T_0)$  in data commons of CEM03.0x and complement them with routines **gambetn** and **gambetp** for their interpolation outside the region covered by our fitting. As shown already above in Fig. 17 and proved in several more figures below, after fitting  $M_j(A, Z, T_0)$ , CEM and LAQGSM describe quite well the measured spectra of all complex particles, providing a much better agreement with experimental data than all their predecessors did.

CEM and LAQGSM predict forward-peaked (in the laboratory system) angular distributions for preequilibrium particles. For instance, CEM03.0x assumes that a nuclear state with a given excitation energy  $E^*$  should be specified not only by the exciton number  $n$  but also by the momentum direction  $\Omega$ . Following Ref. [123], the master equation (11) from Ref. [2] can be generalized for this case provided that the angular dependence for the transition rates  $\lambda_+$ ,  $\lambda_0$ , and  $\lambda_-$  (Eq. (29) is factorized. In accordance with Eqs. (24) and (25), in the CEM it is assumed that

$$\langle \sigma \rangle \rightarrow \langle \sigma \rangle F(\Omega) , \quad (32)$$

where

$$F(\Omega) = \frac{d\sigma^{free}/d\Omega}{\int d\Omega' d\sigma^{free}/d\Omega'} . \quad (33)$$

The scattering cross section  $d\sigma^{free}/d\Omega$  is assumed to be isotropic in the reference frame of the interacting excitons, thus resulting in an asymmetry in both the nucleus center-of-mass and laboratory frames. The angular distributions of preequilibrium complex particles are assumed [2] to be similar to those for the nucleons in each nuclear state.

This calculation scheme is easily realized by the Monte-Carlo technique. It provides a good description of double differential spectra of preequilibrium nucleons and a not-so-good but still satisfactory description of complex-particle spectra from different types of nuclear reactions at incident energies from tens of MeV to several GeV. For incident energies below about 200 MeV, Kalbach [124] has developed a phenomenological systematics for preequilibrium-particle angular distributions by fitting available measured spectra of nucleons and complex particles. As the Kalbach systematics are based on measured spectra, they describe very well the double-differential spectra of preequilibrium particles and generally provide a better agreement of calculated preequilibrium complex-particle spectra with data than does the CEM approach based on Eqs. (32,33). This is why we have incorporated into CEM03.0x and LAQGSM03.0x the Kalbach systematics [124] to describe angular distributions of both preequilibrium nucleons and complex particles at incident energies up to 210 MeV. At higher energies, we use the CEM approach based on Eqs. (32,33).

By “preequilibrium particles” we mean particles which are emitted after the cascade stage of a reaction but before achieving statistical equilibrium at a time  $t_{eq}$ , which is fixed by the condition  $\lambda_+(n_{eq}, E) = \lambda_-(n_{eq}, E)$  from which we get

$$n_{eq} \simeq \sqrt{2gE} . \quad (34)$$

At  $t \geq t_{eq}$  (or  $n \geq n_{eq}$ ), the behavior of the remaining excited compound nucleus is described in the framework of both the Weisskopf-Ewing statistical theory of particle evaporation [125] and fission competition according to Bohr-Wheeler theory [126].

The parameter  $g$  entering into Eqs. (29) and (34) is related to the level-density parameter of single-particle states  $a = \pi^2 g/6$ . At the preequilibrium stage, we calculate the level-density

parameter  $a$  with our own approximation [16] in the form proposed initially by Ignatyuk *et al.* [127], following the method by Iljinov *et al.* [128]:

$$a(Z, N, E^*) = \tilde{a}(A) \left\{ 1 + \delta W_{gs}(Z, N) \frac{f(E^* - \Delta)}{E^* - \Delta} \right\}, \quad (35)$$

where

$$\tilde{a}(A) = \alpha A + \beta A^{2/3} B_s \quad (36)$$

is the asymptotic Fermi-gas value of the level-density parameter at high excitation energies. Here,  $B_s$  is the ratio of the surface area of the nucleus to the surface area of a sphere of the same volume (for the ground state of a nucleus,  $B_s \approx 1$ ), and

$$f(E) = 1 - \exp(-\gamma E). \quad (37)$$

$E^*$  is the total excitation energy of the nucleus, related to the “thermal” energy  $U$  by:  $U = E^* - E_R - \Delta$ , where  $E_R$  and  $\Delta$  are the rotational and pairing energies, respectively.

We use the shell correction  $\delta W_{gs}(Z, N)$  by Möller *et al.* [129] and the pairing energy shifts from Möller, Nix, and Kratz [130]. The values of the parameters  $\alpha$ ,  $\beta$ , and  $\gamma$  were derived in Ref. [16] by fitting the the same data analyzed by Iljinov *et al.* [128] (we discovered that Iljinov *et al.* used  $11/\sqrt{A}$  for the pairing energies  $\Delta$  in deriving their level-density systematics instead of the value of  $12/\sqrt{A}$  stated in Ref. [128] and we also found several misprints in the nuclear level-density data shown in their Tables. 1 and 2 used in the fit). We find:

$$\alpha = 0.1463, \beta = -0.0716, \text{ and } \gamma = 0.0542.$$

As mentioned in Section 3.1, the standard version of the CEM [2] provides an overestimation of preequilibrium particle emission from different reactions we have analyzed (see more details in [17, 18]). One way to solve this problem suggested in Ref. [17] is to change the criterion for the transition from the cascade stage to the preequilibrium one, as described in Section 3.1. Another easy way suggested in Ref. [17] to shorten the preequilibrium stage of a reaction is to arbitrarily allow only transitions that increase the number of excitons,  $\Delta n = +2$ , *i.e.*, only allow the evolution of a nucleus toward the compound nucleus. In this case, the time of the equilibration will be shorter and fewer preequilibrium particles will be emitted, leaving more excitation energy for the evaporation. Such a “never-come-back” approach is used by some other exciton models, for instance, by the Multistage Preequilibrium Model (MPM) used in LAHET [131] and by FLUKA [132]. This approach was used in the CEM2k [17] version of the CEM and it allowed us to describe much better the p+A reactions measured at GSI in inverse kinematics at energies around 1 GeV/nucleon. Nevertheless, the “never-come-back” approach seems unphysical, therefore we no longer use it. We now address the problem of emitting fewer preequilibrium particles in the CEM by following Veselský [133]. We assume that the ratio of the number of quasi-particles (excitons)  $n$  at each preequilibrium reaction stage to the number of excitons in the equilibrium configuration  $n_{eq}$ , corresponding to the same excitation energy, to be a crucial parameter for determining the probability of preequilibrium emission  $P_{pre}$ . This probability for a given preequilibrium reaction stage is evaluated using the formula

$$P_{pre}(n/n_{eq}) = 1 - \exp\left(-\frac{(n/n_{eq} - 1)}{2\sigma_{pre}^2}\right) \quad (38)$$

for  $n \leq n_{eq}$  and equal to zero for  $n > n_{eq}$ . The basic assumption leading to Eq. (38) is that  $P_{pre}$  depends exclusively on the ratio  $n/n_{eq}$  as can be deduced from the results of Böhning [134]

where the density of particle-hole states is approximately described using a Gaussian centered at  $n_{eq}$ . The parameter  $\sigma_{pre}$  is a free parameter and we assume no dependence on excitation energy [133]. Our calculations of several reactions using different values of  $\sigma_{pre}$  show that an overall reasonable agreement with available data can be obtained using  $\sigma_{pre} = 0.4$ – $0.5$  (see Fig. 11 in Ref. [18]). In CEM03.0x, we choose the fixed value  $\sigma_{pre} = 0.4$  and use Eqs. (34,38) as criteria for the transition from the preequilibrium stage of reactions to evaporation, instead of using the “never-come-back” approach along with Eq. (34), as was done in CEM2k.

Algorithms of many preequilibrium routines are changed and almost all these routines are rewritten, which has speeded up the code significantly. Finally, some bugs were fixed as previously mentioned.

Several examples with results from the preequilibrium model used in our current event generators are shown in Figs. 19–24.

The energy spectra of secondary particles emitted from 96 MeV  $n + {}^{56}\text{Fe}$  interactions presented in Fig. 17 show that the main contribution to the total spectra of complex particles as calculated by CEM03.01 comes from preequilibrium emission: The coalescence mechanism contributes only a few percent to the total spectra from these reactions, while evaporation is important only in the production of low energy particles, below  $\sim 30$  MeV. Fig. 19 shows several more detailed spectra for the same reactions, namely, CEM03.01 results for double-differential spectra of  $d$  and  $t$  at eight different angles compared with the measured data [112]. Let us recall that CEM03.0x produces almost all these deuterons and tritons via preequilibrium emission. We see that CEM03.0x describes quite well these double-differential spectra, except the very high-energy tails of spectra at the most forward angles, where we should expect a contribution from direct processes like pick-up and knock-out, not considered so far in our models.

Fig. 20 shows examples of angle-integrated energy spectra, energy-integrated angular distributions, and double-differential spectra of nucleons and complex particles from a reaction induced by intermediate-energy protons, namely from 62.9 MeV  $p + \text{Pb}$ , as calculated by CEM03.01 and compared with the recent measurements by Guertin *et al.* [135]. CEM03.01 produces complex particles from this reaction also mainly via preequilibrium emission, and we see that it describes these experimental spectra quite well too.

Fig. 21 shows another example of double-differential spectra of complex particles from proton-induced reactions, at higher energies, namely CEM03.01 calculated  ${}^4\text{He}$  spectra at 20, 40, 60, 100, 120, and 140 degrees from 160 MeV  $p + {}^{27}\text{Al}$ ,  ${}^{59}\text{Co}$ , and  ${}^{197}\text{Au}$  compared with the Cowley *et al.* data [136]. We see again a good agreement between our calculations and the measurements; the main contribution in the production of these  ${}^4\text{He}$  by CEM03.01 is again from preequilibrium emission.

One more example of double-differential spectra of complex particles from proton-induced reactions, at higher energies, namely CEM03.01 calculated  ${}^3\text{He}$  and  ${}^4\text{He}$  spectra at 20, 90, and 160 degrees from 210, 300, and 480 MeV proton-silver interactions compared with the Green and Korteling data [137] is presented in Fig. 22. Again a fairly good agreement between the calculations and the data can be seen, and again the main contribution in the production of these particles by CEM03.01 is from preequilibrium emission.

Finally, Fig. 23 show an example of double-differential spectra of complex particles from neutron-induced reactions, at even higher energies, namely CEM03.01 calculated double-differential spectra of  $p$ ,  $d$ , and  $t$  at 54, 68, 90, 121, and 164 degrees from interactions of 542 MeV neutrons with copper and bismuth compared with the measurements by Franz *et al.* [138]. We see again a good agreement between the calculations and the data and again the main contribution in the production of  $d$  and  $t$  from these reactions by CEM03.01 is from preequilibrium emission. Let

us note that we analyzed these data in 1992 [26], with the version of CEM we had at that time, CEM92m [78]. If we compare the agreement with the experimental data [138] of the results we got in 1992 [26] with our current CEM03.01 results, there is a tremendous improvement in the description of these data.

To conclude this Section, Fig. 24 shows several examples of gas production cross-section calculations by CEM03.01 from  $n+^{56}\text{Fe}$ ,  $p+^{208}\text{Pb}$ , and  $n+^{238}\text{U}$  reactions compared with experimental data [139]–[141] and results by TALYS from [140], McGNASH [142], and IPPE-99 [143]. The overall agreement of the results by CEM03.01 with these data is similar to that achieved by TALYS, McGNASH, and IPPE-99.

For the production of  $^4\text{He}$  from  $n+^{238}\text{U}$  (bottom plot in Fig. 24), we show not only the total gas production cross section, but also contributions to the total yield from preequilibrium emission, from events with evaporation that are not followed by fission, from evaporation before fission and from evaporation of fission fragments in events with fission, the total evaporation component (both with and without fission), and from coalescence, as calculated by CEM03.01. We see that the preequilibrium contribution to the total yield of  $^4\text{He}$  from this reaction is about one order of magnitude higher than contributions from other reaction mechanisms considered by our model.

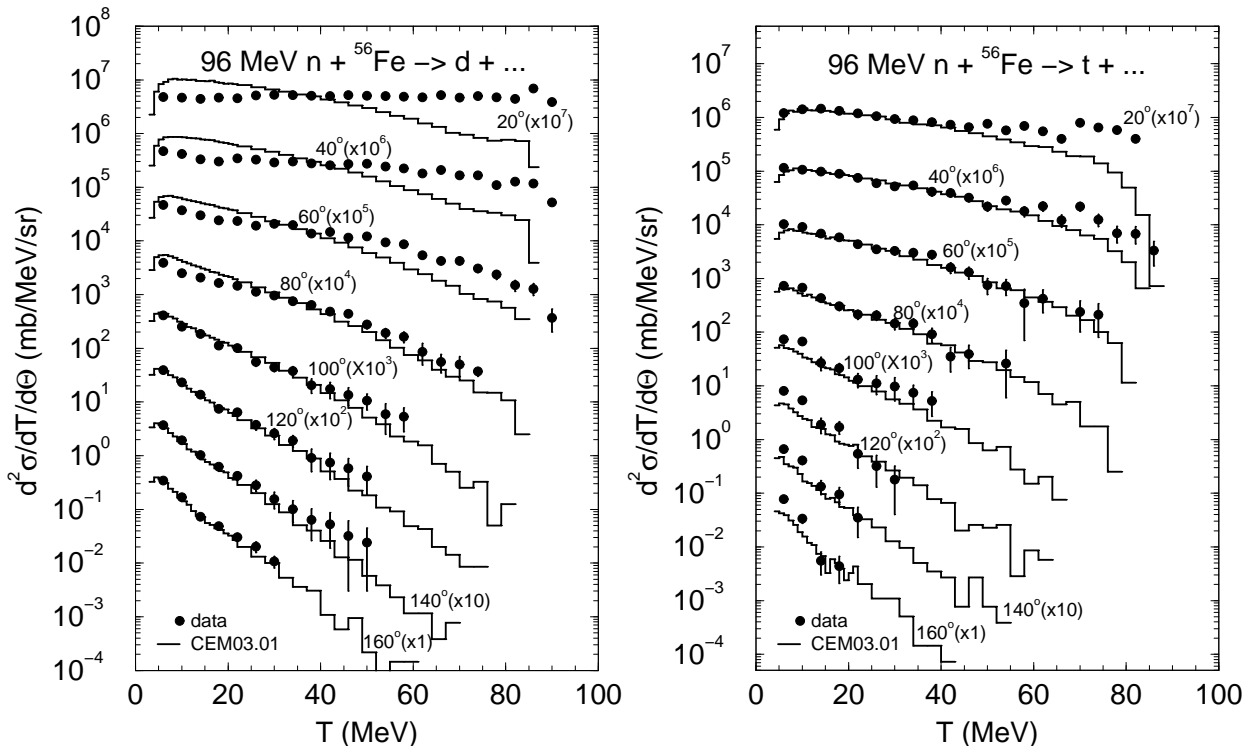


Figure 19: Double-differential spectra of  $d$  and  $t$  at 20, 40, 60, 80, 100, 120, 140, and 160 degrees from 96 MeV  $n + ^{56}\text{Fe}$  calculated by CEM03.01 compared with experimental data by Blideanu *et al.* [112].

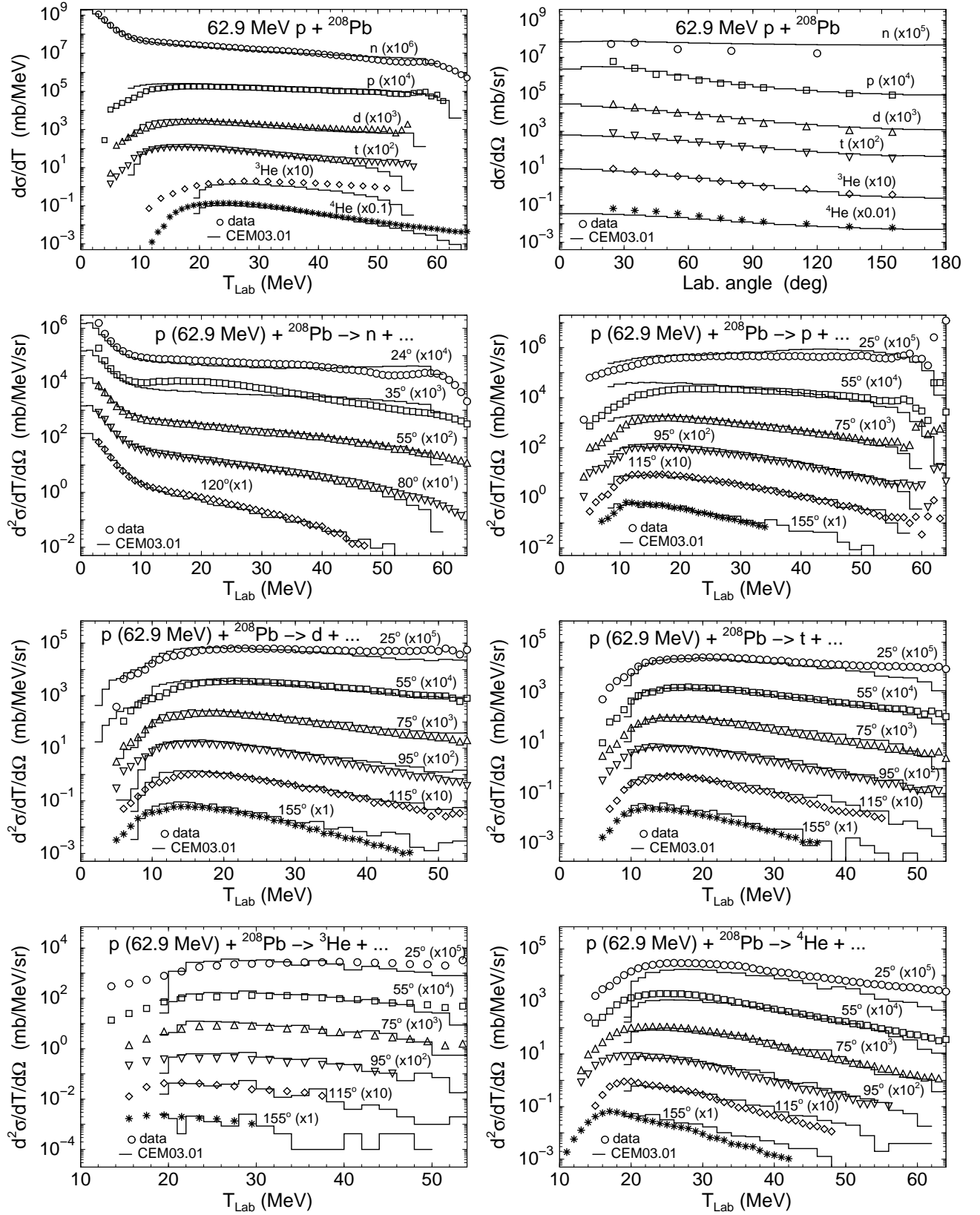


Figure 20: Experimental angle-integrated energy spectra (upper left plot), energy-integrated angular distributions (upper right plot), and double-differential spectra of nucleons and complex particles from 62.9 MeV  $p + \text{Pb}$  [135] compared with CEM03.01 results.

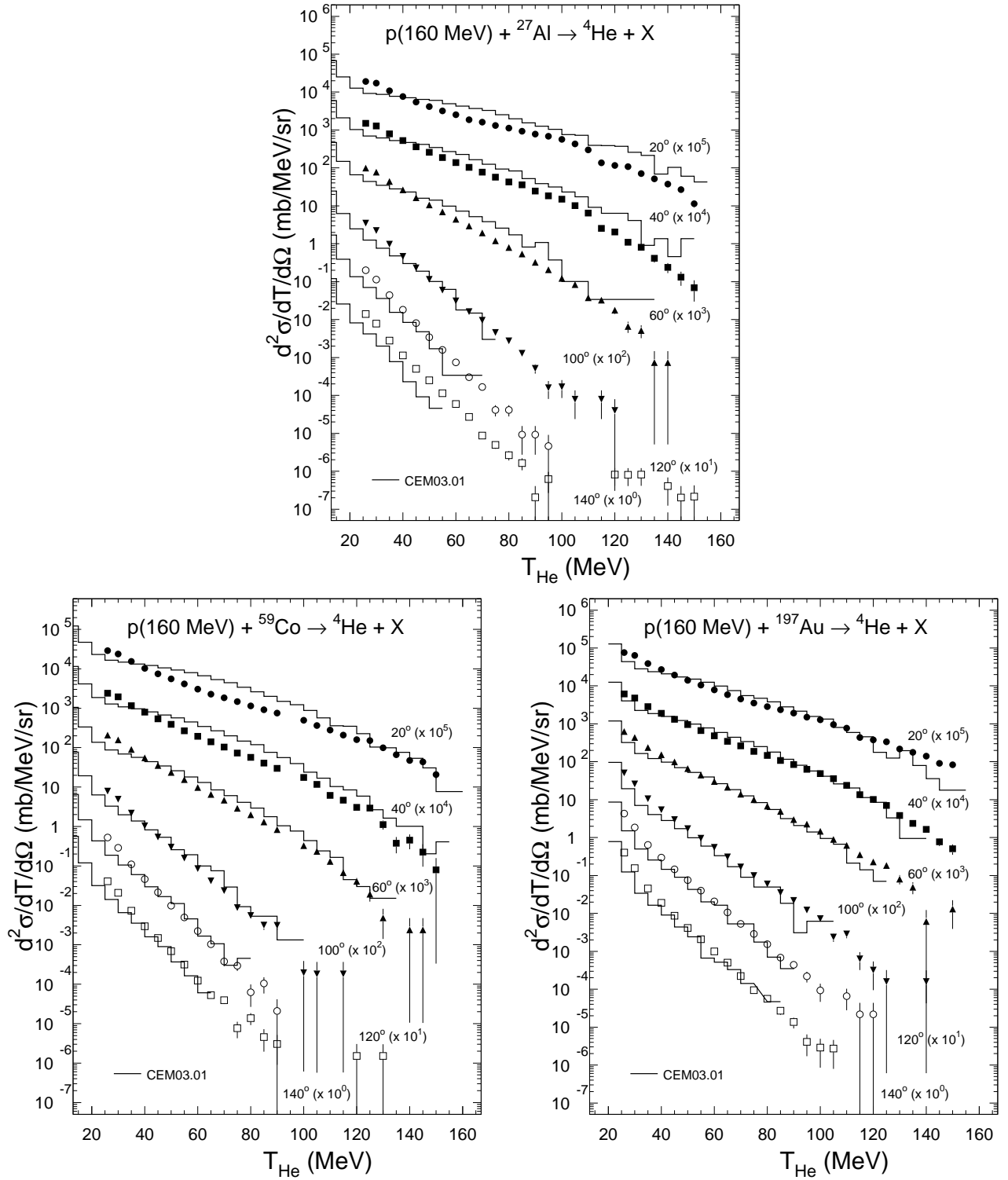


Figure 21: CEM03.01 calculated double-differential spectra of  ${}^4\text{He}$  at 20, 40, 60, 100, 120, and 140 degrees from 160 MeV  $p + {}^{27}\text{Al}$ ,  ${}^{59}\text{Co}$ , and  ${}^{197}\text{Au}$  compared with the Cowley *et al.* data [136].

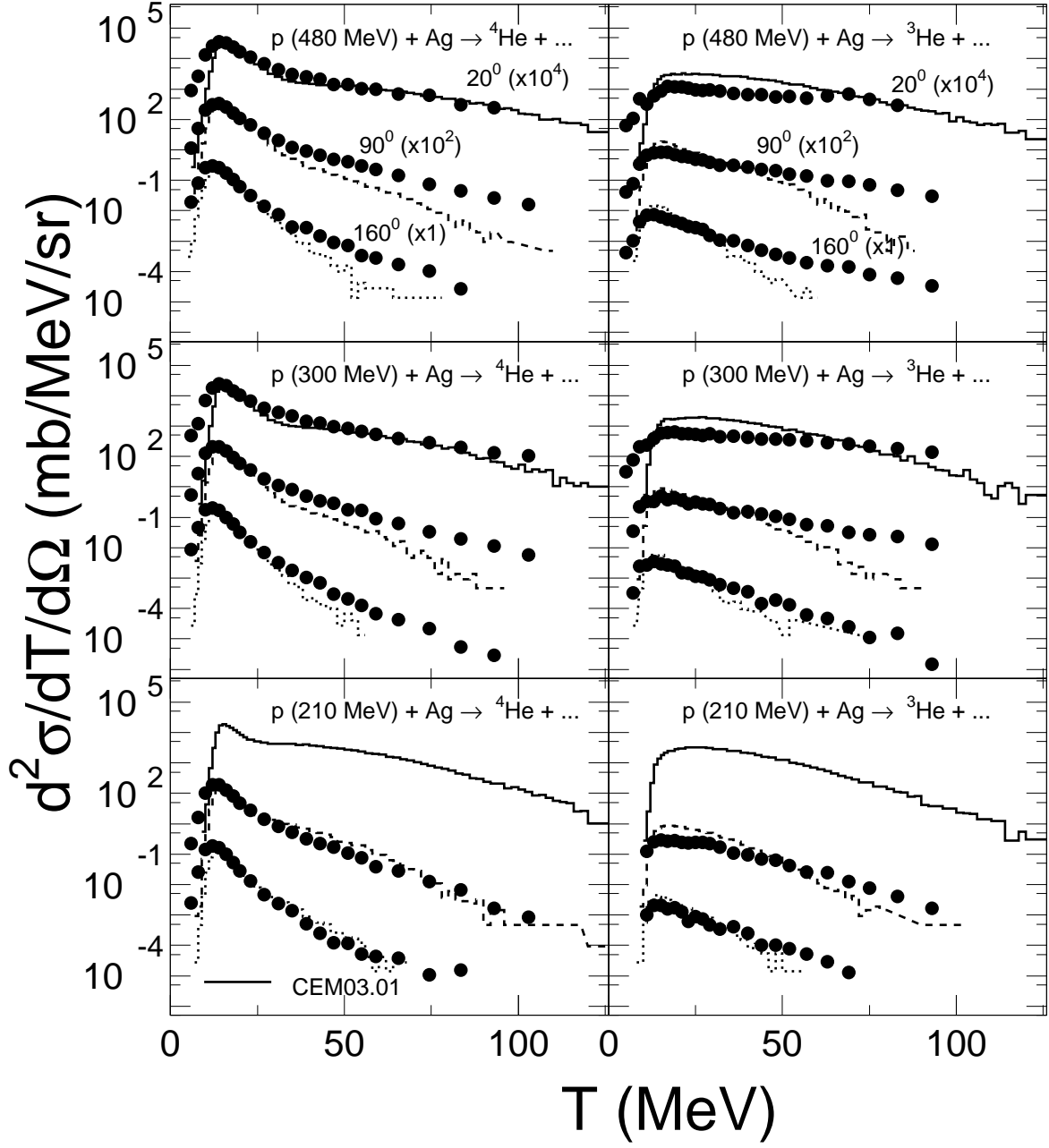


Figure 22: CEM03.01 calculated double-differential spectra of  ${}^3\text{He}$  and  ${}^4\text{He}$  at 20, 90, and 160 degrees from 210, 300, and 480 MeV proton-silver interactions compared with the Green and Korteling data [137].

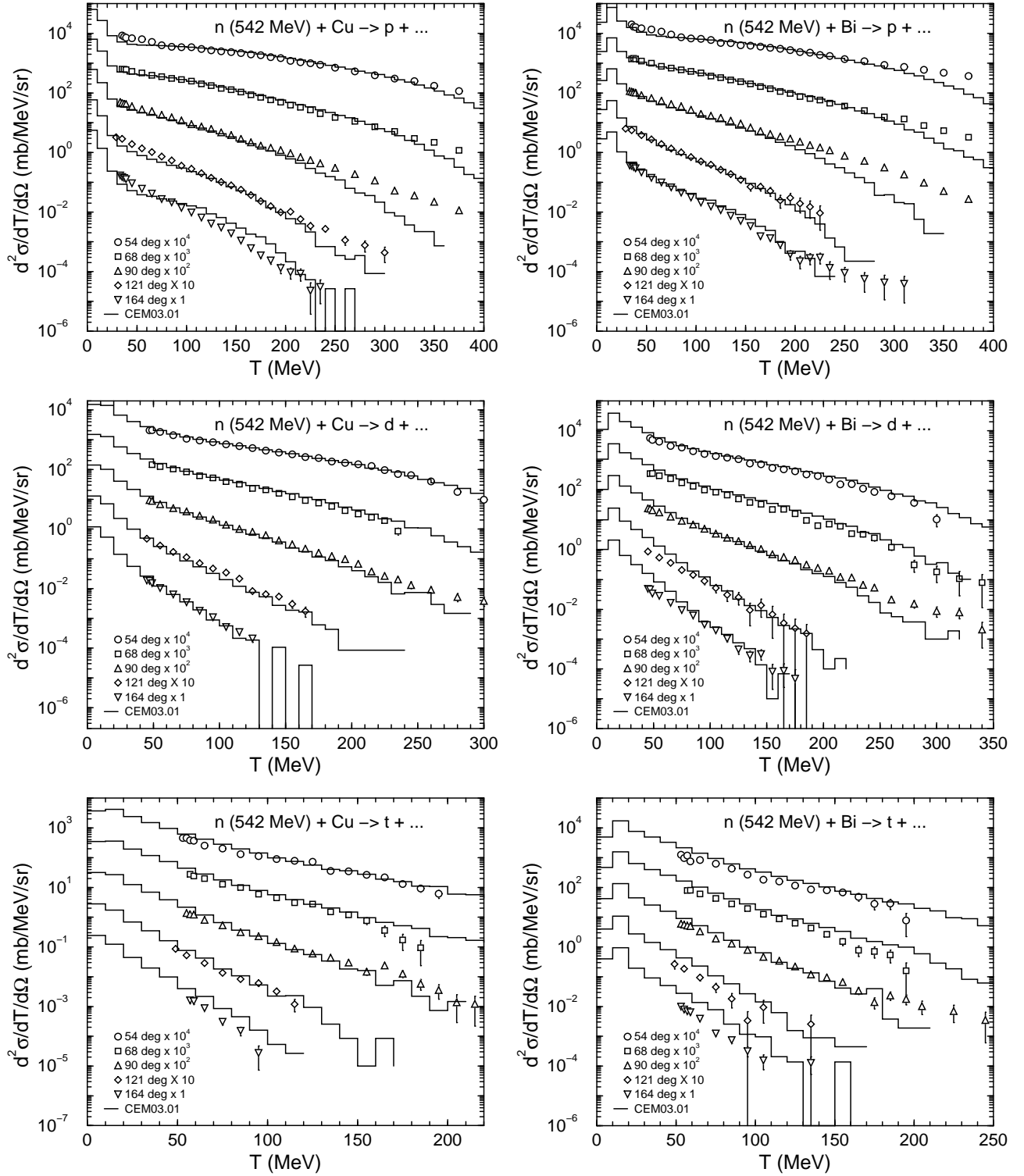


Figure 23: CEM03.01 calculated double-differential spectra of  $p$ ,  $d$ , and  $t$  at 54, 68, 90, 121, and 164 degrees from interactions of 542 MeV neutrons with copper and bismuth compared with the measurements by Franz *et al.* [138].

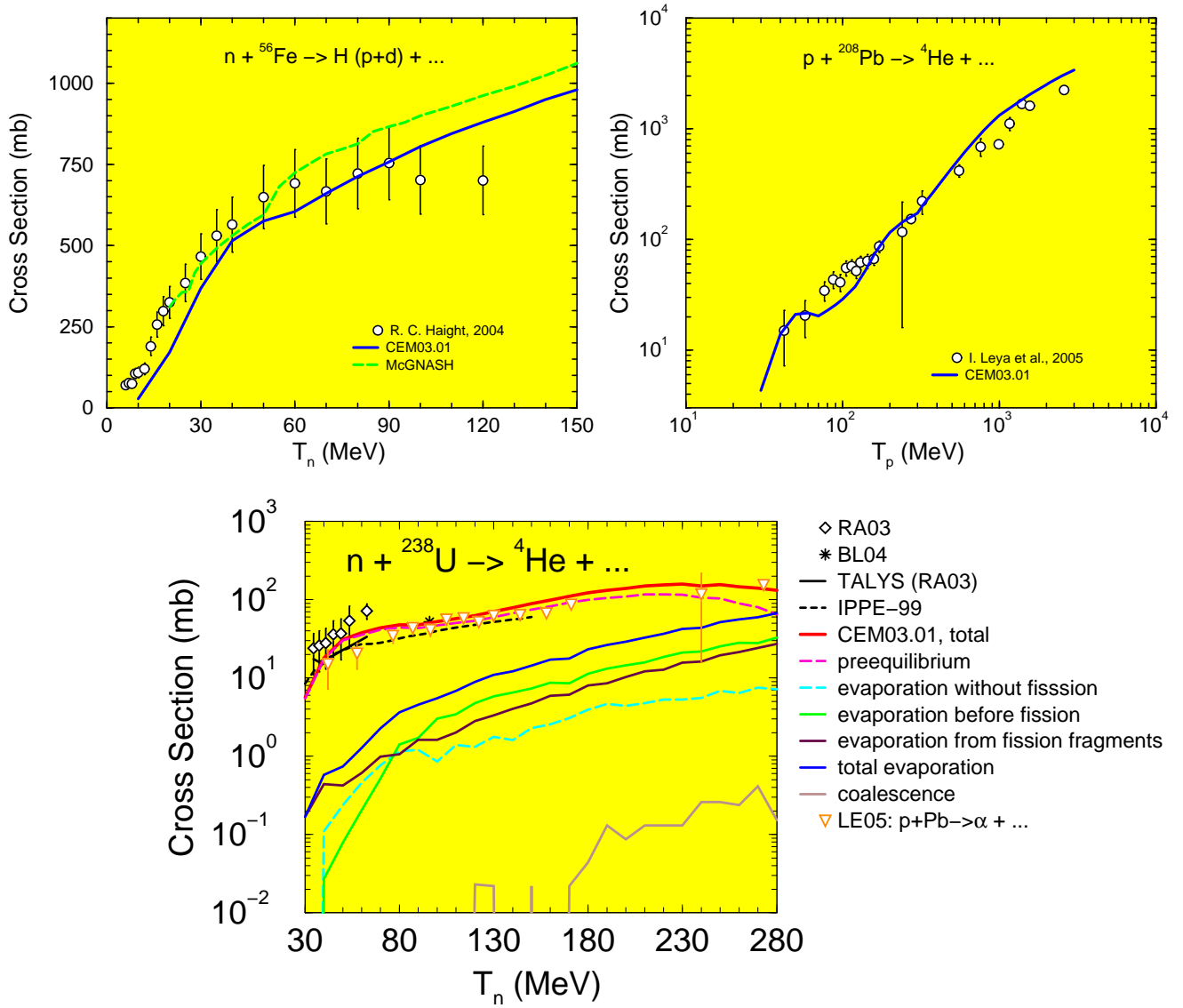


Figure 24: Examples of H ( $p + d$ ) and  ${}^4\text{He}$  total production cross sections calculated by CEM03.01 compared with experimental data [139]–[141] and results by TALYS from [140], McGNASH [142], and IPPE-99 [143]. For the production of  ${}^4\text{He}$  from  $n + {}^{238}\text{U}$  (bottom plot), we show the total cross section as predicted by CEM03.01 with a thick red solid line, as well as contributions to it from preequilibrium emission, from events with evaporation that are not followed by fission, from evaporation before fission, evaporation from fission fragments, total evaporation (both with and without fission), and from coalescence, shown with different color lines as indicated in the legend.

## 6. Evaporation

CEM03.01 and LAQGSM03.01 and their later versions use an extension of the Generalized Evaporation Model (GEM) code GEM2 by Furihata [144]–[146] after the preequilibrium stage of reactions to describe evaporation of nucleons, complex particles, and light fragments heavier than  $^4\text{He}$  (up to  $^{28}\text{Mg}$ ) from excited compound nuclei and to describe their fission, if the compound nuclei are heavy enough to fission ( $Z \geq 65$ ). The GEM is an extension by Furihata of the Dostrovsky evaporation model [147] as implemented in LAHET [131] to include up to 66 types of particles and fragments that can be evaporated from an excited compound nucleus plus a modification of the version of Atchison’s fission model [148]–[150] used in LAHET. Many of the parameters were adjusted by Furihata for a better description of fission reactions when using it in conjunction with the extended evaporation model.

A very detailed description of the GEM, together with a large amount of results obtained for many reactions using the GEM coupled either with the Bertini or ISABEL INC models in LAHET may be found in [144, 145]. Therefore, we present here only the main features of the GEM, following mainly [145] and using as well useful information obtained in private communications with Dr. Furihata.

Furihata did not change in the GEM the general algorithms used in LAHET to simulate evaporation and fission. The decay widths of evaporated particles and fragments are estimated using the classical Weisskopf-Ewing statistical model [125]. In this approach, the decay probability  $P_j$  for the emission of a particle  $j$  from a parent compound nucleus  $i$  with the total kinetic energy in the center-of-mass system between  $\epsilon$  and  $\epsilon + d\epsilon$  is

$$P_j(\epsilon)d\epsilon = g_j\sigma_{inv}(\epsilon)\frac{\rho_d(E-Q-\epsilon)}{\rho_i(E)}\epsilon d\epsilon, \quad (39)$$

where  $E$  [MeV] is the excitation energy of the parent nucleus  $i$  with mass  $A_i$  and charge  $Z_i$ , and  $d$  denotes a daughter nucleus with mass  $A_d$  and charge  $Z_d$  produced after the emission of ejectile  $j$  with mass  $A_j$  and charge  $Z_j$  in its ground state.  $\sigma_{inv}$  is the cross section for the inverse reaction,  $\rho_i$  and  $\rho_d$  are the level densities  $[\text{MeV}]^{-1}$  of the parent and the daughter nucleus, respectively.  $g_j = (2S_j + 1)m_j/\pi^2\hbar^2$ , where  $S_j$  is the spin and  $m_j$  is the reduced mass of the emitted particle  $j$ . The  $Q$ -value is calculated using the excess mass  $M(A, Z)$  as  $Q = M(A_j, Z_j) + M(A_d, Z_d) - M(A_i, Z_i)$ . In GEM2, four mass tables are used to calculate  $Q$  values, according to the following priorities, where a lower priority table is only used outside the range of validity of the higher priority one: (1) the Audi-Wapstra mass table [151], (2) theoretical masses calculated by Möller *et al.* [129], (3) theoretical masses calculated by Comay *et al.* [152], (4) the mass excess calculated using the old Cameron formula [153]. As does LAHET, GEM2 uses Dostrovsky’s formula [147] to calculate the inverse cross section  $\sigma_{inv}$  for all emitted particles and fragments

$$\sigma_{inv}(\epsilon) = \sigma_g \alpha \left(1 + \frac{\beta}{\epsilon}\right), \quad (40)$$

which is often written as

$$\sigma_{inv}(\epsilon) = \begin{cases} \sigma_g c_n (1 + b/\epsilon) & \text{for neutrons} \\ \sigma_g c_j (1 - V/\epsilon) & \text{for charged particles,} \end{cases}$$

where  $\sigma_g = \pi R_b^2$  [fm<sup>2</sup>] is the geometrical cross section, and

$$V = k_j Z_j Z_d e^2 / R_c \quad (41)$$

is the Coulomb barrier in MeV.

One important new ingredient in GEM2 in comparison with LAHET, which considers evaporation of only 6 particles (n, p, d, t,  $^3\text{He}$ , and  $^4\text{He}$ ), is that Furihata includes the possibility of evaporation of up to 66 types of particles and fragments and incorporates into GEM2 several alternative sets of parameters  $b$ ,  $c_j$ ,  $k_j$ ,  $R_b$ , and  $R_c$  for each particle type.

The 66 ejectiles considered by GEM2 for evaporation are selected to satisfy the following criteria: (1) isotopes with  $Z_j \leq 12$ ; (2) naturally existing isotopes or isotopes near the stability line; (3) isotopes with half-lives longer than 1 ms. All the 66 ejectiles considered by GEM2 are shown in Table 1.

Table 1. The evaporated particles considered by GEM2

$Z_j$	Ejectiles							
0	n							
1	p	d	t					
2	$^3\text{He}$	$^4\text{He}$	$^6\text{He}$	$^8\text{He}$				
3	$^6\text{Li}$	$^7\text{Li}$	$^8\text{Li}$	$^9\text{Li}$				
4	$^7\text{Be}$	$^9\text{Be}$	$^{10}\text{Be}$	$^{11}\text{Be}$	$^{12}\text{Be}$			
5	$^8\text{B}$	$^{10}\text{B}$	$^{11}\text{B}$	$^{12}\text{B}$	$^{13}\text{B}$			
6	$^{10}\text{C}$	$^{11}\text{C}$	$^{12}\text{C}$	$^{13}\text{C}$	$^{14}\text{C}$	$^{15}\text{C}$	$^{16}\text{C}$	
7	$^{12}\text{N}$	$^{13}\text{N}$	$^{14}\text{N}$	$^{15}\text{N}$	$^{16}\text{N}$	$^{17}\text{N}$		
8	$^{14}\text{O}$	$^{15}\text{O}$	$^{16}\text{O}$	$^{17}\text{O}$	$^{18}\text{O}$	$^{19}\text{O}$	$^{20}\text{O}$	
9	$^{17}\text{F}$	$^{18}\text{F}$	$^{19}\text{F}$	$^{20}\text{F}$	$^{21}\text{F}$			
10	$^{18}\text{Ne}$	$^{19}\text{Ne}$	$^{20}\text{Ne}$	$^{21}\text{Ne}$	$^{22}\text{Ne}$	$^{23}\text{Ne}$	$^{24}\text{Ne}$	
11	$^{21}\text{Na}$	$^{22}\text{Na}$	$^{23}\text{Na}$	$^{24}\text{Na}$	$^{25}\text{Na}$			
12	$^{22}\text{Mg}$	$^{23}\text{Mg}$	$^{24}\text{Mg}$	$^{25}\text{Mg}$	$^{26}\text{Mg}$	$^{27}\text{Mg}$	$^{28}\text{Mg}$	

GEM2 includes several options for the parameter set in expressions (40,41):

1) The “simple” parameter set is given as  $c_n = c_j = k_j = 1$ ,  $b = 0$ , and  $R_b = R_c = r_0(A_j^{1/3} + A_d^{1/3})$  [fm]; users need to input  $r_0$ .

2) The “precise” parameter set is used in GEM2 as the default, and we use this set in our present work.

A) For all light ejectiles up to  $\alpha$  ( $A_j \leq 4$ ), the parameters determined by Dostrovsky *et al.* [147] are used in GEM2, namely:  $c_n = 0.76 + c_a A_d^{-1/3}$ ,  $b = (b_a A_d^{-2/3} - 0.050)/(0.76 + c_a A_d^{-1/3})$  (and  $b = 0$  for  $A_d \geq 192$ ), where  $c_a = 1.93$  and  $b_a = 1.66$ ,  $c_p = 1 + c$ ,  $c_d = 1 + c/2$ ,  $c_t = 1 + c/3$ ,  $c_{^3\text{He}} = c_\alpha = 0$ ,  $k_p = k$ ,  $k_d = k + 0.06$ ,  $k_t = k + 0.12$ ,  $k_{^3\text{He}} = k_\alpha - 0.06$ , where  $c$ ,  $k$ , and  $k_\alpha$  are listed in Table 2 for a set of  $Z_d$ . Between the  $Z_d$  values listed in Table 2,  $c$ ,  $k$ , and  $k_\alpha$  are interpolated linearly. The nuclear distances are given by  $R_b = 1.5A^{1/3}$  for neutrons and protons, and  $1.5(A_d^{1/3} + A_j^{1/3})$  for d, t,  $^3\text{He}$ , and  $\alpha$ .

Table 2.  $k$ ,  $k_\alpha$ , and  $c$  parameters used in GEM2

$Z_d$	$k$	$k_\alpha$	$c$
$\leq 20$	0.51	0.81	0.0
30	0.60	0.85	-0.06
40	0.66	0.89	-0.10
$\geq 50$	0.68	0.93	-0.10

The nuclear distance for the Coulomb barrier is expressed as  $R_c = R_d + R_j$ , where  $R_d = r_0^c A^{1/3}$ ,  $r_0^c = 1.7$ , and  $R_j = 0$  for neutrons and protons, and  $R_j = 1.2$  for d, t,  $^3\text{He}$ , and  $^4\text{He}$ . We note that several of these parameters are similar to the original values published by Dostrovsky *et al.* [147] but not exactly the same. Dostrovsky *et al.* [147] had  $c_a = 2.2$ ,  $b_a = 2.12$ , and  $r_0^c = 1.5$ . Also, for the  $k$ ,  $k_\alpha$ , and  $c$  parameters shown in Table 2, they had slightly different values, shown in Table 3.

Table 3.  $k_p$ ,  $c_p$ ,  $k_\alpha$ , and  $c_\alpha$  parameters from Ref. [147]

$Z_d$	$k_p$	$c_p$	$k_\alpha$	$c_\alpha$
10	0.42	0.50	0.68	0.10
20	0.58	0.28	0.82	0.10
30	0.68	0.20	0.91	0.10
50	0.77	0.15	0.97	0.08
$\geq 70$	0.80	0.10	0.98	0.06

B) For fragments heavier than  $\alpha$  ( $A_j \geq 4$ ), the “precise” parameters of GEM2 use values by Matsuse *et al.* [154], namely:  $c_j = k = 1$ ,  $R_b = R_0(A_j) + R_0(A_d) + 2.85$  [fm],  $R_c = R_0(A_j) + R_0(A_d) + 3.75$  [fm], where  $R_0(A) = 1.12A^{1/3} - 0.86A^{-1/3}$ .

3) The code GEM2 contains two other options for the parameters of the inverse cross sections.

A) A set of parameters due to Furihata for light ejectiles in combination with Matsuse’s parameters for fragments heavier than  $\alpha$ . Furihata and Nakamura determined  $k_j$  for p, d, t,  $^3\text{He}$ , and  $\alpha$  as follows [146]:

$$k_j = c_1 \log(Z_d) + c_2 \log(A_d) + c_3.$$

The coefficients  $c_1$ ,  $c_2$ , and  $c_3$  for each ejectile are shown in Table 4.

Table 4.  $c_1$ ,  $c_2$ , and  $c_3$  for p, d, t,  $^3\text{He}$ , and  $\alpha$  from [146]

Ejectile	$c_1$	$c_2$	$c_3$
p	0.0615	0.0167	0.3227
d	0.0556	0.0135	0.4067
t	0.0530	0.0134	0.4374
$^3\text{He}$	0.0484	0.0122	0.4938
$\alpha$	0.0468	0.0122	0.5120

When these parameters are chosen in GEM2, the following nuclear radius  $R$  is used in the calculation of  $V$  and  $\sigma_g$ :

$$R = \begin{cases} 0 & \text{for } A = 1, \\ 1.2 & \text{for } 2 \leq A \leq 4, \\ 2.02 & \text{for } 5 \leq A \leq 6, \\ 2.42 & \text{for } A = 7, \\ 2.83 & \text{for } A = 8, \\ 3.25 & \text{for } A = 9, \\ 1.414A_d^{1/3} + 1 & \text{for } A \geq 10. \end{cases}$$

B) The second new option in GEM2 is to use Furihata's parameters for light ejectiles up to  $\alpha$  and the Botvina *et al.* [155] parameterization for inverse cross sections for heavier ejectiles. Botvina *et al.* [155] found that  $\sigma_{inv}$  can be expressed as

$$\sigma_{inv} = \sigma_g \begin{cases} (1 - V/\epsilon) & \text{for } \epsilon \geq V + 1 \text{ [MeV]}, \\ \exp[\alpha(\epsilon - V - 1)]/(V + 1) & \text{for } \epsilon < V + 1 \text{ [MeV]}, \end{cases} \quad (42)$$

where

$$\begin{aligned} \alpha &= 0.869 + 9.91/Z_j, \\ V &= \frac{Z_j Z_d}{r_0^b (A_j^{1/3} + A_d^{1/3})}, \\ r_0^b &= 2.173 \frac{1 + 6.103 \times 10^{-3} Z_j Z_d}{1 + 9.443 \times 10^{-3} Z_j Z_d} \text{ [fm]}. \end{aligned}$$

The expression of  $\sigma_{inv}$  for  $\epsilon < V + 1$  shows the fusion reaction in the sub-barrier region. When using Eq. (42) instead of Eq. (40), the total decay width for a fragment emission can not be calculated analytically. Therefore, the total decay width must be calculated numerically and takes much CPU time.

The total decay width  $\Gamma_j$  is calculated by integrating Eq. (39) with respect to the total kinetic energy  $\epsilon$  from the Coulomb barrier  $V$  up to the maximum possible value,  $(E - Q)$ . The good feature of Dostrovsky's approximation for the inverse cross sections, Eq. (40), is its simple energy dependence that allows the analytic integration of Eq. (39). By using Eq. (40) for  $\sigma_{inv}$ , the total decay width for the particle emission is

$$\Gamma_j = \frac{g_j \sigma_g \alpha}{\rho_i(E)} \int_V^{E-Q} \epsilon \left(1 + \frac{\beta}{\epsilon}\right) \rho_d(E - Q - \epsilon) d\epsilon. \quad (43)$$

The level density  $\rho(E)$  is calculated in GEM2 according to the Fermi-gas model using the expression [156]

$$\rho(E) = \frac{\pi}{12} \frac{\exp(2\sqrt{a(E - \delta)})}{a^{1/4}(E - \delta)^{5/4}}, \quad (44)$$

where  $a$  is the level-density parameter and  $\delta$  is the pairing energy in MeV. As does LAHET, GEM2 uses the  $\delta$  values evaluated by Cook *et al.* [157]. For those values not evaluated by Cook *et al.*,  $\delta$ 's from Gilbert and Cameron [156] are used instead. The simplest option for the level-density parameter in GEM2 is  $a = A_d/8$  [MeV<sup>-1</sup>], but the default is the Gilbert-Cameron-Cook-Ignatyuk (GCCCI) parameterization from LAHET [131]:

$$a = \tilde{a} \frac{1 - e^{-u}}{u} + a_I \left(1 - \frac{1 - e^{-u}}{u}\right), \quad (45)$$

where  $u = 0.05(E - \delta)$ , and

$$\begin{aligned} a_I &= (0.1375 - 8.36 \times 10^{-5} A_d) \times A_d, \\ \tilde{a} &= \begin{cases} A_d/8 & \text{for } Z_d < 9 \text{ or } N_d < 9, \\ A_d(a' + 0.00917S) & \text{for others.} \end{cases} \end{aligned}$$

For deformed nuclei with  $54 \leq Z_d \leq 78$ ,  $86 \leq Z_d \leq 98$ ,  $86 \leq N_d \leq 122$ , or  $130 \leq N_d \leq 150$ ,  $a' = 0.12$  while  $a' = 0.142$  for other nuclei. The shell corrections  $S$  is expressed as a sum of

separate contributions from neutrons and protons, *i.e.*  $S = S(Z_d) + S(N_d)$  from [156, 157] and are tabulated in [144].

The level density is calculated using Eq. (44) only for high excitation energies,  $E \geq E_x$ , where  $E_x = U_x + \delta$  and  $U_x = 2.5 + 150/A_d$  (all energies are in MeV). At lower excitation energies, the following [156] is used for the level density:

$$\rho(E) = \frac{\pi}{12} \frac{1}{T} \exp((E - E_0)/T), \quad (46)$$

where  $T$  is the nuclear temperature defined as  $1/T = \sqrt{a/U_x} - 1.5/U_x$ . To provide a smooth connection of Eqs. (44) and (46) at  $E = E_x$ ,  $E_0$  is defined as  $E_0 = E_x - T(\log T - 0.25 \log a - 1.25 \log U_x + 2\sqrt{aU_x})$ .

For  $E - Q - V < E_x$ , substituting Eq. (46) into Eq. (44) we can calculate the integral analytically, if we neglect the dependence of the level-density parameter  $a$  on  $E$ :

$$\Gamma_j = \frac{\pi g_j \sigma_g \alpha}{12 \rho_i(E)} \{I_1(t, t) + (\beta + V)I_0(t)\}, \quad (47)$$

where  $I_0(t)$  and  $I_1(t, t_x)$  are expressed as

$$\begin{aligned} I_0(t) &= e^{-E_0/T} (e^t - 1), \\ I_1(t, t_x) &= e^{-E_0/T} T \{(t - t_x + 1)e^{t_x} - t - 1\}, \end{aligned}$$

where  $t = (E - Q - V)/T$  and  $t_x = E_x/T$ . For  $E - Q - V \geq E_x$ , the integral of Eq. (43) cannot be solved analytically because of the denominator in Eq. (44). However, it is approximated as

$$\Gamma_j = \frac{\pi g_j \sigma_g \alpha}{12 \rho_i(E)} [I_1(t, t_x) + I_3(s, s_x)e^s + (\beta + V)\{I_0(t_x) - I_2(s, s_x)e^s\}], \quad (48)$$

where  $I_2(s, s_x)$  and  $I_3(s, s_x)$  are given by

$$I_2(s, s_x) = 2\sqrt{2}\{s^{-3/2} + 1.5s^{-5/2} + 3.75s^{-7/2} - (s_x^{-3/2} + 1.5s_x^{-5/2} + 3.75s_x^{-7/2})e^{s_x-s}\},$$

$$\begin{aligned} I_3(s, s_x) &= (\sqrt{2}a)^{-1}[2s^{-1/2} + 4s^{-3/2} + 13.5s^{-5/2} + 60.0s^{-7/2} + 325.125s^{-9/2} \\ &\quad - \{(s^2 - s_x^2)s_x^{-3/2} + (1.5s^2 + 0.5s_x^2)s_x^{-5/2} + (3.75s^2 + 0.25s_x^2)s_x^{-7/2} + (12.875s^2 \\ &\quad + 0.625s_x^2)s_x^{-9/2} + (59.0625s^2 + 0.9375s_x^2)s_x^{-11/2} + (324.8s_x^2 + 3.28s_x^2)s_x^{-13/2}\}e^{s_x-s}], \end{aligned}$$

with  $s = 2\sqrt{a(E - Q - V - \delta)}$  and  $s_x = 2\sqrt{a(E_x - \delta)}$ .

The particle type  $j$  to be evaporated is selected in GEM2 by the Monte-Carlo method according to the probability distribution calculated as  $P_j = \Gamma_j / \sum_j \Gamma_j$ , where  $\Gamma_j$  is given by Eqs. (47) or (48). The total kinetic energy  $\epsilon$  of the emitted particle  $j$  and the recoil energy of the daughter nucleus is chosen according to the probability distribution given by Eq. (39). The angular distribution of ejectiles is simulated to be isotropic in the center-of-mass system.

According to Friedman and Lynch [158], it is important to include excited states in the particle emitted via the evaporation process along with evaporation of particles in their ground states, because it greatly enhances the yield of heavy particles. Taking this into consideration, GEM2 includes evaporation of complex particles and light fragments both in the ground states and excited states. An excited state of a fragment is included in calculations if its half-life  $T_{1/2}(s)$  satisfies the following condition:

$$\frac{T_{1/2}}{\ln 2} > \frac{\hbar}{\Gamma_j^*}, \quad (49)$$

where  $\Gamma_j^*$  is the decay width of the excited particle (resonance). GEM2 calculates  $\Gamma_j^*$  in the same manner as for a ground-state particle emission. The  $Q$ -value for the resonance emission is expressed as  $Q^* = Q + E_j^*$ , where  $E_j^*$  is the excitation energy of the resonance. The spin state of the resonance  $S_j^*$  is used in the calculation of  $g_j$ , instead of the spin of the ground state  $S_j$ . GEM2 uses the ground state masses  $m_j$  for excited states because the difference between the masses is negligible.

Instead of treating a resonance as an independent particle, GEM2 simply enhances the decay width  $\Gamma_j$  of the ground state particle emission as follows:

$$\Gamma_j = \Gamma_j^0 + \sum_n \Gamma_j^n, \quad (50)$$

where  $\Gamma_j^0$  is the decay width of the ground state particle emission, and  $\Gamma_j^n$  is that of the  $n$ th excited state of the particle  $j$  emission which satisfies Eq. (49).

The total-kinetic-energy distribution of the excited particles is assumed to be the same as that of the ground-state particle.  $S_j^*$ ,  $E_j^*$ , and  $T_{1/2}$  used in GEM2 are extracted from the Evaluated Nuclear Structure Data File (ENSDF) database maintained by the National Nuclear Data Center at Brookhaven National Laboratory [159].

Note that when including evaporation of up to 66 particles in GEM2, its running time increases significantly compared to the case when evaporating only 6 particles, up to  ${}^4\text{He}$ . The major particles emitted from an excited nucleus are n, p, d, t,  ${}^3\text{He}$ , and  ${}^4\text{He}$ . For most cases, the total emission probability of particles heavier than  $\alpha$  is negligible compared to those for the emission of light ejectiles. Our detailed study of different reactions (see, *e.g.*, [160] and references therein) shows that if we study only nucleon and complex-particle spectra or only spallation and fission products and are not interested in light fragments, we can consider evaporation of only 6 types of particles in GEM2 and save much time, getting results very close to the ones calculated with the more time consuming “66” option. In CEM03.01 and LAQGSM03.01, we have introduced an input parameter called **nevtype** that defines the number of types of particles to be considered at the evaporation stage. The index of each type of particle that can be evaporated corresponds to the particle arrangement in Table 1, with values, *e.g.*, of 1, 2, 3, 4, 5, and 6 for n, p, d, t,  ${}^3\text{He}$ , and  ${}^4\text{He}$ , with succeeding values up to 66 for  ${}^{28}\text{Mg}$ . All 66 particles that can possibly evaporate are listed in CEM03.01 and LAQGSM03.01 together with their mass number, charge, and spin values in the **block data bdejc**. For all ten examples of inputs and outputs of CEM03.01 included in Appendices 1 and 2 of the CEM03.01 User Manual [23], whose results are plotted in the figures in Appendix 3 of [23], we have performed calculations taking into account only 6 types of evaporated particles (**nevtype** = 6) as well as with the “66” option (**nevtype** = 66) and we provide the corresponding computing time for these examples in the captions to the appropriate figures shown in Appendix 3 of Ref. [23]. The “6” option can be up to several times faster than the “66” option, providing meanwhile almost the same results. Therefore we recommend that users of CEM03.01 and LAQGSM03.01 use 66 for the value of the input parameter **nevtype** only when they are interested in all fragments heavier than  ${}^4\text{He}$ ; otherwise, we recommend the default value of 6 for **nevtype**, saving computing time. Alternatively, users may choose intermediate values of **nevtype**, for example 9 if one wants to calculate the production of  ${}^6\text{Li}$ , or 14 for modeling the production of  ${}^9\text{Be}$  and lighter fragments and nucleons only, while still saving computing time compared to running the code with the maximum value of 66.

Examples of calculation by CEM03.01 the reactions 800 MeV  $p + {}^{197}\text{Au}$  and 1 GeV  $p + {}^{56}\text{Fe}$  using the “6” and “66” options are shown in Figs. 25 and 26.

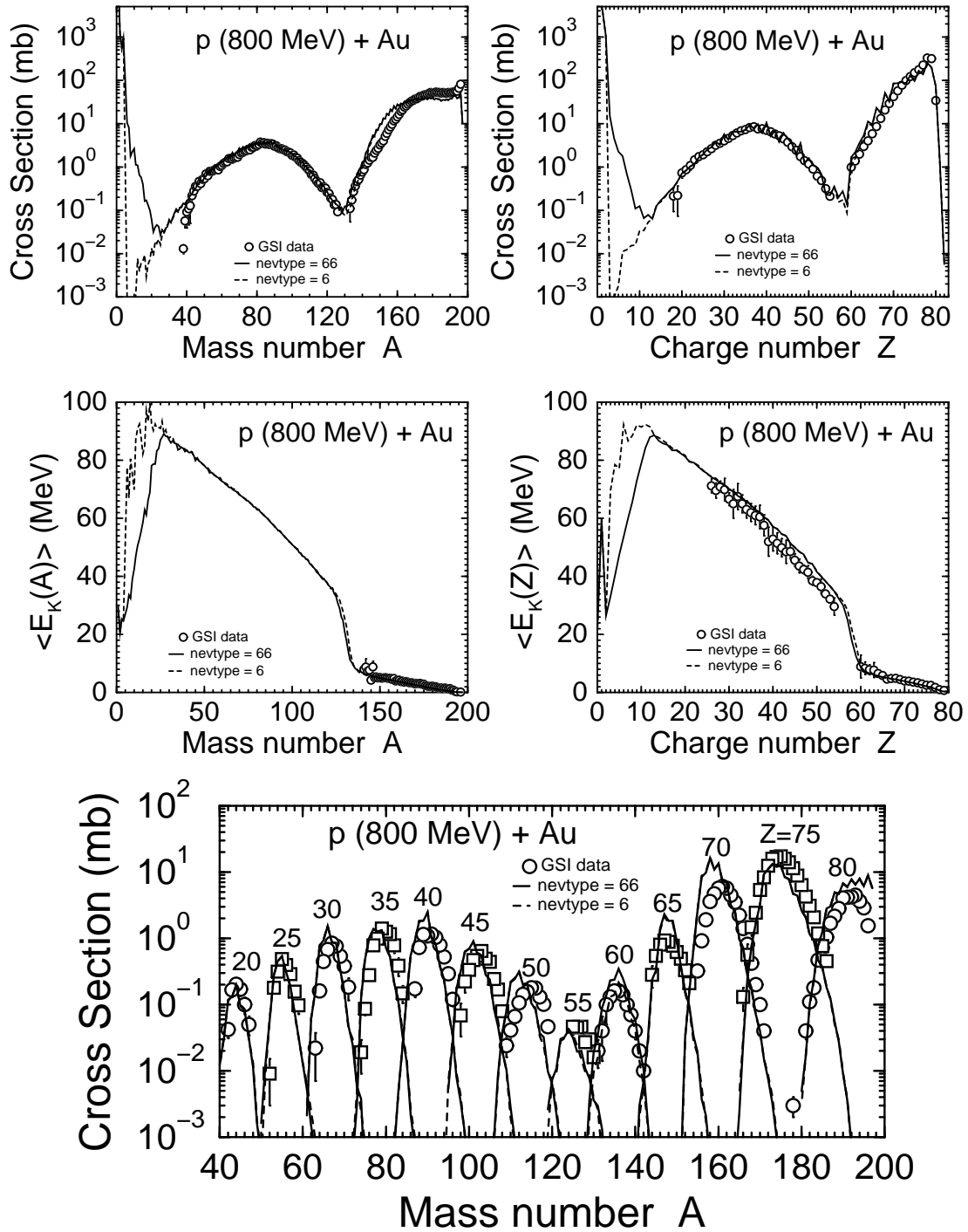


Figure 25: The measured [161] mass and charge distributions of the product yields from the reaction  $800 \text{ MeV/A } ^{197}\text{Au} + p$  and of the mean kinetic energy of these products, and the mass distributions of the cross sections for the production of thirteen elements with the charge  $Z$  from 20 to 80 (open symbols) compared with CEM03.01 results. The results shown in this figure are for ten million simulated inelastic events. The **nevttype=66** option requires 53 hr 34 min 31 sec of computing time on a SunBlade 100, 500 MHz computer, while the **nevttype=6** option requires only 12 hr 48 min 3 sec, providing almost the same results for the spallation and fission products. The fragment ( $2 < Z < 13$ ,  $6 < A < 29$ ) results are very different, therefore we need to use the option **nevttype=66** when we are interested in fragment production.

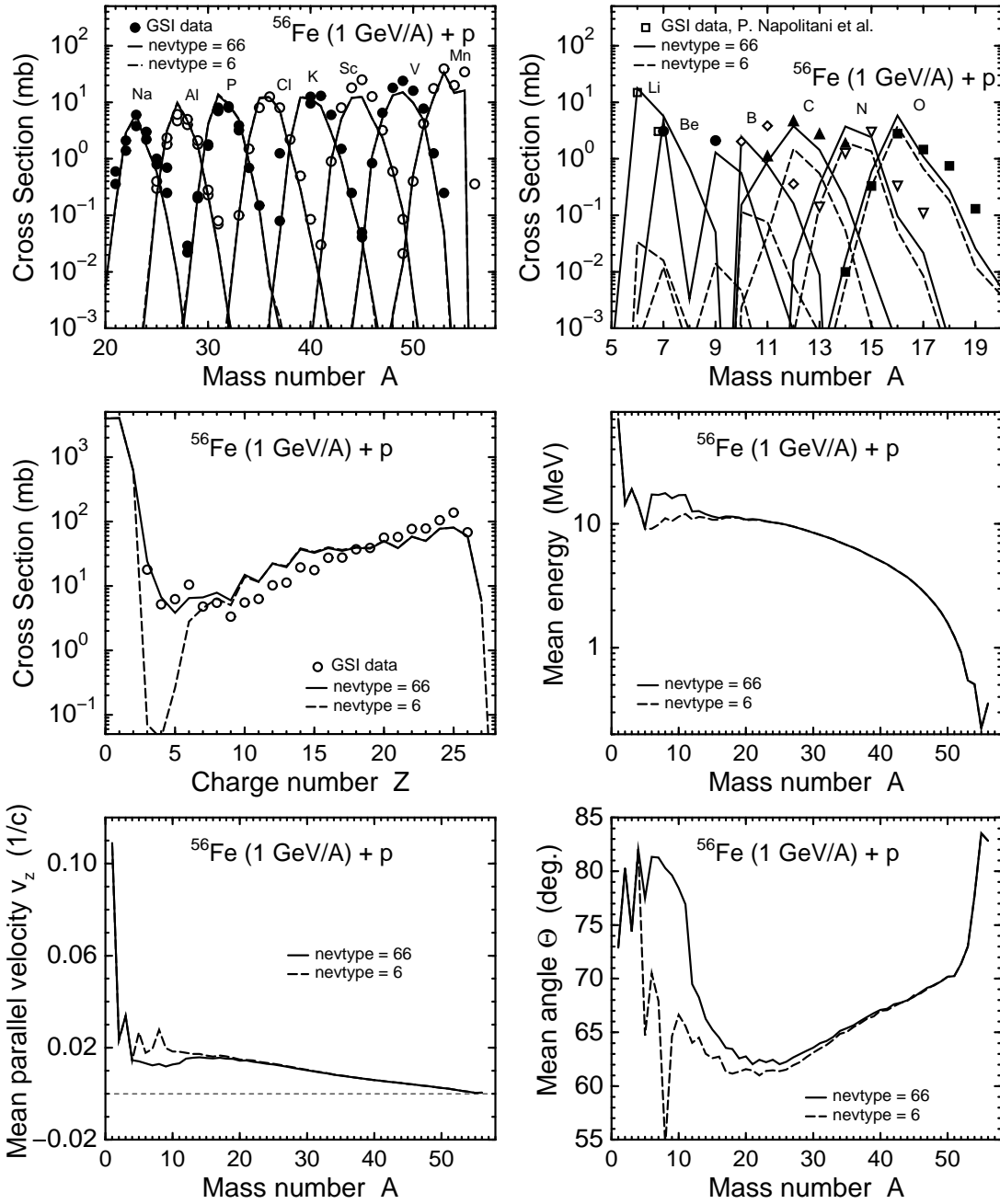


Figure 26: Experimental mass distributions of the yields of eight isotopes from Na to Mn [162] and of all light fragments from Li to O [163] from the reaction 1 GeV/A  $^{56}\text{Fe}+p$  and the charge distribution of the product yield compared with CEM03.01 results. The results shown in this figure are for ten million simulated inelastic events. The **nevtype=66** option requires 27 hr 38 min 37 sec of computing time on a SunBlade 100, 500 MHz computer, while the **nevtype=6** option requires only 8 hr 27 min 48 sec, providing almost the same results for the spallation products. The yields of light fragments, especially of Li and Be, differ by several orders of magnitude, therefore we need to use the option **nevtype > 6** when we are interested in light-fragment production.

Let us note that increasing the number of types of particles that can be evaporated from 6, employed by all old versions of CEM and LAQGSN which use our own evaporation model based on the Weisskopf-Ewing statistical theory of particle evaporation [125] and consider some newer features according to Ref. [128] (see details, e.g., in [9]), to 66 in the 03.01 and later versions, where we replaced our evaporation model with a modification of GEM2 by Furihata [144]–[146] as described above, together with considering the Fermi breakup model to disintegrate exited nuclei with  $A < 13$  in the new versions of our codes, allows us to improve considerably the description of fragment yields from various nuclear reactions. Two examples with such results are shown in Figs. 27 and 28.

Fig. 27 shows an example of an excitation function of interest to space applications used to estimate the risk assessment for electronic devices (SEUs and MBUs), namely  $^{28}\text{Si}(p,x)^7\text{Be}$ , calculated with an already quite old version of CEM, CEM2k [17], and with our recent versions CEM03.01 [23] and CEM03.02 [63] compared with experimental data from our T-16 compilation [164]. CEM2k, which does not consider evaporation of up to 66 types of particles and the Fermi breakup of light excited nuclei, underestimates these data by two orders of magnitude, providing only a tiny production of  $^7\text{Be}$ , only at high incident energies as final residual nuclei produced at the end of the reaction after INC, preequilibrium, and evaporation. The new versions of our codes describe this reaction much better than CEM2k, though there is still room for improvement and we plan a further improvement of the description of fragment production by our codes.

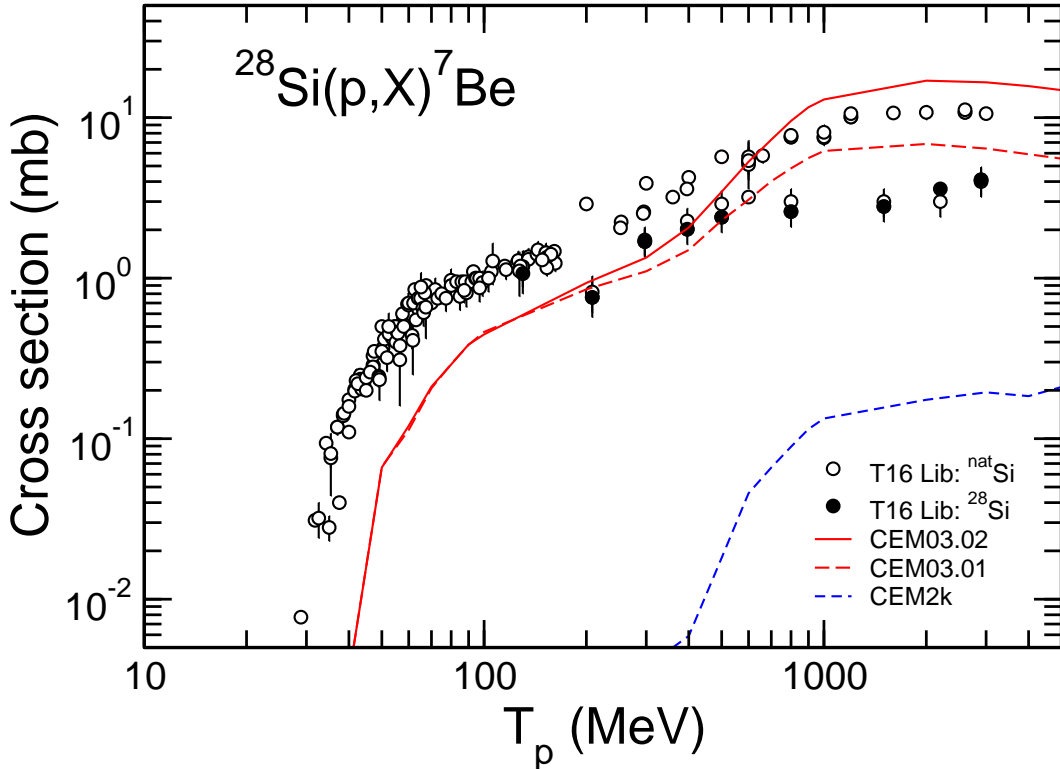


Figure 27: Comparison of the  $^{28}\text{Si}(p,X)^7\text{Be}$  excitation function calculated by CEM2k [17], CEM03.01 [23], and CEM03.02 [63] with experimental data from our T-16 compilation [164].

Fig. 28 compares results from CEM03.01 [23] and from its “S” and “G” modifications described briefly in Section 10, CEM03.S1 and CEM03.G1 [97], for the total production cross sections of Li and Be isotopes produced in interactions of 1.2 GeV protons with thirteen target

nuclei from Al to Th, measured recently at the Cooler Synchrotron Facility COSY of the Forschungszentrum Jülich [165].

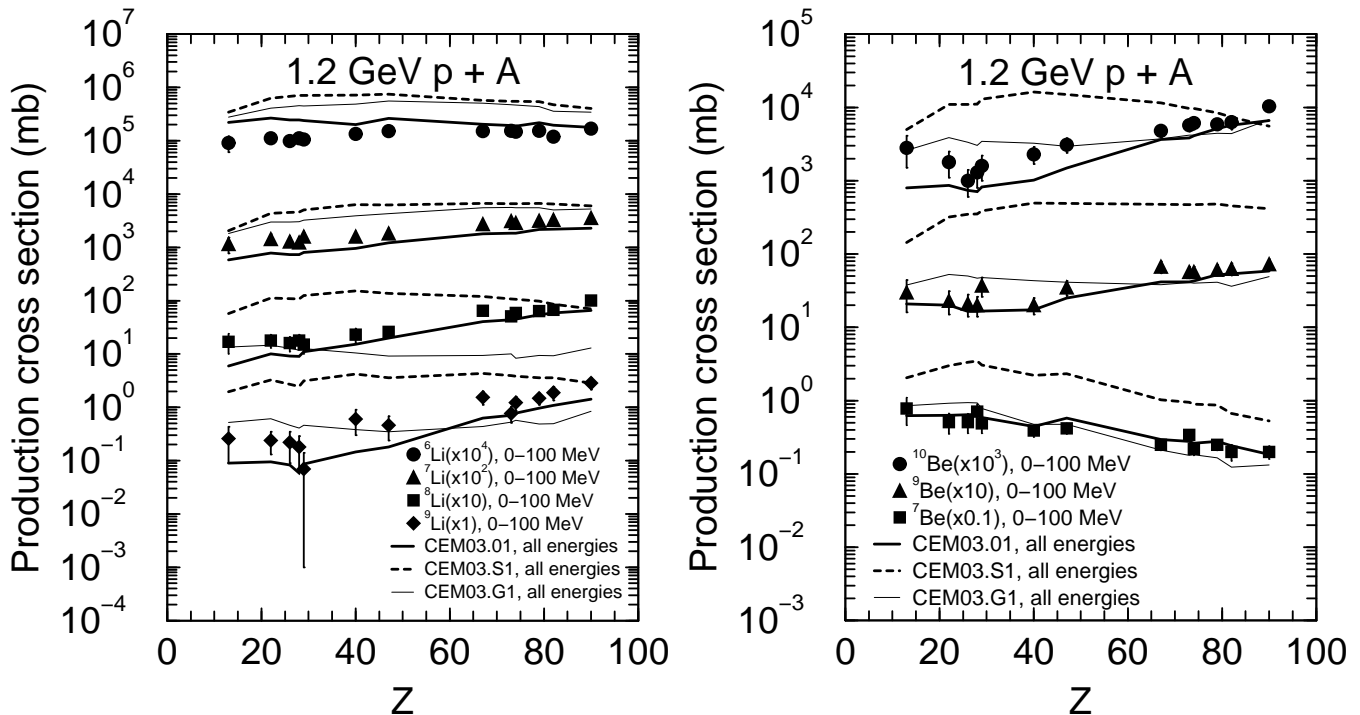


Figure 28: Comparison of measured [165] (symbols) production cross sections of Li and Be isotopes with kinetic energies below 100 MeV for 1.2 GeV proton-induced reactions on targets between Al and Th with results from CEM03.01, CEM03.S1, and CEM03.G1 (lines), as indicated.

We see that on the whole, with only a few exceptions, all versions of our current codes describe reasonably the shape and the absolute values of the measured total production cross sections for all these fragments, while the old versions would produce such fragments only as residual nuclei and would underestimate the data by orders of magnitude, as discussed above. More details on comparisons of our results with the NESSI data [165] may be found in Ref. [97].

However, a reasonable description by our current codes of the experimental integrated fragment yields demonstrated above does not yet assure a similar agreement with the fragment spectra, where we still have some serious problems to solve. Fig. 29 shows examples of some problems we still have in CEM03.03, CEM03.01 [23], as well as in the “S” and “G” versions CEM03.S1 and CEM03.G1 [97] in the description of  ${}^6\text{Li}$  spectra at 20, 45, 60, 90, and 110 degrees from proton-aluminum interactions at 200 MeV measured recently in Ref. [166] (we got very similar results also for the  ${}^7\text{Li}$ ,  ${}^7\text{Be}$ ,  ${}^9\text{Be}$ ,  ${}^{10}\text{Be}$ , and  ${}^{10}\text{B}$  spectra). We see that on the whole, with only a few exceptions, all these recent versions of our codes describe reasonably the low-energy part of the measured spectra, where fragments are produced mostly via evaporation. But all codes fail to reproduce correctly the high-energy tails of the spectra of all the fragments heavier than  ${}^4\text{He}$ . Note that the authors of this experiment [166] have measured similar fragment spectra also from  ${}^{59}\text{Co}$  and  ${}^{197}\text{Au}$ , and the problems with their correct description by our codes for these systems are only graver. We believe that we have these problems (just like other models have; as of today, we do not know any models or codes able to reproduce well all

these data) because the high-energy fragments from these reactions are produced via preequilibrium mechanisms of nuclear reactions, not considered by our current models for fragments heavier than  $^4\text{He}$ . Our models consider preequilibrium emission of particles only up to  $^4\text{He}$ , this is probably the reason why they describe quite well the  $^4\text{He}$  spectra, and not so well but still reasonably the  $^3\text{He}$  spectra, but fail completely to reproduce the high energy tails of all heavier fragments. The incident energy of bombarding protons in these reactions is too low to produce fragments via multigragmentation; this is the reason why the “S” version does not work well here. The “G” version describes production of fragments from these reactions only via fission-like binary decays; this mechanism contributes only to the evaporation part of the spectra, therefore it also fails to reproduce the high-energy results (see more details on the “G” and “S” versions of our codes in Section 10). We plan to address preequilibrium emission of fragments heavier than  $^4\text{He}$  in the future, with a hope to solve these problems.

## 7. Fission

The fission model used in GEM2 is based on Atchison’s model [148, 149] as implemented in LAHET [131], often referred in the literature as the Rutherford Appleton Laboratory (RAL) fission model, which is where Atchison developed it. In GEM2 there are two choices of parameters for the fission model: one of them is the original parameter set by Atchison [148, 149] as implemented in LAHET [131], and the other is a parameter set developed by Furihata [144, 145].

### 7.1. Fission Probability

The Atchison fission model is designed to describe only fission of nuclei with  $Z \geq 70$ . It assumes that fission competes only with neutron emission, *i.e.*, from the widths  $\Gamma_j$  of n, p, d, t,  $^3\text{He}$ , and  $^4\text{He}$ , the RAL code calculates the probability of evaporation of any particle. When a charged particle is selected to be evaporated, no fission competition is taken into account. When a neutron is selected to be evaporated, the code does not actually simulate its evaporation, instead it considers that fission may compete, and chooses either fission or evaporation of a neutron according to the fission probability  $P_f$ . This quantity is treated by the RAL code differently for the elements above and below  $Z = 89$ . The reasons Atchison split the calculation of the fission probability  $P_f$  are: (1) there is very little experimental information on fission in the region  $Z = 85$  to  $88$ , (2) the marked rise in the fission barrier for nuclei with  $Z^2/A$  below about 34 (see Fig. 2 in [149]) together with the disappearance of asymmetric mass splitting, indicates that a change in the character of the fission process occurs. If experimental information were available, a split between regions around  $Z^2/A \approx 34$  would be more sensible [149].

1)  $70 \leq Z_j \leq 88$ . For fissioning nuclei with  $70 \leq Z_j \leq 88$ , GEM2 uses the original Atchison calculation of the neutron emission width  $\Gamma_n$  and fission width  $\Gamma_f$  to estimate the fission probability as

$$P_f = \frac{\Gamma_f}{\Gamma_f + \Gamma_n} = \frac{1}{1 + \Gamma_n/\Gamma_f}. \quad (51)$$

Atchison uses [148, 149] the Weisskopf and Ewing statistical model [125] with an energy-independent pre-exponential factor for the level density (see Eq. (44)) and Dostrovsky’s [147] inverse cross section for neutrons and estimates the neutron width  $\Gamma_n$  as

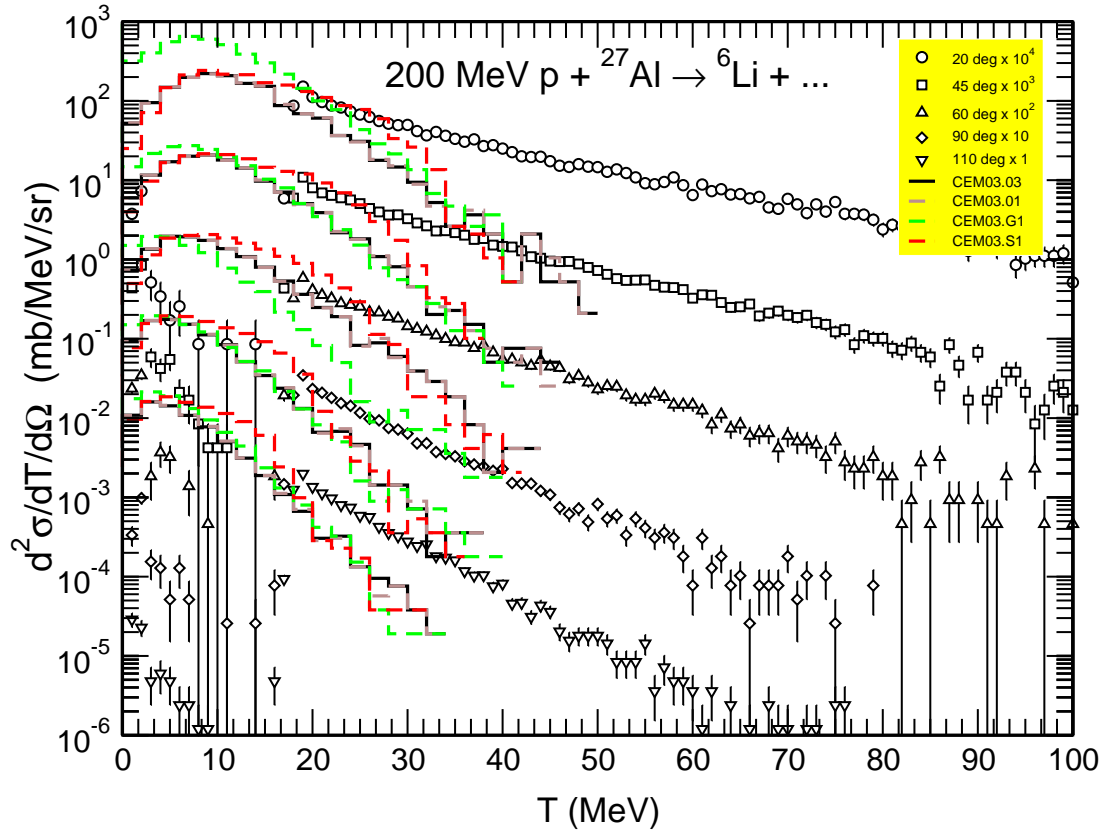
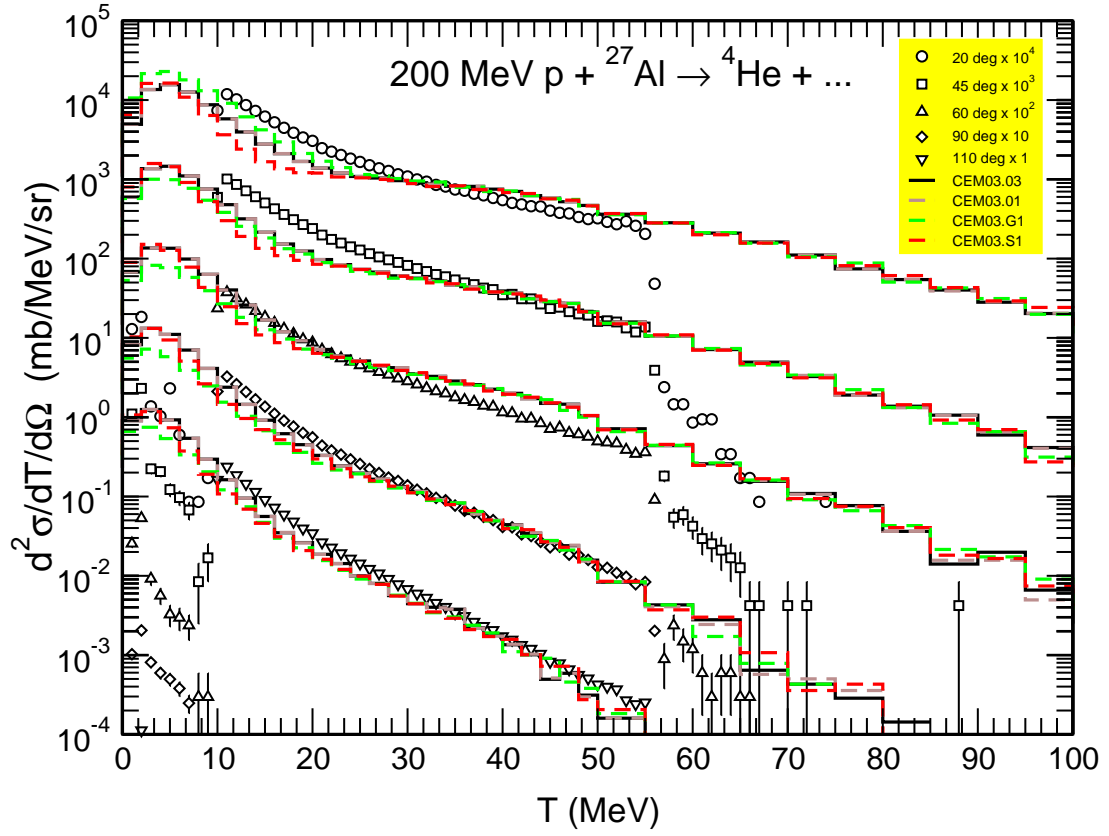


Figure 29: Experimental  ${}^4\text{He}$  and  ${}^6\text{Li}$  spectra at 20, 45, 60, 90, and 110 degrees from proton-aluminum interactions at 200 MeV [166] compared with results from CEM03.03, CEM03.01, CEM03.S1, and CEM03.G1, as indicated.

$$\Gamma_n = 0.352(1.68J_0 + 1.93A_i^{1/3}J_1 + A_i^{2/3}(0.76J_1 - 0.05J_0)), \quad (52)$$

where  $J_0$  and  $J_1$  are functions of the level-density parameter  $a_n$  and  $s_n (= 2\sqrt{a_n(E - Q_n - \delta)})$ ,

$$J_0 = \frac{(s_n - 1)e^{s_n} + 1}{2a_n},$$

$$J_1 = \frac{(2s_n^2 - 6s_n + 6)e^{s_n} + s_n^2 - 6}{8a_n^2}.$$

Note that the RAL model uses a fixed value for the level-density parameter  $a_n$ , namely

$$a_n = (A_i - 1)/8, \quad (53)$$

and this approximation is kept in GEM2 when calculating the fission probability according to Eq. (51), although it differs from the GCCI parameterization (45) used in GEM2 to calculate particle evaporation widths. The fission width for nuclei with  $70 \leq Z_j \leq 88$  is calculated in the RAL model and in the GEM as

$$\Gamma_f = \frac{(s_f - 1)e^{s_f} + 1}{a_f}, \quad (54)$$

where  $s_f = 2\sqrt{a_f(E - B_f - \delta)}$  and the level-density parameter in the fission mode  $a_f$  is fitted by Atchison to describe the measured  $\Gamma_f/\Gamma_n$  to be [149]:

$$a_f = a_n \left( 1.08926 + 0.01098(\chi - 31.08551)^2 \right), \quad (55)$$

and  $\chi = Z^2/A$ . The fission barriers  $B_f$  [MeV] are approximated by

$$B_f = Q_n + 321.2 - 16.7 \frac{Z_i^2}{A} + 0.218 \left( \frac{Z_i^2}{A_i} \right)^2. \quad (56)$$

Note that neither the angular momentum nor the excitation energy of the nucleus are taken into account in finding the fission barriers.

2)  $Z_j \geq 89$ . For heavy fissioning nuclei with  $Z_j \geq 89$  GEM2 follows the RAL model [148, 149] and does not calculate at all the fission width  $\Gamma_f$  and does not use Eq. (51) to estimate the fission probability  $P_f$ . Instead, the following semi-empirical expression obtained by Atchison [148, 149] by approximating the experimental values of  $\Gamma_n/\Gamma_f$  published by Vandenbosch and Huizenga [167] is used to calculate the fission probability:

$$\log(\Gamma_n/\Gamma_f) = C(Z_i)(A_i - A_0(Z_i)), \quad (57)$$

where  $C(Z)$  and  $A_0(Z)$  are constants depending on the nuclear charge  $Z$  only. The values of these constants are those used in the current version of LAHET [131] and are tabulated in Table 5 (note that some adjustments of these values have been done since Atchison's papers [148, 149] were published).

In this approach the fission probability  $P_f$  is independent of the excitation energy of the fissioning nucleus and its angular momentum.

## 7.2. Mass Distribution

The selection of the mass of the fission fragments depends on whether the fission is symmetric or asymmetric. For a pre-fission nucleus with  $Z_i^2/A_i \leq 35$ , only symmetric fission is allowed. For  $Z_i^2/A_i > 35$ , both symmetric and asymmetric fission are allowed, depending on the excitation energy of the fissioning nucleus. No new parameters were determined for asymmetric fission in GEM2.

For nuclei with  $Z_i^2/A_i > 35$ , whether the fission is symmetric or not is determined by the asymmetric fission probability  $P_{asy}$

$$P_{asy} = \frac{4870e^{-0.36E}}{1 + 4870e^{-0.36E}}. \quad (58)$$

Table 5.  $C(Z)$  and  $A_0(Z)$  values used in GEM2

Z	$C(Z)$	$A_0(Z)$
89	0.23000	219.40
90	0.23300	226.90
91	0.12225	229.75
92	0.14727	234.04
93	0.13559	238.88
94	0.15735	241.34
95	0.16597	243.04
96	0.17589	245.52
97	0.18018	246.84
98	0.19568	250.18
99	0.16313	254.00
100	0.17123	257.80
101	0.17123	261.30
102	0.17123	264.80
103	0.17123	268.30
104	0.17123	271.80
105	0.17123	275.30
106	0.17123	278.80

**7.2.a. Asymmetric fission.** For asymmetric fission, the mass of one of the post-fission fragments  $A_1$  is selected from a Gaussian distribution of mean  $A_f = 140$  and width  $\sigma_M = 6.5$ . The mass of the second fragment is  $A_2 = A_i - A_1$ .

**7.2.b. Symmetric fission.** For symmetric fission,  $A_1$  is selected from a Gaussian distribution of mean  $A_f = A_i/2$  and two options for the width  $\sigma_M$  as described below.

The first option for choosing  $\sigma_M$  is the original Atchison approximation:

$$\sigma_M = \begin{cases} 3.97 + 0.425(E - B_f) - 0.00212(E - B_f)^2, \\ 25.27, \end{cases} \quad (59)$$

for  $(E - B_f)$  below or above 100 MeV, respectively. In this expression all values are in MeV and the fission barriers  $B_f$  are calculated according to Eq. (56) for nuclei with  $Z_i \leq 88$ . For

nuclei with  $Z_i > 88$ , the expression by Neuzil and Fairhall [168] is used:

$$B_f = C - 0.36(Z_i^2/A_i), \quad (60)$$

where  $C = 18.8, 18.1, 18.1$ , and  $18.5$  [MeV] for odd-odd, even-odd, odd-even, and even-even nuclei, respectively.

The second option in GEM2 for  $\sigma_M$  (used here) was found by Furihata [144, 145] as:

$$\sigma_M = C_3(Z_i^2/A_i)^2 + C_4(Z_i^2/A_i) + C_5(E - B_f) + C_6. \quad (61)$$

The constants  $C_3 = 0.122$ ,  $C_4 = -7.77$ ,  $C_5 = 3.32 \times 10^{-2}$ , and  $C_6 = 134.0$  were obtained by fitting with GEM2 the recent Russian collection of experimental fission-fragment mass distributions [169]. In this expression, the fission barriers  $B_f$  by Myers and Swiatecki [170] are used. More details may be found in Ref. [145].

### 7.3. Charge Distribution

The charge distribution of fission fragments is assumed to be a Gaussian distribution of mean  $Z_f$  and width  $\sigma_Z$ .  $Z_f$  is expressed as

$$Z_f = \frac{Z_i + Z'_1 - Z'_2}{2}, \quad (62)$$

where

$$Z'_l = \frac{65.5A_l}{131 + A_l^{2/3}}, l = 1 \text{ or } 2. \quad (63)$$

The original Atchison model uses  $\sigma_Z = 2.0$ . An investigation by Furihata [145] suggests that  $\sigma_Z = 0.75$  provides a better agreement with data; therefore  $\sigma_Z = 0.75$  is used in GEM2 and in our code.

### 7.4. Kinetic Energy Distribution

The kinetic energy of fission fragments [MeV] is determined by a Gaussian distribution with mean  $\epsilon_f$  and width  $\sigma_{\epsilon_f}$ .

The original parameters in the Atchison model are:

$$\begin{aligned} \epsilon_f &= 0.133Z_i^2/A_i^{1/3} - 11.4, \\ \sigma_{\epsilon_f} &= 0.084\epsilon_f. \end{aligned}$$

Furihata's parameters in the GEM, which we also use, are:

$$\epsilon_f = \begin{cases} 0.131Z_i^2/A_i^{1/3}, \\ 0.104Z_i^2/A_i^{1/3} + 24.3, \end{cases} \quad (64)$$

for  $Z_i^2/A_i^{1/3} \leq 900$  and  $900 < Z_i^2/A_i^{1/3} \leq 1800$ , respectively, according to Rusanov *et al.* [169]. By fitting the experimental data by Itkis *et al.* [171], Furihata found the following expression for  $\sigma_{\epsilon_f}$

$$\sigma_{\epsilon_f} = \begin{cases} C_1(Z_i^2/A_i^{1/3} - 1000) + C_2, \\ C_2, \end{cases} \quad (65)$$

for  $Z_i^2/A_i^{1/3}$  above and below 1000, respectively, and the values of the fitted constants are  $C_1 = 5.70 \times 10^{-4}$  and  $C_2 = 86.5$ . The experimental data used by Furihata for fitting are the values extrapolated to the nuclear temperature 1.5 MeV by Itkis *et al.* [171]. More details may be found in [145].

We note that Atchison has also modified his original version using recent data and published [172] improved (and more complicated) parameterizations for many quantities and distributions in his model, but these modifications [172] have not been included either in LAHET or in GEM2.

### 7.5. Modifications to GEM2 in CEM03.01 and LAQGSM03.01

First, we fixed several observed uncertainties and small errors in the 2002 version of GEM2 Dr. Furihata kindly sent us. Then, we extended GEM2 to describe fission of lighter nuclei, down to  $Z \geq 65$ , and modified it [20] so that it provides a good description of fission cross sections when it is used after our INC and preequilibrium models.

If we had merged GEM2 with the INC and preequilibrium-decay modules of CEM or of LAQGSM without any modifications, the new code would not describe correctly fission cross sections (and the yields of fission fragments). This is because Atchison fitted the parameters of his RAL fission model when it followed the Bertini INC [173] which differs from ours. In addition, Atchison did not model preequilibrium emission. Therefore, the distributions of fissioning nuclei in  $A$ ,  $Z$ , and excitation energy  $E^*$  simulated by Atchison differ significantly from the distributions we get; as a consequence, all the fission characteristics are also different. Furihata used GEM2 coupled either with the Bertini INC [173] or with the ISABEL [174] INC code, which also differs from our INC, and did not include preequilibrium particle emission. Therefore the distributions of fissioning nuclei simulated by Furihata differ from those in our simulations, so the parameters adjusted by Furihata to work well with her INC are not appropriate for us. To get a good description of fission cross sections (and fission-fragment yields) we have modified at least two parameters in GEM2 as used in CEM03.01 and LAQGSM03.01 (see more details in [18, 19, 42]).

The main parameters that determine the fission cross sections calculated by GEM2 are the level-density parameter in the fission channel,  $a_f$  (or more exactly, the ratio  $a_f/a_n$  as calculated by Eq. (55)) for preactinides, and parameter  $C(Z)$  in Eq. (57) for actinides. The sensitivity of results to these parameters is much higher than to either the fission-barrier heights used in a calculation or other parameters of the model. Therefore we choose [20] to adjust only these two parameters in our merged codes. We do not change the form of systematics (55) and (57) derived by Atchison. We only introduce additional coefficients both to  $a_f$  and  $C(Z)$ , replacing  $a_f \rightarrow C_a \times a_f$  in Eq. (55) and  $C(Z_i) \rightarrow C_c \times C(Z_i)$  in Eq. (57) and fit  $C_a$  and  $C_c$  to experimental proton-induced fission cross sections covered by Prokofiev's systematics [175] for both CEM03.01 and LAQGSM03.01. No other parameters in GEM2 have been changed. For preactinides, we fit only  $C_a$ . The values of  $C_a$  found in our fit to Prokofiev's systematics are close to one and vary smoothly with the proton energy and the charge or mass number of the target. This result gives us some confidence in our procedure, and allows us to interpolate the values of  $C_a$  for nuclei and incident proton energies not analyzed by Prokofiev. For actinides, as described in [18, 19], we have to fit both  $C_a$  and  $C_c$ . The values of  $C_a$  we find are also very close to one, while the values of  $C_c$  are more varied, but both of them change smoothly with the proton energy and  $Z$  or  $A$  of the target, which again allows us to interpolate them for nuclei and energies outside Prokofiev's systematics.

We fix the fitted values of  $C_a$  and  $C_c$  in data blocks in our codes and use the routines **fitafpa**

and **fitafac** to interpolate to nuclei not covered by Prokofiev's systematics. We believe that such a procedure provides a reasonably accurate fission cross-section calculation, at least for proton energies and target nuclei not too far from the ones covered by the systematics.

Let us mention that the situation with the fitting procedure of parameters  $C_a$  and  $C_c$  is quite tricky, as it should be redone after all major improvements of other parts of our codes describing INC, preequilibrium, or evaporation. This is a major minus of such types of models like GEM2 that are based mostly on systematics of available experimental data rather than on fundamental physics. (This was the main reason we started to develop our own improved evaporation and fission models for our codes [19] that would describe experimental data not worse than GEM2 but would be based on physics rather than on systematics of available data; this work is not completed yet, so we have to use GEM2 in our codes so far.) Indeed, after making our major improvements to the INC and preequilibrium parts CEM and LAQGSM as described above, the mean values of the mass and charge numbers,  $A$  and  $Z$  of the excited compound nuclei produced after the preequilibrium stage of nuclear reactions and their mean excitation energy  $E^*$  have changed slightly, which affects the probability of heavy compound nuclei (especially preactinides) to fission. This means that the procedure of fitting the  $C_a$  and  $C_c$  parameters which we performed in [20] to provide the best description by CEM2k and LAQGSM of fission cross sections was no longer correct. We had to redo this fitting for the latest versions of our CEM03.01 and LAQGSM03.01, ensuring that they describe as well as possible fission cross sections from various reactions. Fig. 30 shows examples of fission cross sections for proton-induced reactions on  $^{186}\text{W}$ ,  $^{184}\text{W}$ ,  $^{183}\text{W}$  and  $^{182}\text{W}$ . The improved CEM03.01 reproduces the recent Uppsala measurements [176] of proton-induced fission cross sections.

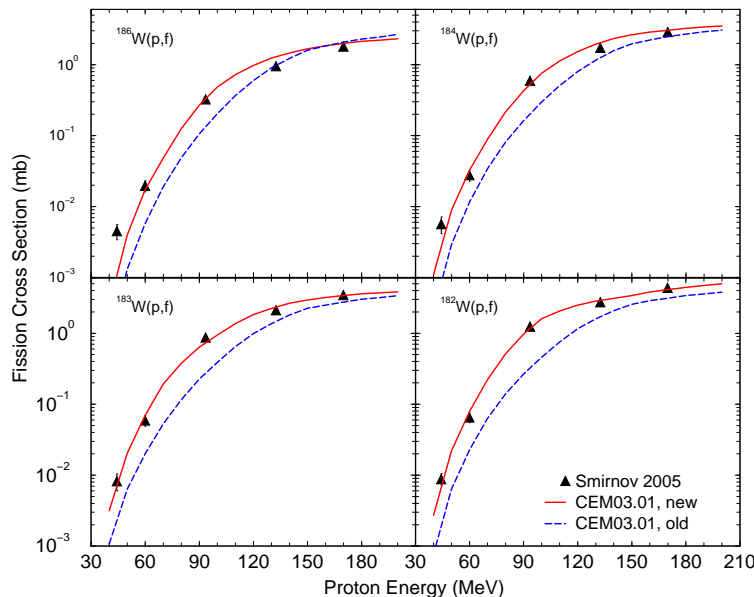


Figure 30: Experimental [176] proton-induced fission cross sections of  $^{186}\text{W}$ ,  $^{184}\text{W}$ ,  $^{183}\text{W}$ , and  $^{182}\text{W}$  compared with improved (red solid lines) and old (blue dashed lines, from [176]) CEM03.01 calculations.

Another example of some problems of the fission model of GEM2 based on systematics of measured data is shown in Fig. 31 for fragment mass distributions from several reactions induced by bremsstrahlung with the maximum energy  $E_0$  of 15, 20, 30, and 70 MeV on  $^{235}\text{U}$  and  $^{238}\text{U}$  targets measured in [177] compared with results by CEM03.02 [63]. We see that the fission

model of GEM2 used in our CEM03.02 describes surprisingly well these mass distributions of fission fragments at  $E_0 = 15, 20$ , and  $30$  MeV, where experimental data were available to fit the mass distribution of fission fragments in the GEM2 systematics, but fails to reproduce correctly such distribution at  $E_0 = 70$  MeV, requiring an additional refitting of the GEM systematics at this energy to improve the agreement with the data.

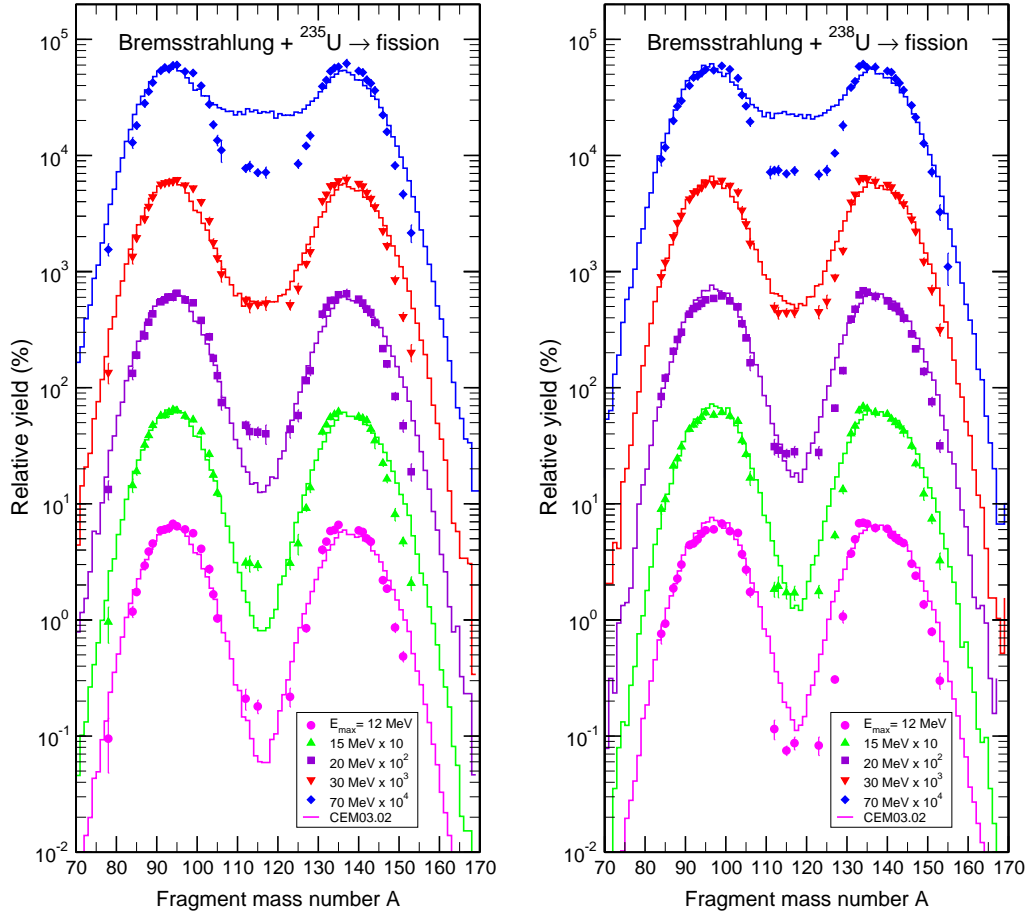


Figure 31: Experimental [177] fission fragment mass distributions (symbols) from reactions induced by bremsstrahlung with the maximum energy  $E_0$  of 15, 20, 30, and 70 MeV on  $^{235}\text{U}$  and  $^{238}\text{U}$  targets compared with results by CEM03.02 [63] (histograms).

Finally, to conclude the fission Section, Figs. 32 and 33 shows examples of spallation, fission, and fragmentation experimental product cross sections from 1 GeV  $p + ^{238}\text{U}$  [107, 108] and 2 GeV  $d + ^{208}\text{Pb}$  [178] measured recently at GSI in inverse kinematics compared with results by CEM03.01 ( $p + \text{U}$ , Fig. 32) and LAQGSM03.01 ( $d + \text{Pb}$ , Fig. 33), respectively. Our models describe quite well the fission- fragment yields, as well as the spallation and fragmentation product cross sections and agree with most of the GSI data with an accuracy of a factor of two or better. Similar agreements are obtained with other reactions measured at GSI in inverse kinematics (see, *e.g.*, [31, 42, 160, 179]).

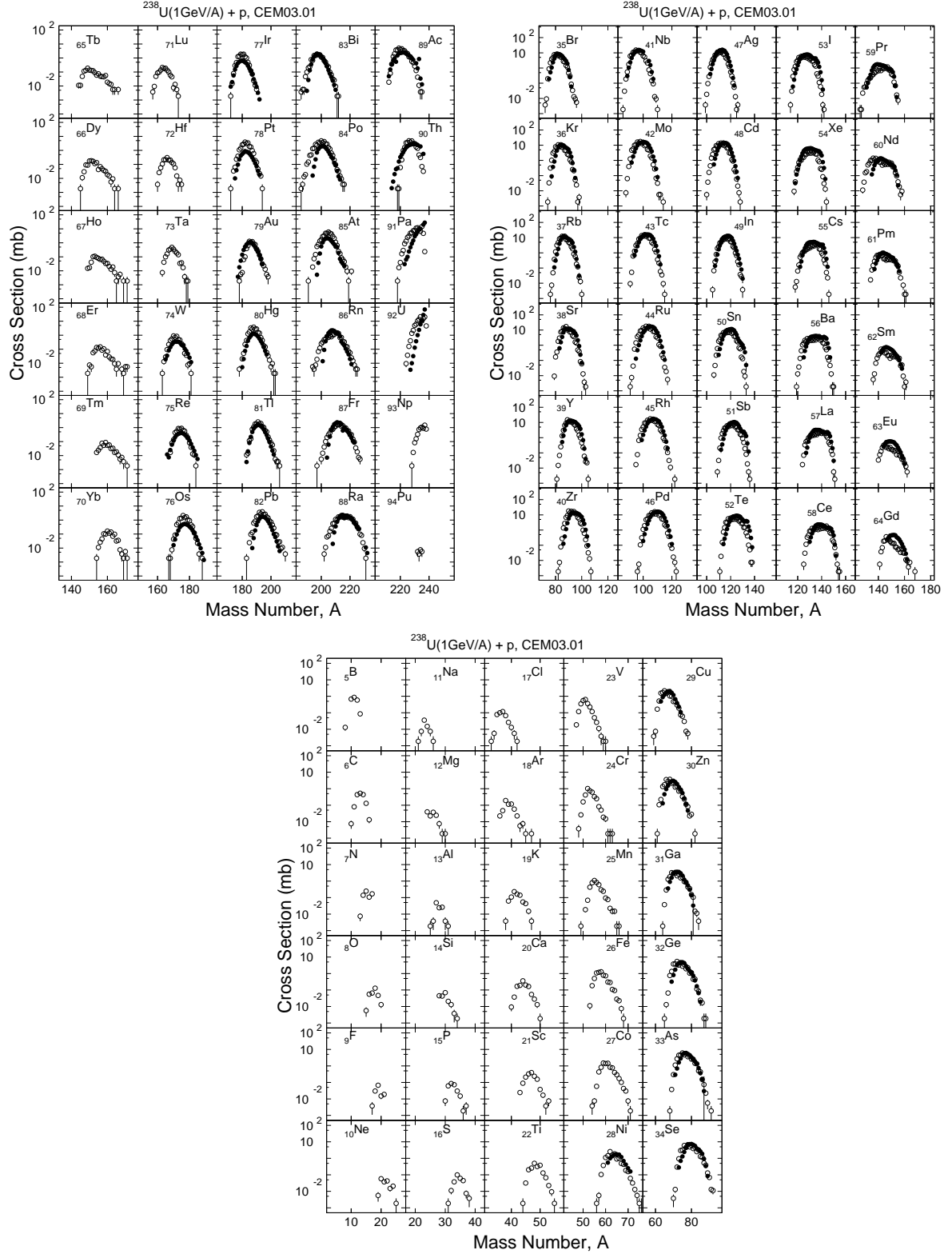


Figure 32: Comparison of measured [107, 108] spallation, fission, and fragmentation cross sections for the reaction  $^{238}\text{U}(1 \text{ GeV/A}) + p$  (filled circles) with our CEM03.01 results (open circles). Experimental data for isotopes from B to Co, from Tb to Ta, and for Np and Pu are not available so we present only our predictions.

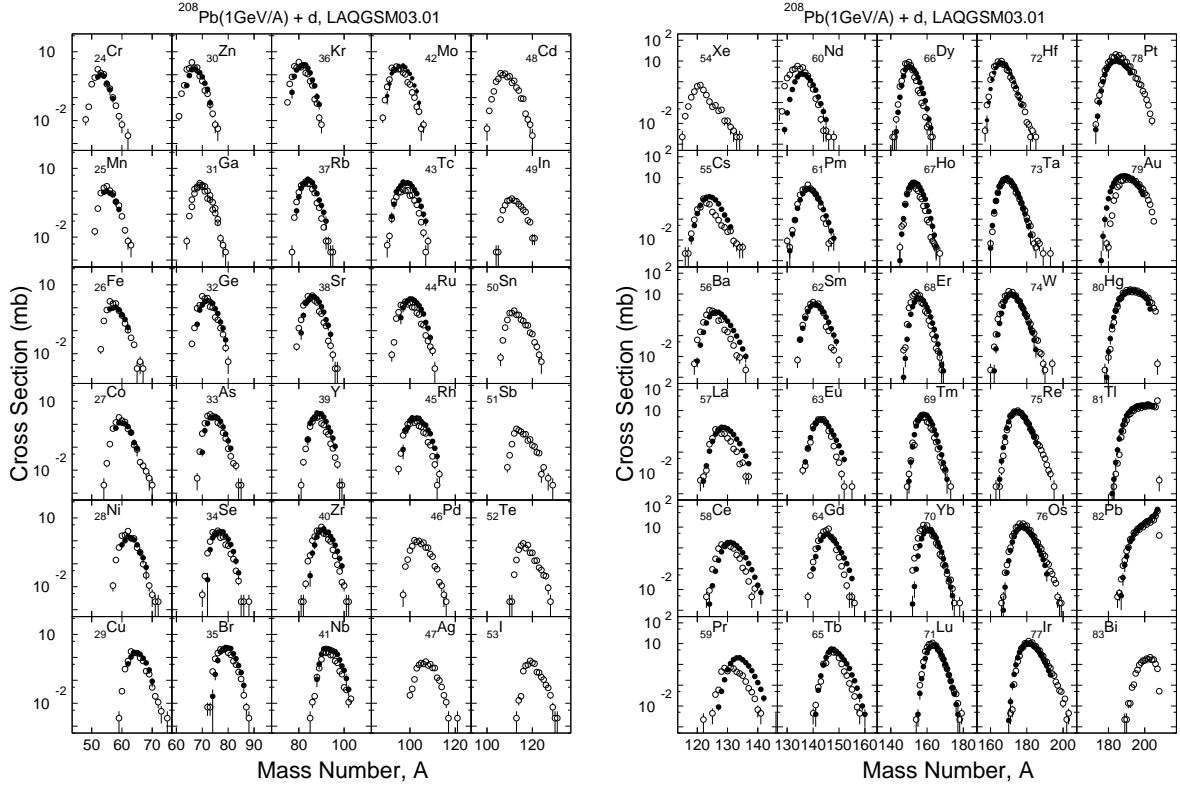


Figure 33: Comparison of measured [178] spallation and fission-product cross sections for the reaction  $^{208}\text{Pb}(1 \text{ GeV/A}) + d$  (filled circles) with our LAQGSM03.01 results (open circles).

## 8. The Fermi Breakup Model

After calculating the coalescence stage of a reaction, CEM03.01 and LAQGSM03.01 move to the description of the last slow stages of the interaction, namely to preequilibrium decay and evaporation, with a possible competition of fission. But as mentioned above, if the residual nuclei have atomic numbers with  $A < 13$ , CEM03.01 and LAQGSM03.01 use the Fermi breakup model [180] to calculate their further disintegration instead of using the preequilibrium and evaporation models. The newer 03.02 versions of our codes use the Fermi breakup model also during the preequilibrium and/or evaporation stages of reactions, when the residual nucleus has an atomic number with  $A < 13$ .

Finally, the latest 03.03 versions of our codes use the Fermi breakup model also to disintegrate the unstable fission fragments with  $A < 13$  that can be produced in very rare cases of very asymmetric fission.

All formulas and details of the algorithms used in the version of the Fermi breakup model developed in the former group of Prof. Barashenkov at Joint Institute for Nuclear Research (JINR), Dubna, Russia and used by our codes may be found in [53]. All the information needed to calculate the breakup of an excited nucleus is its excitation energy  $U$  and the mass and charge numbers  $A$  and  $Z$ . The total energy of the nucleus in the rest frame will be  $E = U + M(A, Z)$ , where  $M$  is the mass of the nucleus. The total probability per unit time for a nucleus to break up into  $n$  components in the final state (*e.g.*, a possible residual nucleus, nucleons, deuterons, tritons, alphas, *etc.*) is given by

$$W(E, n) = (V/\Omega)^{n-1} \rho_n(E), \quad (66)$$

where  $\rho_n$  is the density of final states,  $V$  is the volume of the decaying system and  $\Omega = (2\pi\hbar)^3$  is the normalization volume. The density  $\rho_n(E)$  can be defined as a product of three factors:

$$\rho_n(E) = M_n(E)S_nG_n. \quad (67)$$

The first one is the phase space factor defined as

$$M_n(E) = \int_{-\infty}^{+\infty} \cdots \int_{-\infty}^{+\infty} \delta\left(\sum_{b=1}^n \vec{p}_b\right) \delta\left(E - \sum_{b=1}^n \sqrt{p_b^2 + m_b^2}\right) \prod_{b=1}^n d^3p_b, \quad (68)$$

where  $\vec{p}_b$  are fragment momenta. The second one is the spin factor

$$S_n = \prod_{b=1}^n (2s_b + 1), \quad (69)$$

which gives the number of states with different spin orientations. The last one is the permutation factor

$$G_n = \prod_{j=1}^k \frac{1}{n_j!}, \quad (70)$$

which takes into account identical particles in the final state ( $n_j$  is the number of components of  $j$ -type particles and  $k$  is defined by  $n = \sum_{j=1}^k n_j$ ). For example, if we have in the final state six particles ( $n = 6$ ) and two of them are alphas, three are nucleons, and one is a deuteron, then  $G_6 = 1/(2!3!1!) = 1/12$ . For the non-relativistic case, the integration in Eq. (68) can be evaluated analytically (see, *e.g.*, [53]) and the probability for a nucleus to disintegrate into  $n$  fragments with masses  $m_b$ , where  $b = 1, 2, 3, \dots, n$  is

$$W(E, n) = S_n G_n \left(\frac{V}{\Omega}\right)^{n-1} \left(\frac{1}{\sum_{b=1}^n m_b} \prod_{b=1}^n m_b\right)^{3/2} \frac{(2\pi)^{3(n-1)/2}}{\Gamma(3(n-1)/2)} E^{(3n-5)/2}, \quad (71)$$

where  $\Gamma(x)$  is the gamma function.

The angular distribution of  $n$  emitted fragments is assumed to be isotropic in the c.m. system of the disintegrating nucleus and their kinetic energies are calculated from momentum-energy conservation. The Monte-Carlo method is used to randomly select the decay channel according to probabilities defined by Eq. (71). Then, for a given channel, the code calculates kinematic quantities for each fragment according to the  $n$ -body phase space distribution using Kopylov's method [181]. Generally, the Fermi breakup model considers formation of fragments only in their ground and those low-lying states which are stable for nucleon emission. However, as already mentioned in Section 2, several unstable fragments with large lifetimes:  ${}^5\text{He}$ ,  ${}^5\text{Li}$ ,  ${}^8\text{Be}$ ,  ${}^9\text{B}$ , *etc.* are considered as well by the initial version of the Fermi breakup model code as described in Ref. [53]. The randomly chosen channel will be allowed to decay only if the total kinetic energy  $E_{kin}$  of all fragments at the moment of breakup is positive, otherwise a new simulation will be performed and a new channel will be selected. The total kinetic energy  $E_{kin}$  can be calculated according to the equation:

$$E_{kin} = U + M(A, Z) - E_{Coulomb} - \sum_{b=1}^n (m_b + \epsilon_b), \quad (72)$$

where  $m_b$  and  $\epsilon_b$  are masses and excitation energies of the fragments, respectively, and  $E_{Coulomb}$  is the Coulomb barrier for the given channel. It is approximated by

$$E_{Coulomb} = \frac{3}{5} \frac{e^2}{r_0} \left(1 + \frac{V}{V_0}\right)^{-1/3} \left( \frac{Z^2}{A^{1/3}} - \sum_{b=1}^n \frac{Z_b^2}{A_b^{1/3}} \right), \quad (73)$$

where  $A_b$  and  $Z_b$  are the mass number and the charge of the  $b$ -th particle of a given channel, respectively.  $V_0$  is the volume of the system corresponding to normal nuclear density and  $V = kV_0$  is the decaying system volume (we assume  $k = 1$  in our codes).

Thus, the Fermi breakup model we use has only one free parameter,  $V$  or  $V_0$ , the volume of the decaying system, which is estimated as follows:

$$V = 4\pi R^3/3 = 4\pi r_0^3 A/3, \quad (74)$$

where we use  $r_0 = 1.4$  fm.

There is no limitation on the number  $n$  of fragments a nucleus may break up into in our version of the breakup model, in contrast to implementations in other codes, such as  $n \leq 3$  in MCNPX, or  $n \leq 7$  in LAHET.

In comparison with its initial version as described in [53], the Fermi breakup model used in CEM03.02 and LAQGSM03.02 has been modified [63] to decay the unstable light fragments that were produced by the original code. As mentioned above, the initial routines that describe the Fermi breakup model were written more than twenty years ago in the group of Prof. Barashenkov at JINR, Dubna, and unfortunately had some problems. First, those routines allowed in rare cases production of some light unstable fragments like  ${}^5\text{He}$ ,  ${}^5\text{Li}$ ,  ${}^8\text{Be}$ ,  ${}^9\text{B}$ , *etc.* as a result of a breakup of some light excited nuclei. Second, they allowed very rarely even production of “neutron stars” (or “proton stars”), *i.e.*, residual “nuclei” produced via Fermi breakup that consist of only neutrons (or only protons). Lastly, those routines could even crash the code, due to cases of division by 0. All these problems of the Fermi breakup model routines were addressed and solved in CEM03.02 [63]; the changes were then put in LAQGSM03.02 [63]. Several bugs are also fixed. However, even after solving these problems and after implementing the improved Fermi breakup model into CEM03.02 and LAQGSM03.02 [63], our event generators still could produce some unstable products via very asymmetric fission, when the excitation energies of those fragments were below 3 MeV so they were not checked and disintegrated with the Fermi breakup model. Our analysis [12] had shown that such events could occur very rarely, in less than 0.0006% of all simulated events, so that production of such unstable nuclides affects by less than 0.0006% the other correct cross sections calculated by our codes. However, these unstable nuclides are not physical and should be eliminated. This was the reason why a universal checking of all unstable light products has been incorporated into CEM03.03 and LAQGSM03.03. Such unstable products are forced to disintegrate via Fermi breakup independently of their excitation energy. The latest versions of the CEM03 and LAQGSM03 event generators do not produce any such unstable products.

Examples of several results from CEM03.02 compared with results from CEM03.01 and from the older versions CEM95 and CEM2k and with experimental data for a number of reactions relevant to the Fermi breakup model are presented Figs. 34 to 36. Fig. 34 presents the mass distribution of the product yields from the reaction 730 MeV  $p + {}^{27}\text{Al}$  calculated with CEM03.01 without considering the Fermi breakup mode during the preequilibrium and evaporation stages of reactions and with CEM03.02 that does consider this mode during these stages and uses an extended version of the model without unstable products, as described

above. CEM03.01 provides a small yield of unphysical unstable  ${}^5\text{He}$  (just like the older versions CEM95 and CEM2k do), while the newer version does not produce such unstable nuclides. The results from CEM03.02 also agree a little better with available experimental data (red squares on Fig. 34) than those from CEM03.01. Similar results are obtained for several other reactions on other light targets.

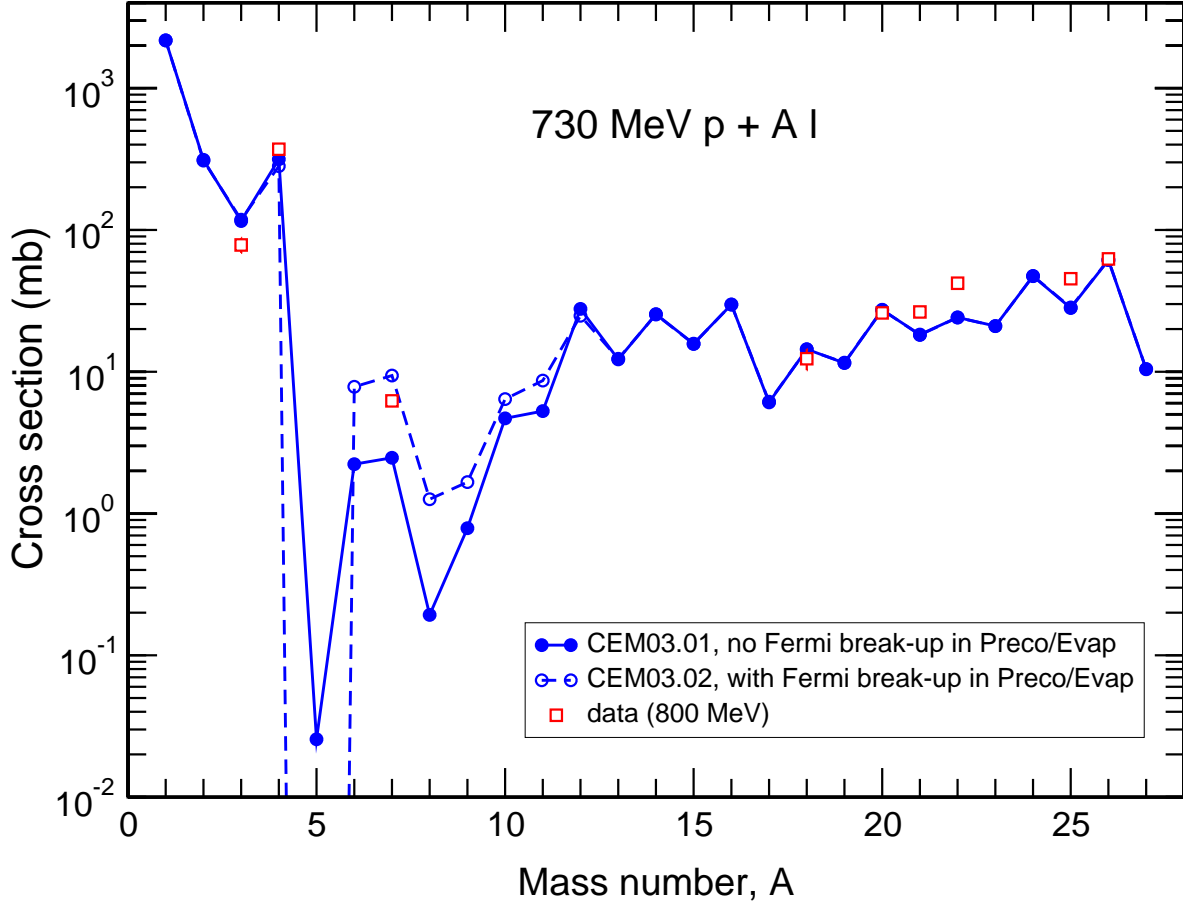


Figure 34: Mass distribution of the product yields from the reaction  $730 \text{ MeV p} + {}^{27}\text{Al}$  calculated with CEM03.01 without considering the Fermi breakup mode during the preequilibrium and evaporation stages of reactions (solid circles connected with a solid line) and with the improved version of the code CEM03.02 that does consider the Fermi breakup mode during the preequilibrium and evaporation stages of reactions (open circles connected with a dashed line), compared with experimental data available at a nearby energy of 800 MeV from the T-16 Lib compilation [164] (open red squares).

Our results show that CEM03.02 and LAQGSM03.02 do not predict unstable unphysical nuclides and describe the yields of most products a little better than the 03.01 or older versions of CEM and LAQGSM. The question about how the spectra of different particles from different nuclear reactions are described by the 03.02 version in comparison with older versions of our codes is not obvious. We studied this question on several reactions and Fig. 35 presents examples of particle spectra calculated with CEM03.01 and CEM03.02 for the reaction  $730 \text{ MeV p} + \text{Al}$ . We see that spectra of  $n$ ,  $p$ ,  $d$ ,  $t$ ,  ${}^3\text{He}$ , and  ${}^4\text{He}$  calculated by CEM03.02 that uses the Fermi breakup model to describe disintegration of exited nuclei with  $A < 13$  are almost the same as such spectra calculated by CEM03.01 which uses the preequilibrium and evaporation models

to describe such reactions when  $A > 12$  after the INC stage of reactions. This result is very interesting from a physical point of view; it is not trivial at all and could not be forecast easily in advance. We see that spectra of these particles predicted by different models are almost the same. In other words, the theoretical spectra of particles do not depend much on the models we use to calculate them, but depend mostly on the final phase space calculated by these models: If the phase spaces calculated by different models are correct and near to each other, than the spectra of secondary particles calculated by these models would be also near to each other and would be not very sensitive to the dynamics of reactions considered (or not) by the models we use.

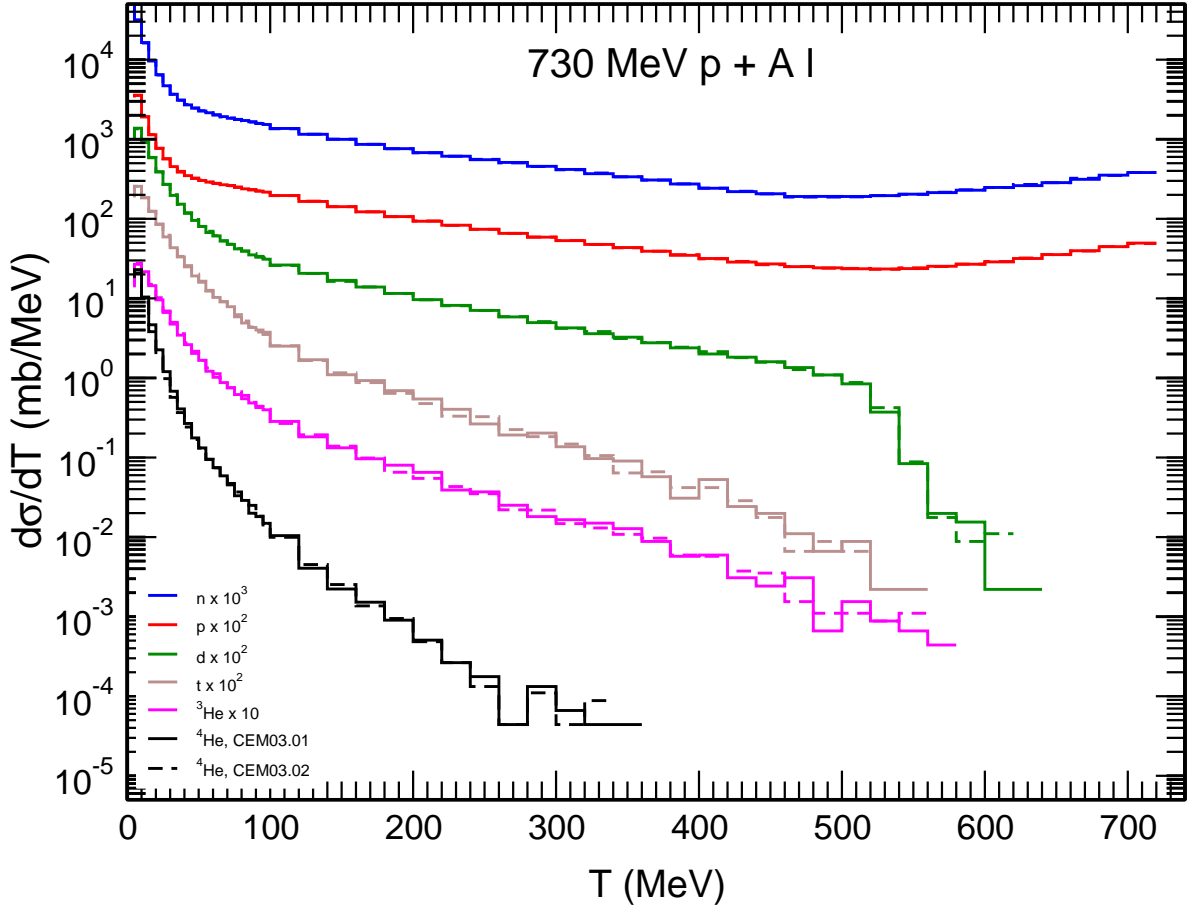


Figure 35: Angle-integrated energy spectra of secondary  $n$ ,  $p$ ,  $d$ ,  $t$ ,  ${}^3\text{He}$ , and  ${}^4\text{He}$  from the reaction  $730 \text{ MeV } p + {}^{27}\text{Al}$  calculated with CEM03.01 without considering the Fermi breakup mode during the preequilibrium and evaporation stages of reactions (solid histograms) and with CEM03.02 that does consider the Fermi breakup mode during the preequilibrium and evaporation stages of reactions (dashed histograms).

Fig. 36 shows examples of double differential experimental neutron spectra at 15, 30, 60, 90, 120, and 150 deg from 3.0, 1.5, 0.8, and 0.597 GeV  $p + \text{Al}$  (symbols) compared with results by CEM03.01 without considering the Fermi breakup mode during the preequilibrium and evaporation stages of reactions (dashed histograms), with CEM03.02 that does consider this mode during the preequilibrium and evaporation stages of reactions (solid histograms), and with the old version of the code, CEM95 [9]. We see that the results from CEM03.02 and CEM03.01 agree much better with the data at neutron energies of 20–100 MeV (where

the contribution from the preequilibrium mode is the most important) than the results from CEM95 do. Results from CEM03.02 for these neutron spectra are nearly identical to those from CEM03.01, just as observed for the energy spectra of n, p, d, t,  $^3\text{He}$ , and  $^4\text{He}$  shown in Fig. 35.

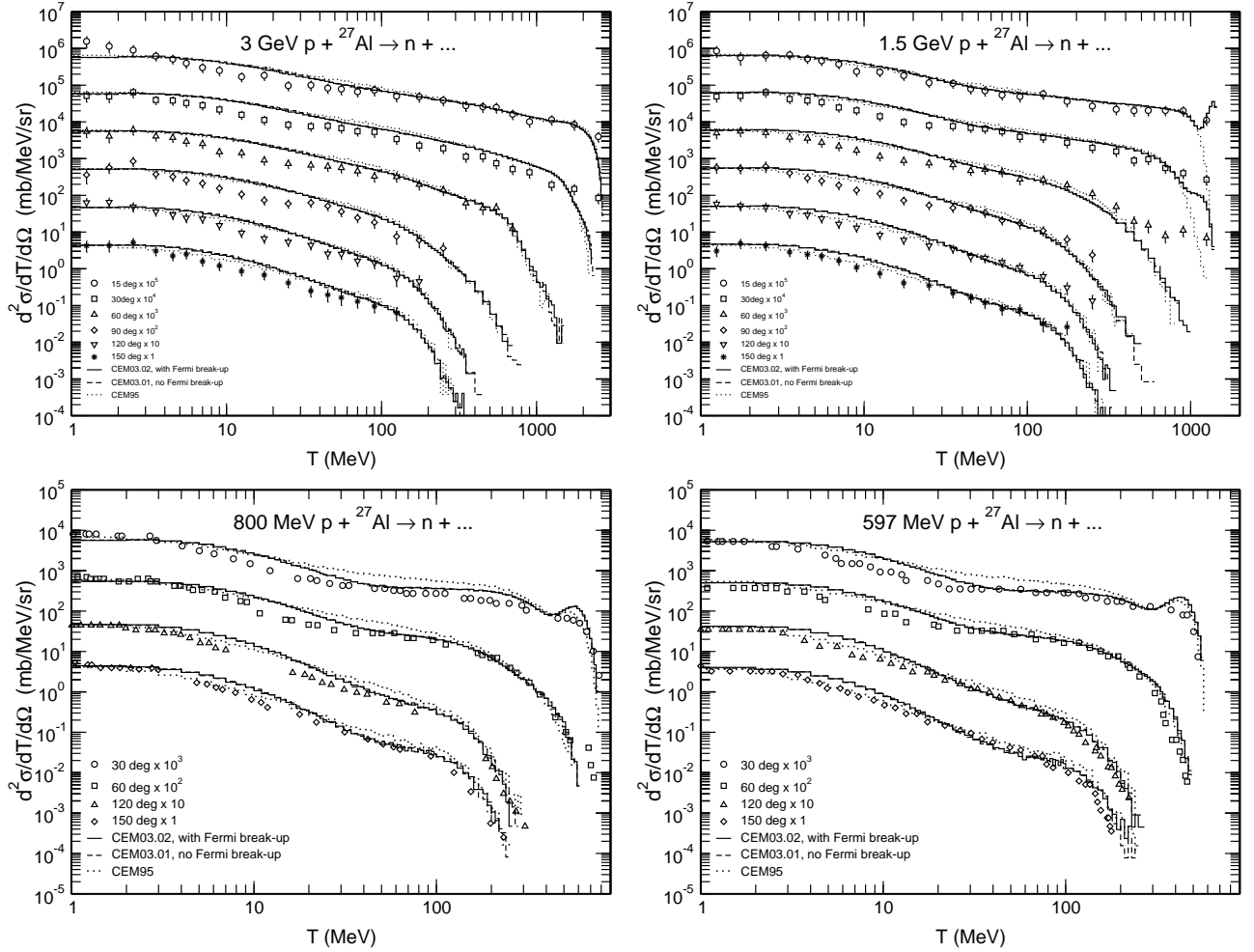


Figure 36: Experimental [182]–[184] double differential neutron spectra at 15, 30, 60, 90, 120, and 150 deg from 3.0, 1.5, 0.8, and 0.597 GeV p + Al (symbols) compared with results from CEM03.01 without considering the Fermi breakup mode during the preequilibrium and evaporation stages of reactions (dashed histograms), with CEM03.02 which does consider this mode during the preequilibrium and evaporation stages of reactions (solid histograms), and with the old version of the code, CEM95 [9].

## 9. Reactions Involving Pions and Photons; Excitation Functions

Protons from the beam and energetic secondary particles generate in ADS targets and surrounding shielding not only nucleons, complex particles, and fragments heavier than  $^4\text{He}$  (in addition to residual nuclei), but also pions of different energies. The transport codes used in ADS applications should be able to describe correctly their spectra and yields, to transport them, and to consider their further interactions with nuclei. We have shown that our event generators describe reasonably well spectra and yields of nucleon and complex particles from various reactions, and a little worse but still reasonably the yields and low energy part of spectra

of fragments heavier than  ${}^4\text{He}$ , with still retaining some unsolved problems for the high energy part of fragment spectra. Here, we demonstrate that our codes describe reasonably well also pion spectra from different reactions as well as various pion-induced reactions.

Fig. 37 shows an example of  $\pi^+$  spectra from 562.5 MeV  $n + \text{Cu}$  calculated by CEM03.01 compared with the LANL measurements by Brooks *et. al.* [185]. We see a reasonably good agreement of CEM03.01 calculations with these pion spectra. Similar results are obtained with our codes for other pion spectra (and for the integrated pion yield) measured in various reactions induced by different projectiles at different energies (see, *e.g.*, [22, 24, 42] and Fig. 12 above).

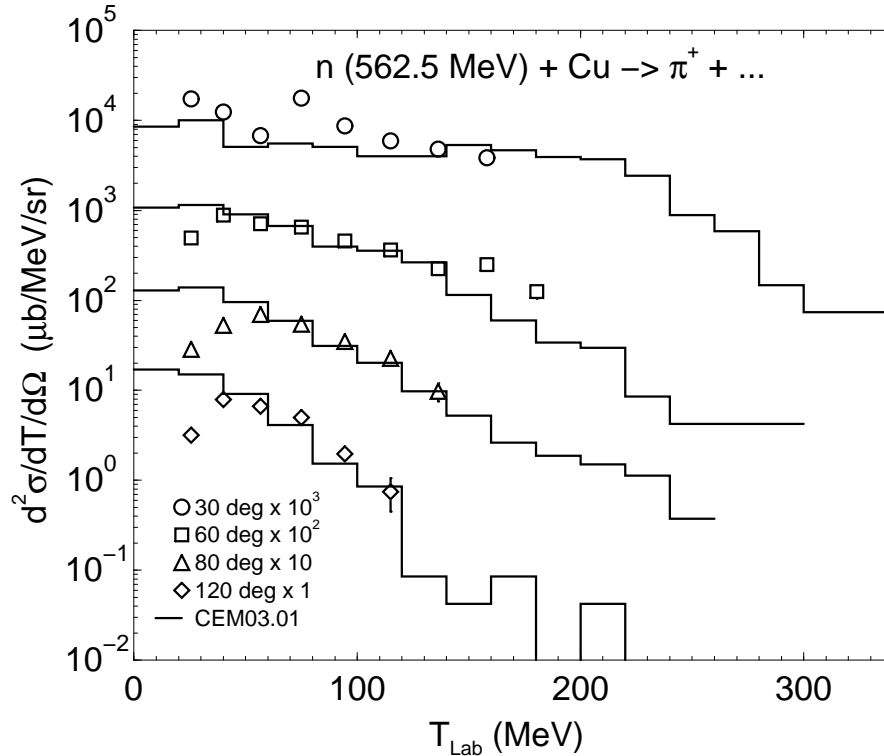


Figure 37: Experimental  $\pi^+$  spectra from 562.5 MeV  $n + \text{Cu}$  [185] compared with CEM03.01 results [23].

Fig. 38 shows an example of neutron spectra from 1.5 GeV  $\pi^+ + \text{Fe}$  calculated by CEM03.01 compared with experimental data by Nakamoto *et. al.* [186]. We see again a reasonably good agreement of our results with these measured data. We obtain similar results for other pion-induced reactions.

The secondary neutral pions produced in ADS targets and shielding materials would decay later into two photons, as their mean life is of only  $(8.4 \pm 0.6) \times 10^{-17}$  s. That is, the transport codes should transport the produced photons and our event generators should be able to describe properly their further interactions with various nuclei.

If the photon energy is above several GeV, such photonuclear interactions are calculated in transport codes using our high-energy event generator LAQGSM03.01. Several examples of results by LAQGSM03.01 for photonuclear reactions are shown in Fig. 14 of Section 3.2; more results for other high-energy photonuclear reactions may be found in Refs. [24, 88].

Interaction of photons of lower energies with nuclei are calculated in transport codes using our low-energy event generator CEM03.01. Figs. 39 and 40 show examples of proton spectra

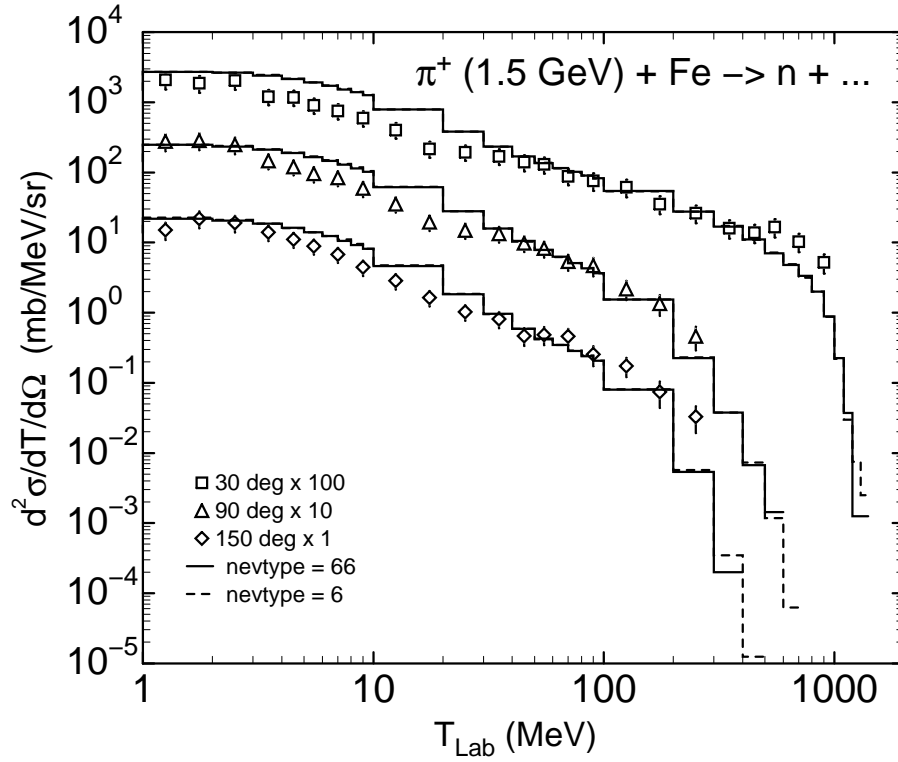


Figure 38: Experimental neutron spectra from 1.5 GeV  $\pi^+$  + Fe [186] compared with CEM03.01 results [23]. The results shown in this figure are for one million simulated inelastic events. The **nevtype=66** option (see Section 6) requires 3 hr 30 min 52 sec of computing time on a SunBlade 100, 500 MHz computer, while the **nevtype=6** option requires only 1 hr 51 min 58 sec, providing almost the same results.

from 300 MeV  $\gamma$ + $^{64}\text{Cu}$  and isotopic yields of products produced by bremsstrahlung reactions on  $^{197}\text{Au}$  and  $^{209}\text{Bi}$  at  $E_0 = 1$  GeV calculated by CEM03.01 compared with experimental data [187, 188]. Figs. 39 and 40 demonstrate that CEM03.01 allows us to describe reasonably well many photonuclear reactions needed for ADS and other applications, as well as to analyze mechanisms of photonuclear reactions for fundamental studies (see [22] for more details).

It is well known that the most difficult characteristics of nuclear reactions to be described by any theoretical model are excitation functions, *i.e.*, cross sections for the production of a given isotope as functions of the energy of the projectile. We have studied with different versions of our models several thousands of excitations functions for various reactions (see, *e.g.*, [38, 39, 76, 189, 190, 191] and references therein); therefore, we limit ourself here to analysis of only a few recent measurements published only recently [192] and calculated with CEM03.03 just the day before our present Advanced Workshop.

Figs. 41 to 43 show excitation functions for the production of  $^3\text{He}$ ,  $^4\text{He}$ ,  $^{21}\text{Ne}$ , and  $^{38}\text{Ar}$  from interactions of protons with Iron and Nickel measured recently by Ammon *et al.* [192] compared with our CEM03.03 results, with results by TALYS [193] and by INCL/ABLA [72, 195] from [192], with systematics by Konobeev and Korovin [194] (for  $^3\text{He}$  and  $^4\text{He}$  from p+Fe), with previous measurements by other authors, and with our predictions for the p+Fe excitation functions we published in 1997 [76]. On the whole, CEM03.03 is able to reproduce quite well these new measurements.

It is interesting to observe on the right panels of Figs. 41 and 42 that the CEM95 [9] version

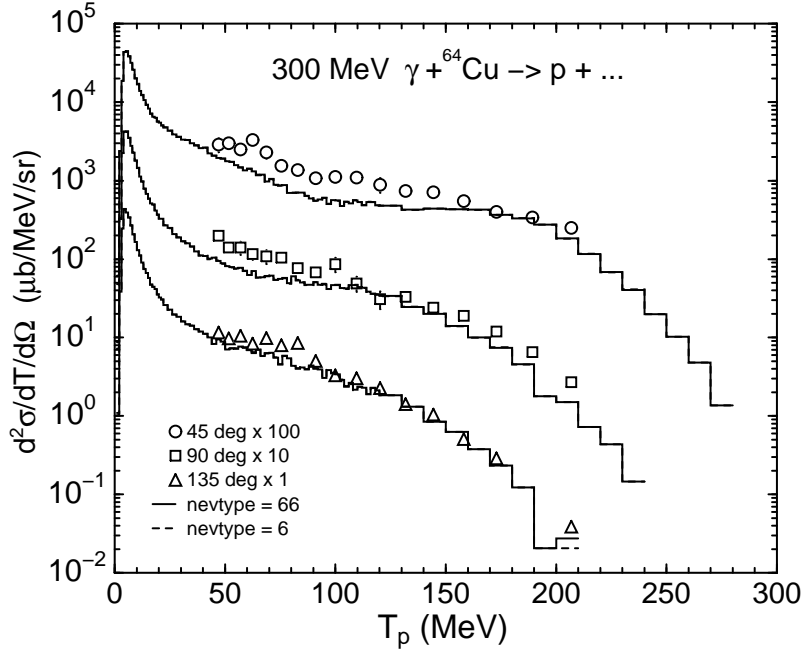


Figure 39: Proton spectra at 45°, 90°, and 135° from the reaction 300 MeV  $\gamma + {}^{64}\text{Cu} \rightarrow p + \dots$ . Symbols are experimental data from [187] and histograms are CEM03.01 results [23].

of CEM predicted these  $p+\text{Fe}$  excitation functions reasonably well: the old CEM95 predictions [76] agree quite well with the recently measured data [192].

We observe some disagreements of our results with the new data, especially for the production of  ${}^{21}\text{Ne}$  at low energies from both Fe and Ni, indicating us that there are still problems to be solved in CEM03.03 and we have to improve further our models to describe properly this type of reaction. We see that TALYS [193] and INCL/ABLA [72, 195] also encounter difficulties in reproducing these data, indicating similar problems occur with other models.

## 10. CEM03.S1, CEM03.G1, LAQGSM03.S1, and LAQGSM03.G1

From the results presented already and in the cited references, we can conclude that CEM03.01 and LAQGSM03.01 and their later 03.02 and 03.03 versions are able to predict well a large variety of nuclear reactions of interest to ADS. Therefore, they can be employed with confidence as reliable event generators in transport codes used as “workhorses” for ADS and other applications. This is true only if we are not interested in the production of intermediate-mass fragments from not too heavy targets at not too high energies, targets that do not fission from an “orthodox” point of view, therefore not producing such fragments. To be able to predict production of intermediate-mass fragments from not too heavy targets at such intermediate energies with our codes, we still need to solve some problems, just as do authors of other similar Monte-Carlo codes.

Such a problem is presented in the low-energy parts of the  $\text{Fe}(p,x){}^{21}\text{Ne}$  and  $\text{Ni}(p,x){}^{21}\text{Ne}$  excitation functions shown in Figs. 42 and 43; two more examples, for other reactions, are

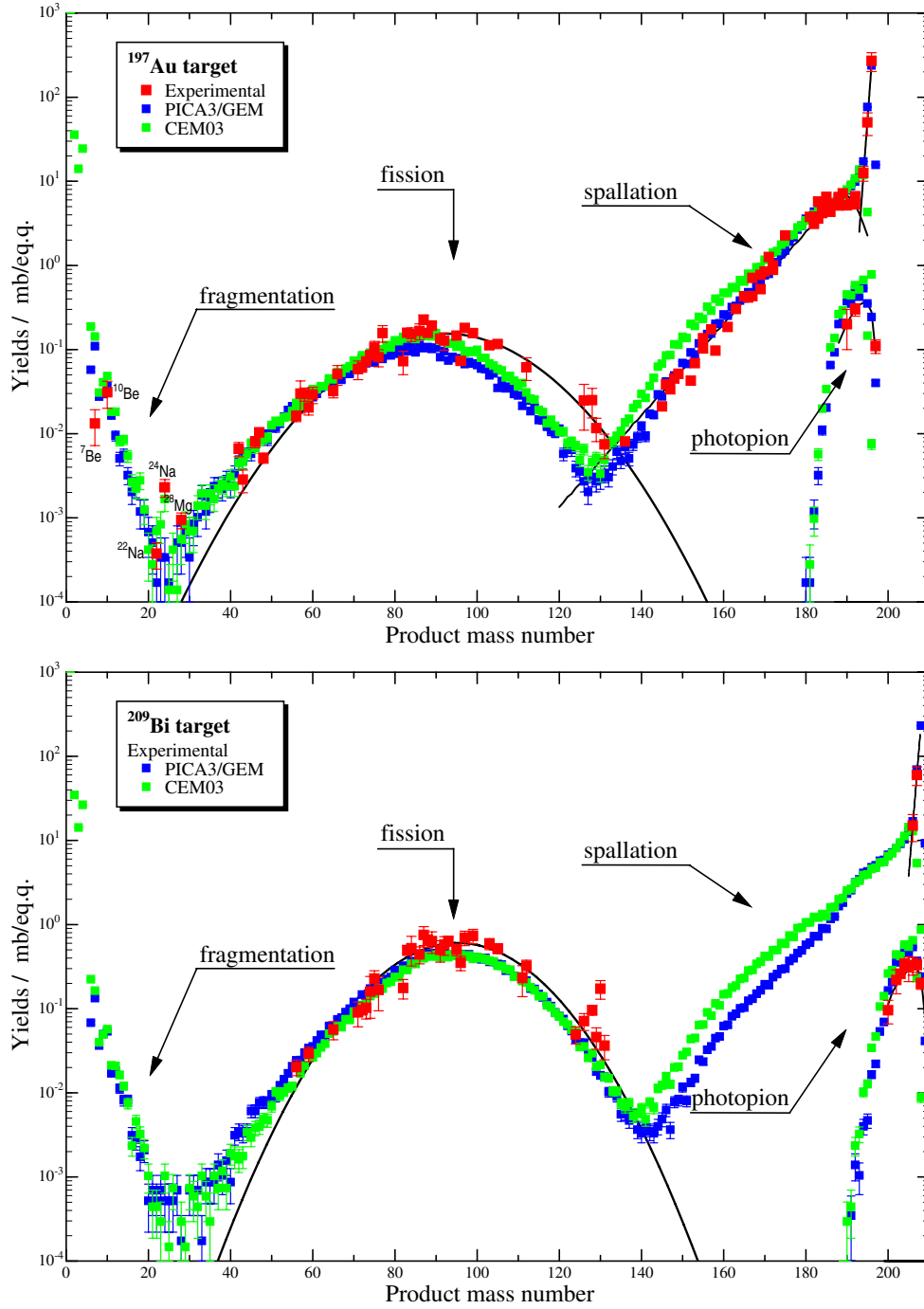


Figure 40: Comparison of CEM03.01 results (green symbols) for the isotopic yields of products produced by bremsstrahlung reactions on  $^{197}\text{Au}$  and  $^{209}\text{Bi}$  at  $E_0 = 1$  GeV with experimental data (red symbols) from the review [188] and calculations by PICA3/GEM (blue symbols); the PICA3/GEM results are from several publications and are presented in Fig. 18 of [188] with the corresponding citations. The mass yields for the fission products shown by black curves represent approximations based on experimental data by Prof. Sakamoto's group. This figure was done for us by Dr. Hiroshi Matsumura by adding our CEM03.01 results to Fig. 18 of the review [188].

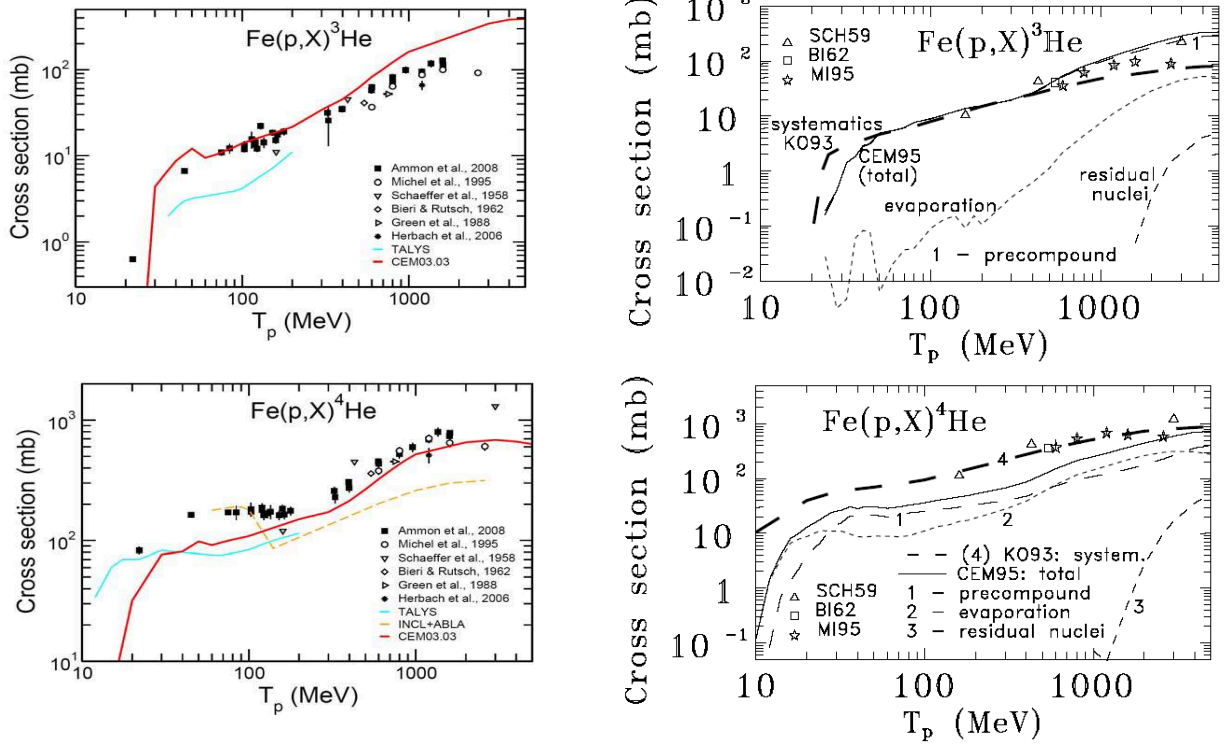


Figure 41: Excitation functions for the production of  ${}^3\text{He}$  and  ${}^4\text{He}$  from  $p+\text{Fe}$ . **Left panel:** Recent measurements by Ammon *et al.* [192] (filled squares) compared with our CEM03.03 results (red lines), with results by TALYS [193] (blue line) from [192], and with previous measurements shown with different symbols, as indicated (see references to old data in [192]). **Right panel:** The same excitation functions as on the left, but predicted twelve years ago [76] with the CEM95 version of CEM (solid lines), compared with the experimental data available at that time (see references in [76] and [192]), and with systematics by Konobeev and Korovin [194] (thick long-dashed lines). Contributions from preequilibrium emission, evaporation, and from residual nuclei to the total CEM95 yields are shown by thin dashed lines, as indicated.

indicated in Figs. 44 and 45. Fig. 44 shows the mass distribution of the product yields from the reaction 660 MeV  $p + {}^{129}\text{I}$  measured recently at JINR, Dubna [37] compared with our calculations with three recent versions of CEM. The standard version of CEM03.01 does not describe production of isotopes with mass number  $26 < A < 63$  from this reaction observed in the experiment [37]. These products are too heavy to be evaporated from compound nuclei and the target is too light to fission in GEM2, therefore not producing these isotopes as fission fragments (CEM03.01 and LAQGSM03.01 consider only “conventional” fission of preactinides and actinides and do not consider at all fission of nuclei with  $Z < 65$ ).

Fig. 45 shows a comparison [21] of the mass distributions of the yields of eight isotopes from Na to Mn produced in the reactions 1500, 1000, 750, 500, and 300 MeV/A  ${}^{56}\text{Fe} + p$  measured recently at GSI [162] with three recent versions of LAQGSM. We see that the standard version of LAQGSM03, referred as “03.01”, fails to reproduce correctly production of fission-like heavy fragments from reactions with a medium-mass nuclear target at intermediate energies (see the solid lines on the bottom two panels of Fig. 45), just as do all previous versions, the standard CEM03.01 and its predecessors, and most other currently available models (see, *e.g.*, [162, 196]). As already mentioned above, such nuclear targets are considered too light to fission in conventional codes (including GEM2 and all models currently employed in large-scale

transport codes). Similarly, the fragments are too light to be produced as spallation residues at these intermediate energies and too heavy to be produced via standard evaporation models.

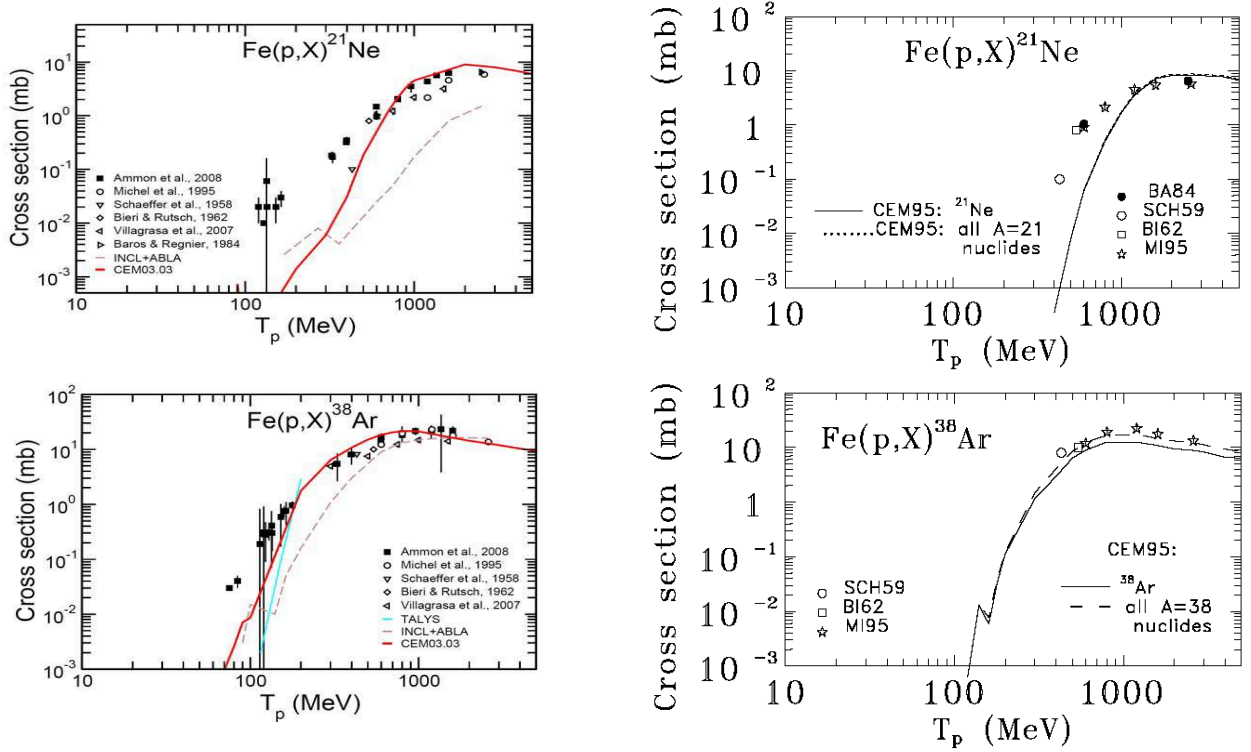


Figure 42: Excitation functions for the production of  $^{21}\text{Ne}$  and  $^{38}\text{Ar}$  from  $p+\text{Fe}$ . **Left panel:** Recent measurements by Ammon *et al.* [192] (filled squares) compared with our CEM03.03 results (red lines), with results from TALYS [193] (blue solid line), and from INCL/ABLA [72, 195] (dashed brown line) from [192], and with previous measurements shown with different symbols, as indicated (see references to old data in [192]). **Right panel:** The same excitation functions as on the left, but predicted twelve years ago [76] with the CEM95 version of CEM, compared with experimental data available at that time (see references in [76] and [192]), as indicated.

We note that the problem of a reliable description of intermediate-mass fragments from not too heavy targets is still unresolved not only in our standard versions of CEM and LAQGSM, but also in most other similar Monte-Carlo codes. Fig. 46 and 47 prove this with an example of comparison [191] the mass distributions of  $^{56}\text{Fe}(p,x)$  reaction products measured at ITEP [191] and GSI [162] at 300 and 1000 MeV energies with results from 15 different code systems: MCNPX (INCL, CEM2k, BERTINI, ISABEL), LAHET (BERTINI, ISABEL), CEM03 (.01, .G1, .S1), LAQGSM03 (.01, .G1, .S1), CASCADE-2004, LAHETO, and BRIEFF (see references and details in [191]). We see that all these models give a sufficiently good description of the mass yields of the products close to target nucleus mass ( $A > 35\text{--}40$ ). In the mass range  $A < 30$ , however, a good description of the measured product nuclide yields is only given by the models that, apart from the conventional evaporation of nucleons and complex particles up to  $^4\text{He}$ , allow for evaporation of heavy clusters (the CEM and LAQGSM versions).

We also note that none of these models gives a good quantitative description of the whole set of experimental data. However, as can be seen from Fig. 47, while still having these problems, our CEM and LAQGSM codes provide the lowest mean deviation factors between the calculated

and measured [162, 191] cross sections, averaged over all energies of the beams and detected products in comparison with other models (see more details in [191]).

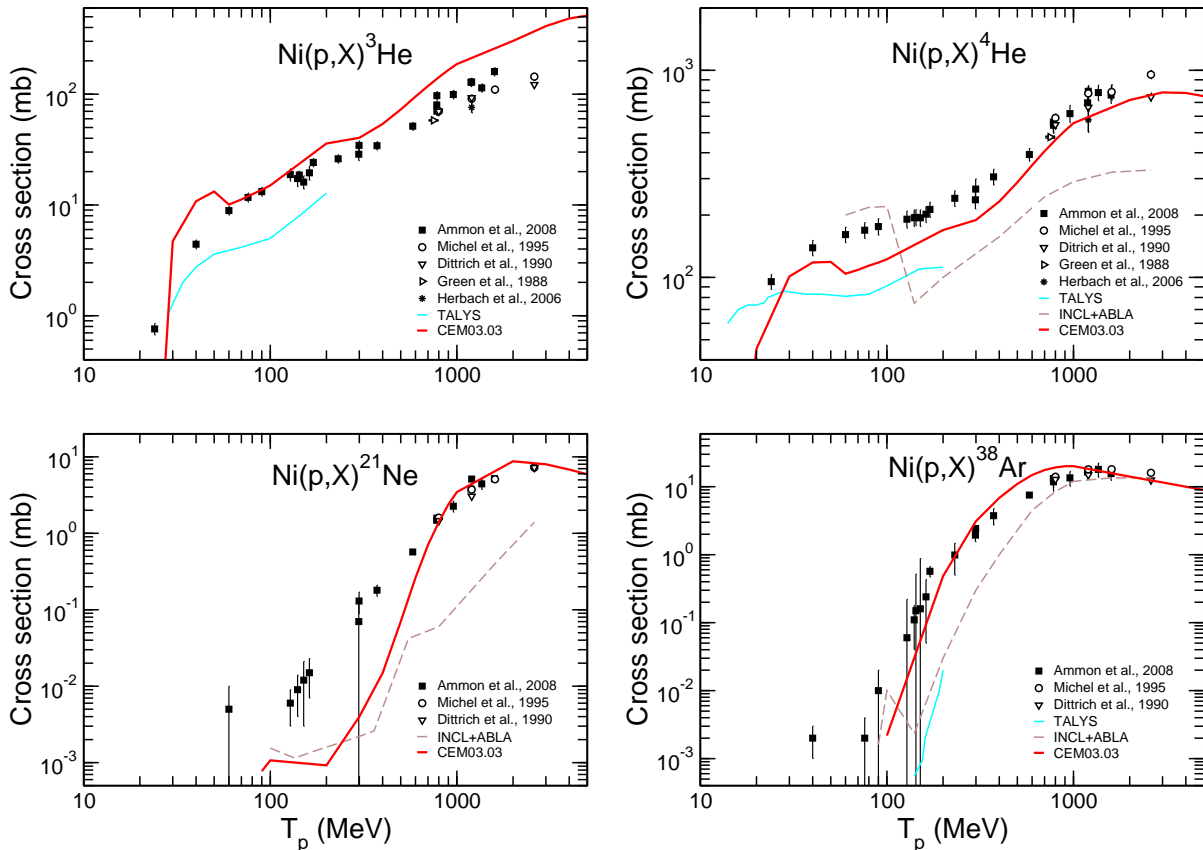


Figure 43: Excitation functions for the production of  ${}^3\text{He}$ ,  ${}^4\text{He}$ ,  ${}^{21}\text{Ne}$  and  ${}^{38}\text{Ar}$  from  $p + \text{Ni}$ . Recent measurements by Ammon *et al.* [192] (filled squares) compared with our CEM03.03 results (red lines), with results from TALYS [193] (blue solid line), and from INCL/ABLA [72, 195] (dashed brown line) from [192], and with previous measurements shown with different symbols, as indicated (see references to old data in [192]).

We have addressed this problem in two different ways [21, 97, 196]:

1) By implementing into CEM03.01 and LAQGSM03.01 the Statistical Multifragmentation Model (SMM) by Botvina *et al.* [155], [197]–[201], to consider multifragmentation as a mode competitive to evaporation of particles and light fragments, when the excitation energy  $E^*$  of a compound nucleus produced after the preequilibrium stage of a reaction is above  $2 \times A$  MeV. This way, we have produced the “S” version of our codes (“S” stands for SMM), CEM03.S1 and LAQGSM03.S1.

CEM03.S1 and LAQGSM03.S1 are exactly the same as CEM03.01 and LAQGSM03.01, but consider also multifragmentation of excited nuclei produced after the preequilibrium stage of reactions, when their excitation energy is above  $2 \times A$  MeV, using SMM. In SMM, within the total accessible phase space, a micro-canonical ensemble of all breakup configurations, composed of nucleons and excited intermediate-mass fragments governs the disassembly of the hot remnant. The probability of different channels is proportional to their statistical weight. Several different breakup partitions of the system are possible. When after the preequilibrium stage of a reaction  $E^* > 2 \times A$  MeV and we “activate” SMM to calculate multifragmentation

in the 03.S1 codes, the competitive evaporation process are calculated also with a version of the evaporation model by Botvina *et al.* from SMM, rather than using GEM2, as we do always in the standard 03.01 versions and in 03.S1 when  $E^* \leq 2 \times A$  MeV and SMM is not invoked.

A very detailed description of SMM together with many results obtained for many reactions may be found in [155], [197]–[201] and references therein; many details on SMM are presented in the first paper of Ref. [97], therefore we do not repeat this here.

2) By replacing the Generalized Evaporation Model GEM2 by Furihata [144]–[146] used in CEM03.01 and LAQGSM03.01 with the fission-like binary-decay model GEMINI of Charity [202]–[207] which considers production of all possible fragments. This way, we have produced the “G” version of our codes (“G” stands for GEMINI), CEM03.G1 and LAQGSM03.G1.

CEM03.G1 and LAQGSM03.G1 are exactly the same as CEM03.01 and LAQGSM03.01, but use GEMINI instead of using GEM2. Within GEMINI, a special treatment based on the Hauser-Feshbach formalism is used to calculate emission of the lightest particles, from neutrons and protons up to beryllium isotopes. The formation of heavier nuclei than beryllium is modeled according to the transition-state formalism developed by Moretto [208]. All asymmetric divisions of the decaying compound nuclei are considered in the calculation of the probability of successive binary-decay configurations. GEMINI is described in details in the original publications [202]–[208]; many details on GEMINI may be found also in the first paper of Ref. [97], therefore we do not elaborate here.

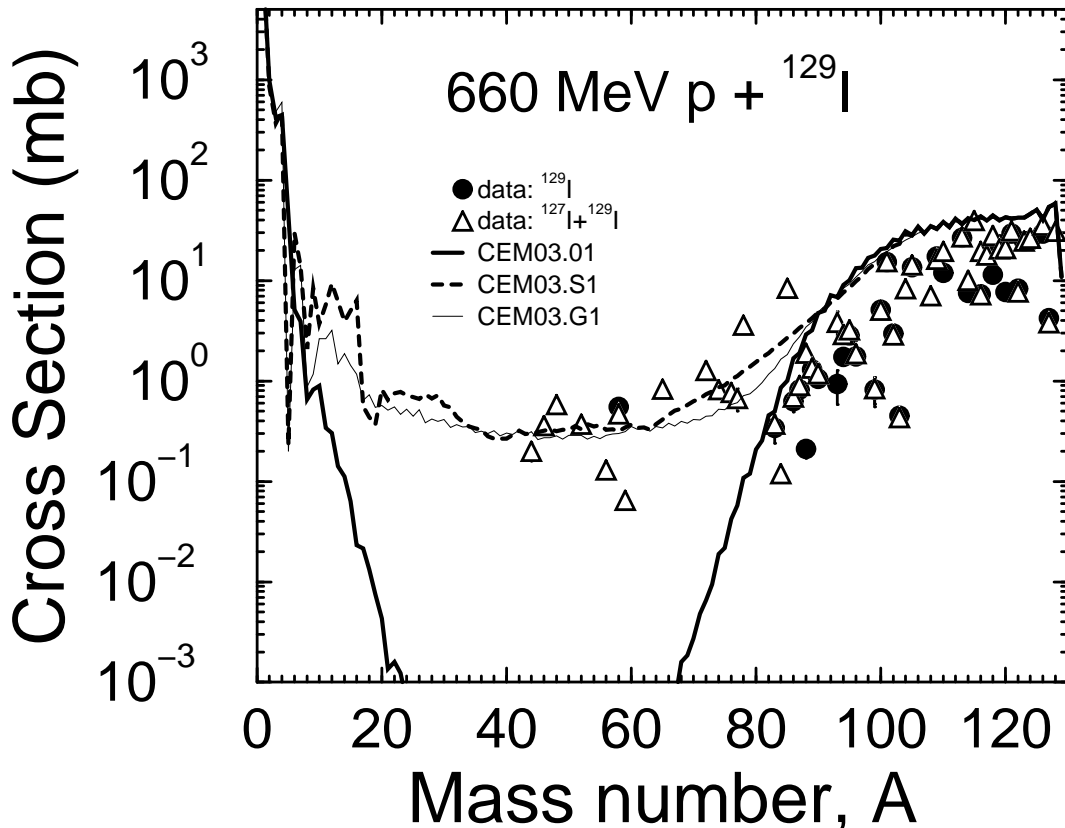


Figure 44: Experimental [37] mass number distribution of the product yield from 660 MeV p +  $^{129}\text{I}$  compared with calculations by CEM03.01 (thick solid line), CEM03.S1 (thick dashed line), and CEM03.G1 (solid thin line), as indicated

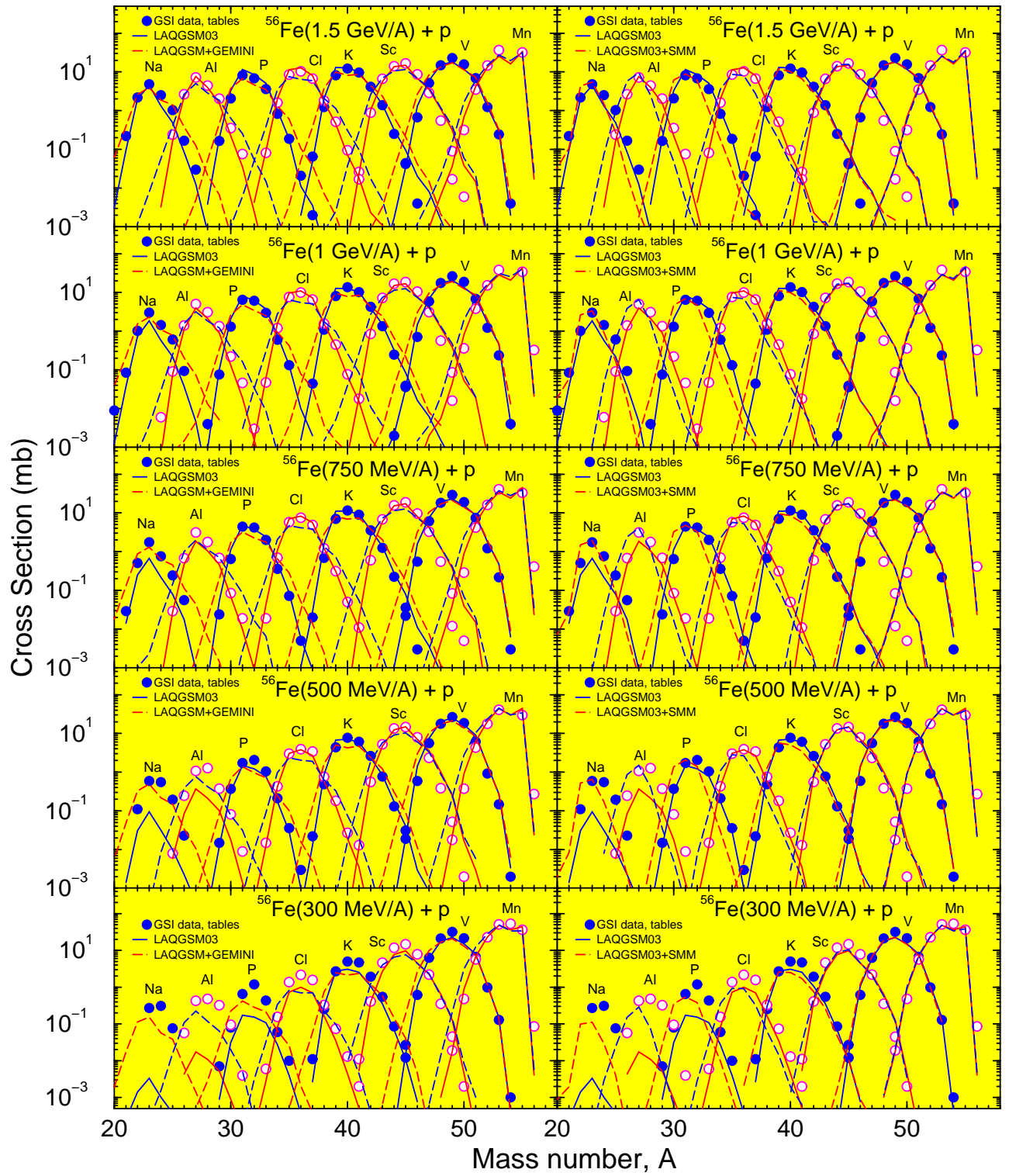


Figure 45: Experimental [162] mass distributions of the yields of eight isotopes from Na to Mn produced in the reactions 1500, 1000, 750, 500, and 300 MeV/A  $^{56}\text{Fe} + p$  compared with LAQGSM03 (solid lines on both panels), LAQGSM03+GEMINI (dashed lines, left panel), and LAQGSM03+SMM (dashed lines, right panel) results, respectively.

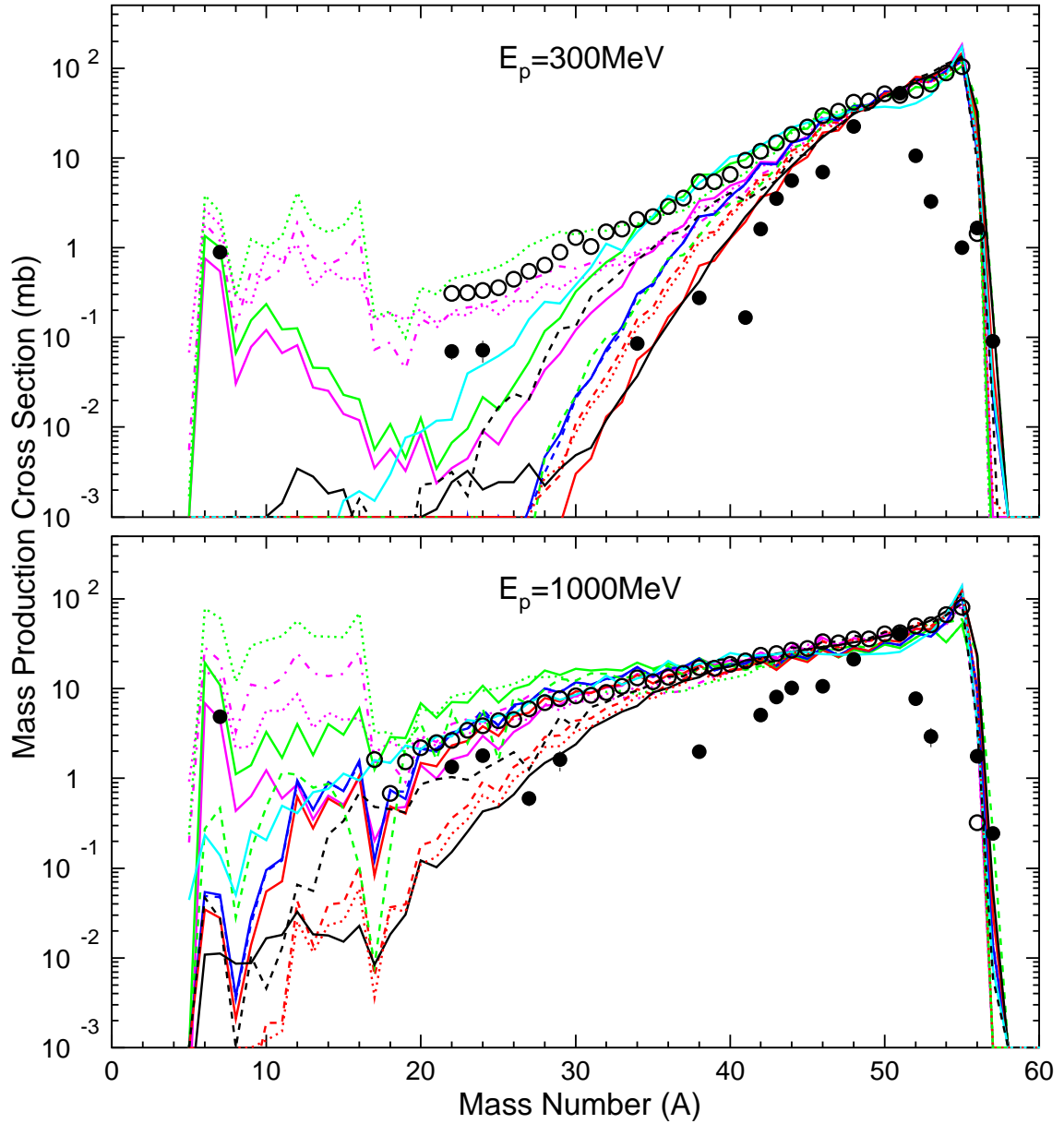


Figure 46: Mass distributions of  $^{56}\text{Fe}(p,x)$  reaction products measured at ITEP (filled circles) [191] and GSI (open circles) [162] for 300 and 1000 MeV energies compared with results by 14 codes shown with different lines as following: INCL/MCNPX (solid black), BRIEFF1.5.4g (dashed black), CEM03.01 (solid green), CEM2k/MCNPX (dashed green), CEM03.G1 (dotted green), BERTINI (MCNPX - solid blue, LAHET - dashed blue), ISABEL (MCNPX - solid red, LAHET - dashed red, LAHETO - dotted red), LAQGSM03.01 (solid magenta), LAQGSM03.G1 (dotted magenta), LAQGSM03.S1 (dashed-dotted magenta), CASCADE-2004 (cyan). This figure is adopted from Ref. [191], where more details on this comparison may be found.

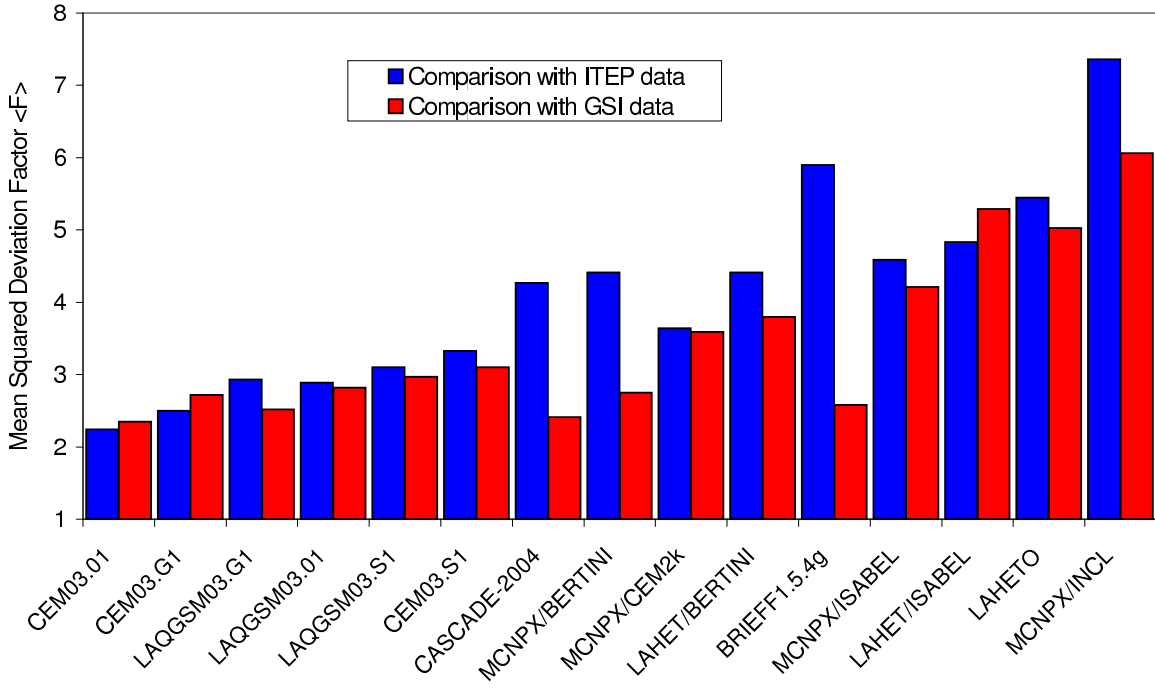


Figure 47: The predictive power of each tested code for the data shown in Fig. 46: the mean-square deviation factors between calculations and measured cross sections averaged over all energies and all products (see details in [191]).

Results by “S” and “G” versions of our codes are shown together with standard 03.01 results in Figs. 44, 45, and 46 (see also Figs. 28 and 29 in Section 6). We see that both “S” and “G” versions reproduce almost equally well the yields of intermediate-mass fragments from these reactions, that can not be described by the standard CEM03.01 and LAQGSM03.01.

From one point of view, this is an achievement, as, with the “S” and “G” versions, we are able to describe reasonably well the reactions where the standard 03.01 versions do not work. On the other hand, this also makes the situation more intricate, as from these (and other similar) results we can not choose easily between the “S” and “G” versions, that makes more difficult to determine the real mechanisms of such reactions. We think that for such intermediate-energy proton-induced reactions the contribution of multifragmentation to the production of heavy fragments should not be very significant due to the relatively low excitation energies involved. Such fragments are more likely to be produced via the fission-like binary decays modeled by GEMINI. Multifragmentation processes are important and should be considered in reactions involving higher excitation energies; at excitations probably higher than the 2 MeV/nucleon considered here. We conclude [21] that it is impossible to make a correct choice between fission-like and fragmentation reaction mechanisms involved in these (or other similar) reactions merely by comparing model results with the measurements of only product cross sections; addressing this question will probably require analysis of two- or multi-particle correlation measurements. Our conclusion [21] was confirmed by the recent coincidence measurements and calculations of residual and light particles in 1 GeV/A  $^{56}\text{Fe} + \text{p}$  by Gentil *et al.* [209, 210].

Several more examples of the difficult situation with determination of the mechanisms of fragment production from reactions induced by intermediate-energy projectiles using the “S” and “G” versions of our codes are presented below in Figs. 48 to 51.

Fig. 48 shows data recently measured at GSI [211] on mass- and charge-product yield distributions and mean kinetic energies of all products as a function of the product mass

number from the reaction 1 GeV/nucleon  $^{136}\text{Xe} + p$  compared with calculations by the standard CEM03.03 and LAQGSM03.03, as well as by their “S” versions. More results for this reaction may be found in Ref. [212]. We see that the standard 03.03 versions of both CEM and LAQGSM codes fail to reproduce production of intermediate mass fragments with  $20 < A < 70$  from this reaction. With the “S” versions, we performed calculations for several different values of the excitations energy  $E^*$  of the nuclei produced after the preequilibrium stage of reactions when we start to consider multifragmentation as a competitive to evaporation mechanism of nuclear reactions, namely, at  $E^* > 2, 4, 4.5$ , and 5 MeV/nucleon in the case of CEM03.S1, and  $E^* > 1.5, 2$ , and 4 MeV/nucleon for LAQGSM03.S1. We see that the best agreement of results by LAQGSM03.S1 (solid red lines in Fig. 48) with the GSI data [211] were achieved for  $E^* > 2$  MeV/nucleon, just as Dr. Botvina suggested to us and how it was implemented in both LAQGSM03.S1 and CEM03.S1 versions of our codes. But in the case of CEM03.S1 (solid blue lines in Fig. 48), we got the best agreement with the data for a higher energy, namely  $E^* > 4.5$  MeV/nucleon.

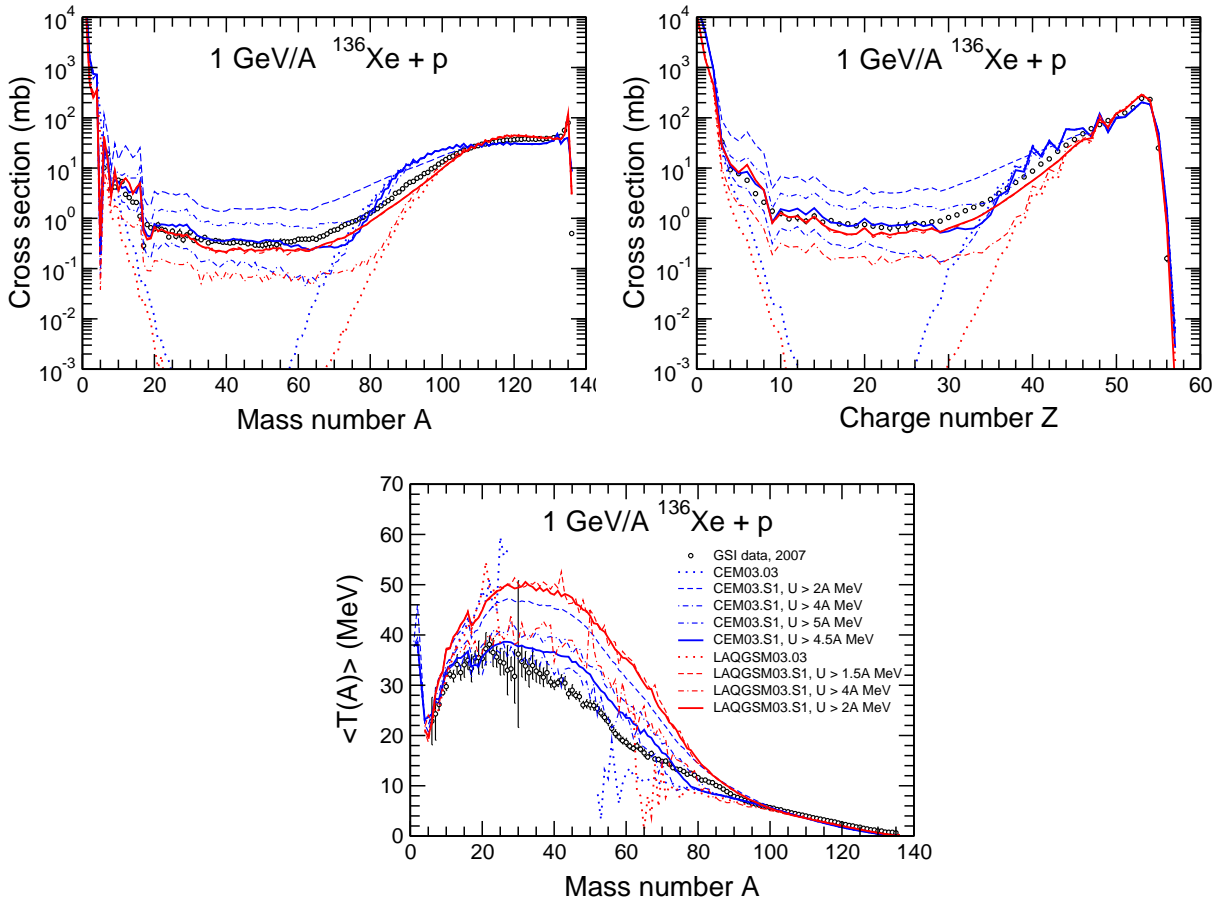


Figure 48: Mass- and charge-product yield distributions and mean kinetic energy of all products as functions of the product mass number from the reaction 1 GeV/nucleon  $^{136}\text{Xe} + p$  [211] (open circles) recently measured at GSI compared with calculations by the standard CEM03.03 and LAQGSM03.03 (dotted lines), as well as by their “S” versions (solid and dot-dashed lines) for different values of the excitations energy  $E^*$  of the nuclei produced after the preequilibrium stage of reactions above which we start to consider multifragmentation as a competitive reaction mechanism, namely, at  $E^* > 2, 4, 4.5$ , and 5 MeV/nucleon in the case of CEM03.S1, and  $E^* > 1.5, 2$ , and 4 MeV/nucleon for LAQGSM03.S1, as indicated.

The fact that we get different “best” values of  $E^*$  when we need to “activate” multifragmentation as a competition to the simple evaporation mechanism in different codes is not contradictory and does imply anything physical: The INC of CEM is completely different from the one of LAQGSM, therefore the mean mass  $\langle A \rangle$  and charge number  $\langle Z \rangle$  of residual nuclei produced after the preequilibrium stage of a reaction with an excitation  $E^*$  higher than a certain values, *e.g.*, 2 MeV/nucleon, should be also different, as should be the distributions of such nuclei with respect to their  $E^*$ . This results in turn in different fragments produced via multifragmentation from this reaction as predicted by CEM03.S1 and LAQGSM03.S1. If we would use another INC, *e.g.*, INCL [72], followed or not by preequilibrium emission, we would get still another “best” value of  $E^*$  when we need to start considering multifragmentation, as another INC would predict other values of  $\langle A \rangle$ ,  $\langle Z \rangle$ , and distributions of  $E^*$ . This makes the situation of considering multifragmentation by different codes more intricate: the condition of its “activation” seems to be model-dependent.

This situation becomes even more unclear if we refer to the results shown in Fig. 49; the same data [211] can be reproduced, even a little better, with the “G” versions of our codes, without considering multifragmentation at all.

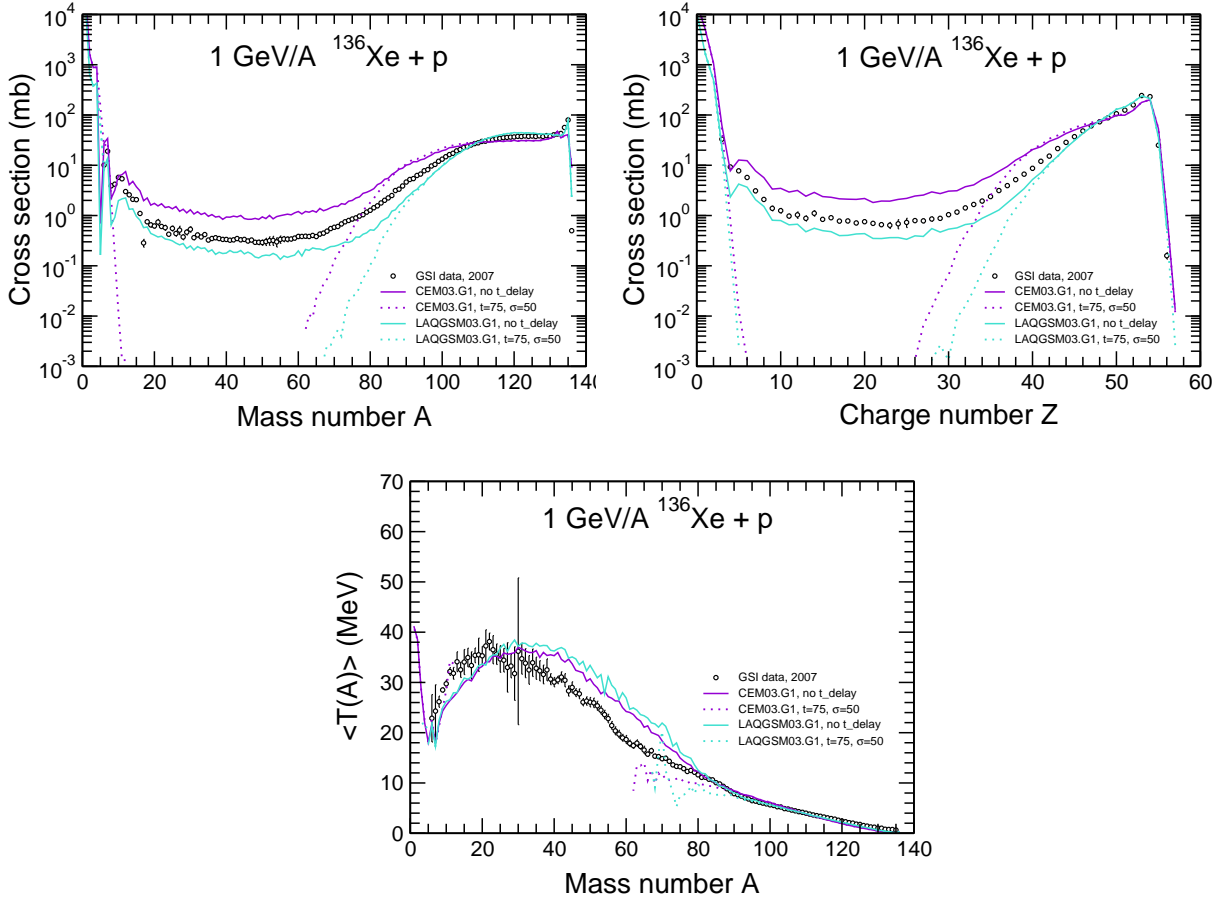


Figure 49: The same experimental data [211] as in previous figure, but compared with results of calculations by CEM03.G1 (violet lines) and LAQGSM03.G1 (turquoise lines), as indicated.

As described above, CEM03.G1 and LAQGSM03.G1 are exactly the same as CEM03.01 and LAQGSM03.01, only replacing GEM2 [144]–[146] with GEMINI [202]–[207]. As can be seen from Figs. 28, 29, 49, 50, and from results presented in Refs. [97, 196, 212], the “G”

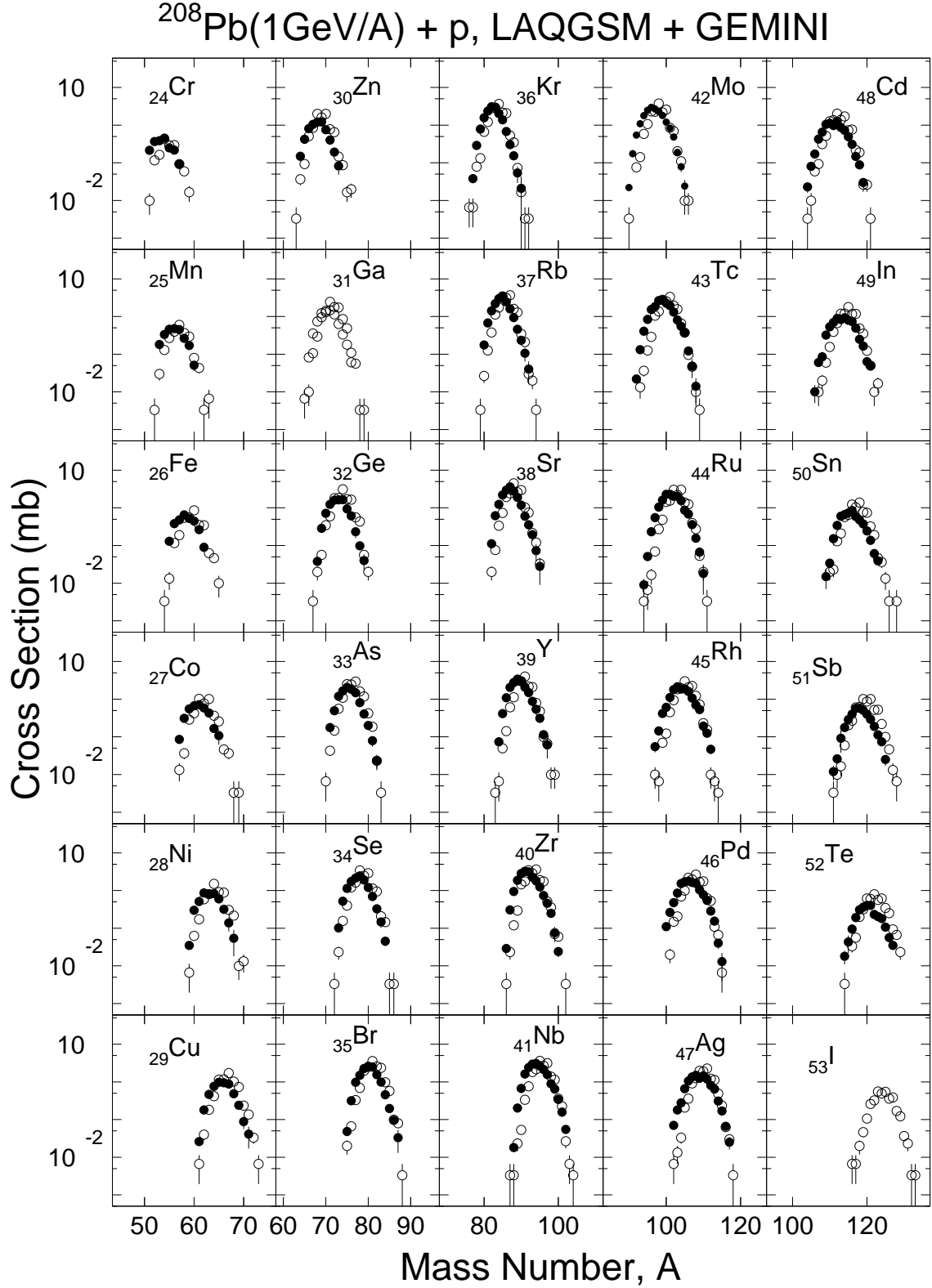


Figure 50: Comparison of all measured [213] cross sections of fission products from the reaction 1 GeV/nucleon  $^{208}\text{Pb}$  on  $p$  (filled circles) with LAQGSM+GEMINI (LAQGSM03.G1) results (open circles). Experimental data for isotopes of Ga and I are not available, so we present only our predictions.  $t_{\text{delay}} = 75$  and  $\text{sig\_delay} = 50$  are used in GEMINI to calculate this reaction.

version of our codes allows us to describe well many fission and fragmentation reactions, especially on targets below the actinide region, where the standard versions of our codes using GEM2 may not work well.

We find that: 1) GEMINI merged with CEM or LAQGSM provides reasonably good results for medium-heavy targets without a fission delay time; 2) For preactinides, we have to use  $t_{\text{delay}} = 50\text{--}70$  and  $\text{sig\_delay} = 1\text{--}50$ , otherwise GEMINI provides too much fission—this may be related to the calculation of fission barriers of preactinides without strong ground-state shell corrections in the 2002 version of GEMINI we use; 3) The current version of GEMINI does not work well for low-energy fission of actinides (see Fig. 51).

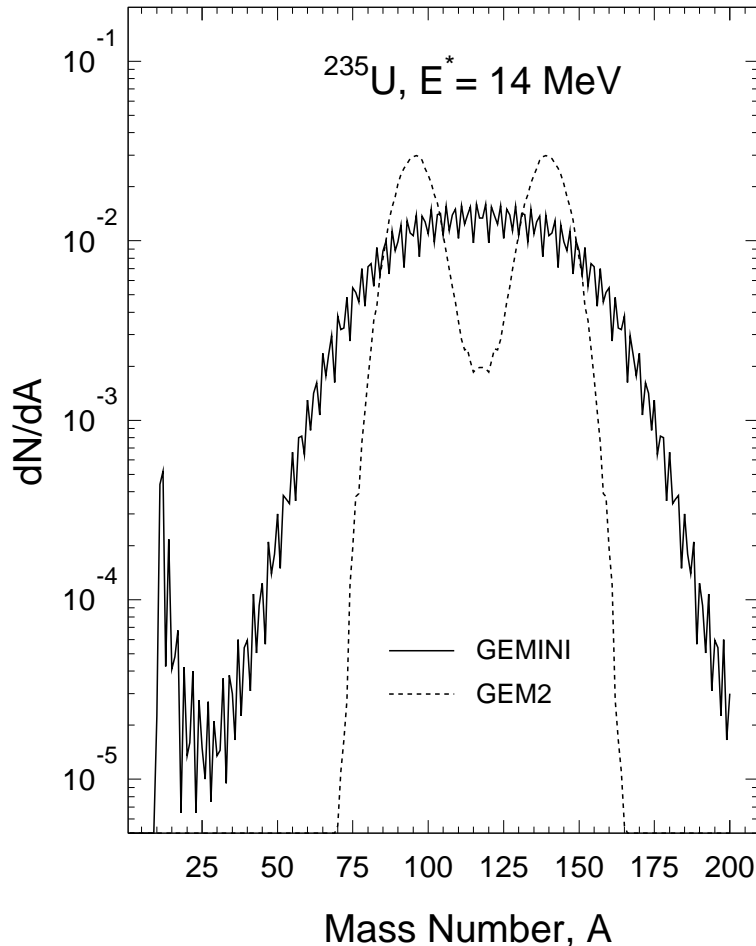


Figure 51: Mass distributions of fission fragments from the compound nucleus  $^{235}\text{U}$  with an excitation of 14 MeV as predicted by GEMINI (solid line) and GEM2 (dashed line), respectively (adopted from [196]). No delay time in GEMINI for fission is used here.

The physical basis of these shortcomings of GEMINI are understood and are discussed along with possible solutions to be employed in future versions of GEMINI by Dr. Charity at this Workshop [207].

## 11. Summary

Improved versions of the cascade-exciton model of nuclear reactions and of the Los Alamos quark-gluon string model have been developed recently at LANL and implemented in the codes

CEM03.01 and LAQGSM03.01, and in their slightly corrected 03.02 and 03.03 versions. The recent versions of our codes describe quite well and much better than their predecessors a large variety of nuclear reactions of interest to ADS, as well as reactions at higher energies of interest to NASA, accelerator shielding, astrophysics, and other applications, up to  $\sim 1$  TeV/nucleon. (Energies above about 5 GeV are only accessible to LAQGSM.)

What is more, our codes provide reasonable results even for low-energy reactions, where they are not easy to justify from a fundamental physics point of view (see e.g., [21]).

We observe that codes developed for applications must not only describe reasonably well arbitrary reactions without any free parameters, but also not require too much computing time. Our own exercises on many different nuclear reactions with MCNPX [52] and LAHET [114, 131] transport codes using different event generators show that the current version of CEM is a little faster than the Bertini [173] and ISABEL [174] options for INC in these transport codes, and is several times faster than the INCL/ABLA [72, 195] option. The computing time of LAQGSM for heavy-ion reactions was tested recently by Dr. Gomez [214] with MCNPX in comparison with PHITS [215], on simulations of a 400 MeV/nucleon uranium beam on a 0.2-cm thick lithium target. He found that PHITS using the Quantum Molecular Dynamics (QMD) model to simulate heavy-ion reactions requires 210 times more computing time than LAQGSM does, making it very difficult if not impossible to use in applications requiring fast results, for example in real-time beam monitoring of positron emitting fragments used for PET tomography in heavy-ion cancer therapy; LAQGSM does not have these problems, providing quite fast and reliable results.

Both our CEM and LAQGSM event generators still have some problems in a reliable description of some fragments from intermediate-energy nuclear reactions on medium-mass nuclei, just as other similar modern Monte-Carlo codes do. To address these problems, we developed “S” and “G” modifications of our codes, that consider multifragmentation of nuclei formed after the preequilibrium stage of reactions when their excitation energy is above  $2-5 \times A$  MeV using the Statistical Multifragmentation Model (SMM) code by Botvina *et al.* [155], [197]–[201], and the fission-like binary-decay model GEMINI by Charity [202]–[207], respectively. The “S” and “G” versions of our codes allow us to describe many fragmentation reactions that we are not able to reproduce properly with the standard version of our codes. However, there are still some problems to be solved in understanding the “true” mechanisms of fragment productions from many reactions, therefore we consider the present “S” and “G” versions of our codes only as working modifications and they are not yet implemented as event generators into our transport codes, in contrast to our “standard” 03.01, 03.02, and 03.03 versions used as event generators.

The latest versions of our 03.01, 03.02, and 03.03 CEM and LAQGSM codes have been or are being incorporated as event generators into the transport codes MCNP6 [216], MCNPX [52], and MARS [51]. CEM03.01 was made available to the public via RSICC at Oak Ridge and NEA/OECD in Paris as the Code Package PSR-0532. We also plan to make LAQGSM03.01 and the latest 03.03 versions of our codes available to the public via RSICC and NEA/OECD in the future.

## Acknowledgments

We thank the Organizers of this Workshop, especially Dr. Sylvie Leray, for inviting us to present these lectures and for financial support. We are grateful to ICTP and IAEA for kind hospitality. These lectures were written with support from the US Department of Energy.

## References

- [1] K. K. Gudima, S. G. Mashnik, and V. D. Toneev, JINR Communications P2-80-774 and P2-80-777, Dubna (1980).
- [2] K. K. Gudima, S. G. Mashnik, and V. D. Toneev, Nucl. Phys. **A401** (1983) 329–361.
- [3] V. S. Barashenkov and V. D. Toneev, *Interaction of High Energy Particle and Nuclei with Atomic Nuclei*, Atomizdat, Moscow (1972).
- [4] V. S. Barashenkov *et al.*, Usp. Fiz. Nauk **109**, (1973) 91–136 [Sov. Phys. Usp. **16** (1973) 31–52].
- [5] K. K. Gudima, G. A. Ososkov, and V. D. Toneev, Yad. Fiz. **21** (1975) 260–272 [Sov. J. Nucl. Phys. **21** (1975) 138–143].
- [6] S. G. Mashnik and V. D. Toneev, JINR Communication P4-8417, Dubna (1974).
- [7] T. Gabriel, G. Maino, and S. G. Mashnik, JINR Preprint E2-94-424, Dubna (1994); Proc. XII Int. Sem. on High Energy Phys. Problems *Relativistic Nuclear Physics & Quantum Chromodynamics*, Dubna, Russia, September 12–17, 1994, Eds. A. M. Baldin and V. V. Burov, Dubna, JINR Publish Department, 1997, JINR E1,2-97-79, pp. 309–318.
- [8] S. G. Mashnik, Izv. RAN, Ser. Fiz. **60** (1996) 73–84 [Bull. of the Russian Acad. Sci., Physics, **60** (1996) 58–67].
- [9] S. G. Mashnik, *User Manual for the Code CEM95*, (1995), Bogoliubov Laboratory of Theoretical Physics, Joint Institute for Nuclear Reserach, Dubna, Russia; OECD Nuclear Energy Agency Data Bank, Le Seine Saint-Germain 12, Boulevard des Iles, F-92130 Issy-les-Moulineaux, Paris, France <http://www.nea.fr/abs/html/iaea1247.html>; Radiation Safety Information Computational Center (RSICC), Oak Ridge, USA, <http://www-rsicc.ornl.gov/codes/psr/psr3/psr-357.html>.
- [10] M. Blann, H. Gruppelaar, P. Nagel, and J. Rodens, *International Code Comparison for Intermediate Energy Nuclear Data*, NEA OECD, Paris (1994).
- [11] P. Nagel, J. Rodens, M. Blann, and H. Gruppelaar, Nucl. Sci. Eng. **119** (1995) 97–107.
- [12] S. G. Mashnik *et al.*, LANL Report LA-UR-07-6198; E-print: arXiv:0709.173v1 [nucl-th] 12 Sep 2007.
- [13] K. K. Gudima, S. G. Mashnik, A. J. Sierk, LANL Report LA-UR-01-6804, Los Alamos, 2001.
- [14] N. S. Amelin, K. K. Gudima, V. D. Toneev, Sov. J. Nucl. Phys. **51** (1990) 327–333; [Yad. Fiz. **51** (1990) 512–523]. Sov. J. Nucl. Phys. **51** (1990) 1093–1101; [Yad. Fiz. **51** (1990) 1730–1743]. Sov. J. Nucl. Phys. **52** (1990) 1722–178, [Yad. Fiz. **52** (1990) 272–282], and references therein.
- [15] S. G. Mashnik and A. J. Sierk, LANL Report LA-UR-98-5999 (1998); E-print: nucl-th/9812069; Proc. SARE-4, Knoxville, TN, September 13–16, 1998, edited by Tony A. Gabriel (ORNL, 1999), pp. 29–51.
- [16] A. J. Sierk and S. G. Mashnik, LANL Report LA-UR-98-5998 (1998); E-print: nucl-th/9812070; Proc. SARE-4, Knoxville, TN, September 13–16, 1998, edited by Tony A. Gabriel (ORNL, 1999), pp. 53–67.
- [17] S. G. Mashnik and A. J. Sierk, Proc. AccApp00, November 12–16, 2000, Washington, DC (USA), ANS, La Grange Park, IL, 2001, pp. 328–341; E-print: nucl-th/0011064.

- [18] S. G. Mashnik, K. K. Gudima, and A. J. Sierk, LANL Report LA-UR-03-2261, Los Alamos (2003); E-print: nucl-th/0304012; Proc. SATIF-6, April 10–12, 2002, Stanford Linear Accelerator Center, CA 94025, USA, (NEA/OECD, Paris, France, 2004), pp. 337–366.
- [19] S. G. Mashnik, A. J. Sierk, and K. K. Gudima, LANL Report LA-UR-02-5185, Los Alamos (2002); E-print: nucl-th/0208048.
- [20] M. Baznat, K. Gudima, and S. Mashnik, LANL Report LA-UR-03-3750, Los Alamos (2003); Proc. AccApp03, San Diego, California, June 1–5, 2003, (ANS, La Grange Park, IL 60526, USA, 2004), pp. 976–985; E-print: nucl-th/0307014.
- [21] S. G. Mashnik *et al.*, LA-UR-05-0711, Los Alamos (2005); E-print: nucl-th/0502019; Proc. ND2004, September 26–October 1, 2004, Santa Fe, NM, USA, edited by R. C. Haight, M. B. Chadwick, T. Kawano, and P. Talou, (AIP Conf. Proc. **769**, Melville, New York, 2005), pp. 1188–1192.
- [22] S. G. Mashnik *et al.*, LANL Report LA-UR-05-2013, Los Alamos (2005), E-print: nucl-th/0503061; J. Nucl. Radiochem. Sci. **6** (2005) A1–A19.
- [23] S. G. Mashnik *et al.*, LANL Report LA-UR-05-7321, Los Alamos (2005); RS-ICC Code Package PSR-532; <http://www-rsicc.ornl.gov/codes/psr/psr5/psr532.html>; <http://www.nea.fr/abs/html/psr-0532.html>.
- [24] S. G. Mashnik *et al.*, LANL Report LA-UR-05-2686, Los Alamos (2005).
- [25] M. G. Gornov, *et al.*, Yad. Fiz. **47** (1988) 959–967 [Sov. J. Nucl. Phys. **47** (1988) 612–617]; Yad. Fiz. **47** (1988) 1193–1200 [Sov. J. Nucl. Phys. **47** (1988) 760–764].
- [26] S. G. Mashnik, JINR Preprint E2-92-320, Dubna, 1992; Nucl. Phys. **A568** (1994) 703–726.
- [27] S. G. Mashnik *et al.*, Phys. Rev. C **61** (2000) 034601.
- [28] R. J. Peterson *et al.*, Euro. Phys. J. A **10** (2001) 69–71; A. V. Prokofiev, S. G. Mashnik, and A. J. Sierk, Nucl. Sci. Eng. **131** (1999) 78–95.
- [29] Yu. E. Titarenko *et al.*, Phys. Rev. C **65** (2002) 064610.
- [30] K. A. Van Riper, S. G. Mashnik, and W. B. Wilson, Nucl. Instr. Meth. A **463** (2001) 576–585.
- [31] S. G. Mashnik *et al.*, Advances in Space Research **34** (2004) 1288–1296; E-print: nucl-th/0210065.
- [32] A. Fokin *et al.*, Phys. Rev. **C60** (1999) 024601.
- [33] V. Yu. Alexakhin *et al.*, Phys. At. Nucl. **63** (2000) 1673–1678.
- [34] N. S. Amelin *et al.*, Phys. Rev. **C47** (1993) 002299.
- [35] N. S. Amelin *et al.*, Phys. Rev. **C44** (1991) 001541.
- [36] N. S. Amelin *et al.*, Phys. Rev. Lett. **67** (1991) 001523.
- [37] J. Adam *et al.*, Pis'ma v EChAYa **1** (2004) 53–64.
- [38] Yu. E. Titarenko *et al.*, Yad. Fiz. **70** (2007) 1188–1192 [Phys. At. Nucl. **70** (2007) 1149–1153].
- [39] Yu. E. Titarenko *et al.*, Pramana – J. Phys. **68** (2007) 289–295.

- [40] A. R. Balabekyan *et al.*, Yad. Fiz. **69** (2006) 1520–1530 [Phys. At. Nucl. **69** (2006) 1485–1495].
- [41] A. R. Balabekyan *et al.*, E-print: nucl-ex/0603022, Phys. At. Nucl. **70** (2007) 1889–1897.
- [42] S. G. Mashnik *et al.*, E-print: nucl-th/0510070; Journal of Physics: Conference Series, **41** (2006) 340–351.
- [43] C. Y. Fu, T. A. Gabriel, and R. A. Lillie, Proc. SATIF-3, Sendai, Japan, May 12–13, 1997, NEA/OECD, 1998, pp. 49–60.
- [44] T. Sato *et al.*, Proc. MC2000, Lisbon, Portugal, 2000, edited by A. Kling, F. J. C. Barão, M. Nakagawa, L. Távora, and P. Vaz, Springer, Berlin, (2001), pp. 1139–1144.
- [45] A. V. Ignatyuk *et al.*, Proc. XV Workshop on Physics of Nuclear Fission, Obninsk, 3–6 October, 2000, [www-w2k.gsi.de/charms/Preprints/Obninsk2000/Cascado-v7.pdf](http://www-w2k.gsi.de/charms/Preprints/Obninsk2000/Cascado-v7.pdf).
- [46] A. V. Ignatyuk *et al.*, Proc. ND2004, September 26–October 1, 2004, Santa Fe, NM, USA, edited by R. C. Haight, M. B. Chadwick, T. Kawano, and P. Talou, (AIP Conf. Proc. **769**, Melville, New York, 2005), pp. 1307–1312.
- [47] S. Yavshits *et al.*, Voprosy Atomnoj Nauki i Tekhniki, seriya Yadernye Konstanty (Nuclear Constants) **1** (2000) 62–70 (in Russian), translated to English in Report INDC(CCP)-430 (2001), pp. 83–94.
- [48] Zs. Schram, Gy. Kluge, and K. Sailer, IAEA Report INDC(HUN)-023/L, Vienna, Austria, June 1987.
- [49] T. Nishida, Y. Nakahara, and T. Tsutsui, JAERI-M-86-116 (1986); JAERI-M-87-088 (1987); T. Nishida, H. Takada, and Y. Nakahara, Proc. Int. Conf. on Nuclear Data for Science and Technology, Jülich, Germany, May 13–17, 1991, Ed. S. M. Qaim, Springer-Verlag, Berlin (1992), pp. 152–157; H. Takada *et al.*, pp. 121–136 in Ref. [10].
- [50] V. S. Barashenkov *et al.*, JINR Communication P2-85-173, Dubna (1985).
- [51] N. V. Mokhov, Fermilab-FN-628, 1995; more references and many details on MARS may be found at the Web page <http://www-ap.fnal.gov/MARS/>.
- [52] *MCNPX User's Manual, Version 2.3.0*, L. S. Waters, Ed., LANL Report LA-UR-02-2607 (April, 2002); more references and many details on MCNPX may be found at the Web page <http://mcnpx.lanl.gov/>.
- [53] N. Amelin, CERN/IT/ASD Report CERN/IT/99/6, Geneva, Switzerland and JINR LHE, Dubna, Russia; [http://wwwinfo.cern.ch/asd/geant/geant4\\_public/G4UsersDocuments/Overview/html/index.html/](http://wwwinfo.cern.ch/asd/geant/geant4_public/G4UsersDocuments/Overview/html/index.html/).
- [54] V. Lara, Proc. MC2000, Lisbon, Portugal, 2000, edited by A. Kling, F. J. C. Barão, M. Nakagawa, L. Távora, and P. Vaz, Springer, Berlin, (2001), pp. 1039–1044; V. Lara and J. P. Wellisch, [chep2000.pd.infn.it/short\\_p/spa\\_a096.pdf](http://chep2000.pd.infn.it/short_p/spa_a096.pdf); more references and many details on GEANT4 may be found at the Web page <http://wwwasd.web.cern.ch/wwwasd/geant4/geant4.html>.
- [55] N. M. Sobolevsky, CCC-667 SHIELD, RSICC Computer Code Collection, ORNL, 1998; A. V. Dementyev and N. M. Sobolevsky, Radiation Measurements **30** (1999) 553–557; more references and many details on SHIELD may be found at the Web pages <http://www.nea.fr/abs/html/iaea1287.html>; <http://www-rsicc.ornl.gov/codes/ccc/cc6/cc6-667.html>.

- [56] I. I. Degtyarev *et al.*, Proc. Fourth Int. Workshop on Simulating Accelerator Radiation Environments (SARE-4), Knoxville, TN, September 13–16, 1998, edited by Tony A. Gabriel, ORNL, 1999, pp. 141–149; I. I. Degtyarev *et al.*, Proc. of the 2001 Particle Accelerator Conference, Chicago, USA, Voprosy Atomnoi Nauki i Tekhniki **01-1** (2001) 2796–2798.
- [57] S. E. Chigrinov *et al.*, Proc. Int. Conf. on Accelerator-Driven Transmutation Technologies and Applications (ADTT'99), Praha, Czech Republic, June 7–11, 1999, paper Mo-O-C12 on the Conference CD-ROM and Web page [http://fjfi.cvut.cz/con\\_adtt99](http://fjfi.cvut.cz/con_adtt99).
- [58] C. Y. Fu and T. A. Gabriel, Proc. Fourth Int. Workshop on Simulating Accelerator Radiation Environments (SARE-4), Knoxville, TN, September 13–16, 1998, ORNL, 1999, pp. 23–27; T. A. Gabriel and L. A. Carlson, Proc. Joint Int. Conf. on Mathematical Methods and Supercomputing for Nuclear Applications, Satatoga Springs, NY, Oct. 6–10, 1997, [http://www.osti.gov/bridge/product.biblio.jsp?osti\\_id=527544](http://www.osti.gov/bridge/product.biblio.jsp?osti_id=527544).
- [59] N. Yoshizawa, K. Ishibashi, and H. Takada, J. Nucl. Sci. Techn. **32** (1995) 601–607; H. Takada *et al.*, pp. 121–136 in Ref. [10].
- [60] V. S. Barashenkov *et al.*, Atomnaya Energiya **87** (1999) 283–286 [Atomic Energy **87** (1999) 742–744].
- [61] A. V. Sannikov and E. N. Savitskaya, Nucl. Instr. Meth. A **450** (2000) 127–137.
- [62] H. Kumawat and V. S. Barashenkov, Eur. Phys. J. **A26** (2005) 61–67; V. Kumar, H. Kumawat, and M. Sharma Pramana **68** (2007) 315–324.
- [63] S. G. Mashnik, R. E. Prael, and K. K. Gudima, LANL Report LA-UR-06-8652, Los Alamos (2007).
- [64] M. L. Goldberger, Phys. Rev. **74** 1268 (1948) 1269–1277.
- [65] R. Serber, Phys. Rev. **72** (1947) 1114–1115.
- [66] V. S. Barashenkov, K. K. Gudima, and V. D. Toneev, JINR Communication P2-4065, Dubna, 1968.
- [67] V. S. Barashenkov, K. K. Gudima, and V. D. Toneev, JINR Communication P2-4066, Dubna, 1968; Acta Physica Polonica **36** (1969) 415–432.
- [68] K. K. Gudima, A. S. Iljinov, and V. D. Toneev, JINR Communication P2-4661, Dubna, 1969.
- [69] V. S. Barashenkov *et al.*, Nucl. Phys. **A231** (1974) 462–476.
- [70] J. S. Levinger, Phys. Rev. **84** (1951) 43–51; Phys. Lett. B **82** (1979) 181–182.
- [71] W. O. Lock and D. F. Measday, *Intermediate Energy Nuclear Physics*, London, Methuen; [Distributed in the U.S.A. by Barnes and Noble, 1970].
- [72] J. Cugnon, C. Volant, and S. Vuillier, Nucl. Phys. **A620** (1997) 475–509; A. Boudard *et al.*, Phys. Rev. C **66** (1002) 044615; these proceedings; Th. Aoust and J. Cugnon, Eur. Phys. J. A **21** (2004) 79–85.
- [73] H. Duarte, Proc. Int. Conf. on Accelerator-Driven Transmutation Technologies and Applications (ADTT'99), Praha, Czech Republic, June 7–11, 1999, paper Mo-O-C17 on the Conference CD-ROM and Web page [http://fjfi.cvut.cz/con\\_adtt99](http://fjfi.cvut.cz/con_adtt99); Phys. Rev. C **75** (2007) 024611.
- [74] A. S. Iljinov *et al.*, Nucl. Phys. **A616** (1997) 575–605.

- [75] S. J. Lindenbaum and R. M. Sternheimer, Phys. Rev. **105** (1957) 1874–1899.
- [76] S. G. Mashnik *et al.*, LANL Report LA-UR-97-2905, Los Alamos (1997), <http://t2.lanl.gov/publications/publications.html>.
- [77] C. H. M. Broeders and A. Yu. Konobeev, Nucl. Instr. Meth. B **234** (2005) 387–411.
- [78] S. G. Mashnik, pp. 107–120 in [10].
- [79] K. K. Gudima, S. G. Mashnik, and V. D. Toneev, Proc. Europhysics Topical Conference June 21–25, 1982, Smollenice, Neutron Induced Reactions. Physics and Applications **10** (1982) 347–351.
- [80] R. K. Tripathi, F. A. Cucinotta, and J. W. Wilson, Nucl. Instr. Meth. B **117** (1996) 347–349.
- [81] C. Kalbach, J. Phys. G **24** (1998) 847–866.
- [82] M. V. Kossov, Eur. Phys. J. A **14** (2002) 377–392.
- [83] V. S. Barashenkov, *Cross Sections of Interactions of Particles and Nuclei with Nuclei*, JINR, Dubna, Russia (1993); tabulated data are available from the NEA/OECD Data Bank Web site at <http://www.nea.fr/html/dbdata/baras.html>.
- [84] M. Blann, Phys. Rev. C **54** (1996) 1341–1349; M. Blann and M. B. Chadwick, Phys. Rev. C **57** (1998) 233–243.
- [85] M. B. Chadwick *et al.*, IAEA-TECDOC-1178, IAEA, Vienna, October 2000, <http://www.nds-iaea.or.at/photonuclear/>; *IAEA Photonuclear Data Library. Cross Sections and Spectra up to 140 MeV*, LANL Report LA-UR-02-2002, LANL, Los Alamos, 20 January 2002, <http://t2.lanl.gov/data/photonuclear.html>.
- [86] F. X. Gallmeier, Radiat. Prot. Dosimetry **116** (2005) 264–269.
- [87] J. Ouyang, Ph.D. thesis U. of Colorado (LANL Report No. LA-12457-T, UC-413, 1992).
- [88] K. K. Gudima and S. G. Mashnik, Proc. 11th Internat. Conf. on Nuclear Reaction Mechanisms, Varenna, Italy, June 12–16, 2006, edited by E. Gadioli (2006) pp. 525–534; E-print: nucl-th/0607007.
- [89] V. D. Toneev and K. K. Gudima, Nucl. Phys. **A400** (1983) 173c–190c.
- [90] N. S. Amelin, K. K. Gudima, and V. D. Toneev, Yad. Fiz. **51** (1990) 512–523 [Sov. J. Nucl. Phys. **51** (1990) 327–333]; N. S. Amelin, K. K. Gudima, and V. D. Toneev, Yad. Fiz. **52** (1990) 272–282 [Sov. J. Nucl. Phys. **52** (1990) 172–178].
- [91] N. S. Amelin, JINR-86-802, Dubna (1986).
- [92] A. B. Kaidalov, Yad. Fiz. **45** (1987) 1452–1461 [Sov. J. Nucl. Phys. **45** (1987) 902–907].
- [93] N. S. Amelin, V. S. Barashenkov, and N. V. Slavin, Yad. Fiz. **40** (1984) 1560–1569 [Sov. J. Nucl. Phys. **40** (1984) 991–996].
- [94] N. S. Amelin and A. I. Ostrovidov, Yad. Fiz. **50** (1989) 486–492 [Sov. J. Nucl. Phys. **50** (1989) 302–305].
- [95] V. D. Toneev, N. S. Amelin, and K. K. Gudima, GSI Preprint GSI-89-52, Darmstadt (1989).
- [96] V. D. Toneev *et al.*, Nucl. Phys. **A519** (1990) 463c–478c.

- [97] S. G. Mashnik *et al.*, Research Note X-3-RN(U)06-07, LANL Report LA-UR-06-1764, Los Alamos (2006); S. G. Mashnik, K. K. Gudima, and M. I. Baznat, LANL Report LA-UR-06-1955, Los Alamos (2006); E-print: nucl/th-0603046.
- [98] W.-M. Yao *et al.*, J. Phys. G **33** (2006) 1; <http://pdg.lbl.gov/>.
- [99] I. Chemakin *et al.* Phys. Rev. C **77** (2008) 015209; Erratum, *ibid.* 049903(E).
- [100] C. Zeitlin *et al.*, Nucl. Phys. **A784** (2007) 341.
- [101] K. V. Alanakyan *et al.*, *Yad. Fiz.* **25** (1977) 545–554 [*Sov. J. Nucl. Phys.* **25** (1977) 292–297].
- [102] K. V. Alanakyan *et al.*, *Yad. Fiz.* **34** (1981) 1494–1503 [*Sov. J. Nucl. Phys.*, **34** (1981) 828–833]; *Nucl. Phys.* **A367** (1981) 429–445.
- [103] Y. Iwata, *et al.*, Phys. Rev. C **64** (2001) 054609.
- [104] K. Niita, *et al.*, Phys. Rev. C **52** (1995) 2620–2635.
- [105] H. W. Bertini, *et al.*, ORNL Report ORNL-TM-4134, Oak Ridge (1974).
- [106] H. Iwase *et al.*, E-print: nucl-th/0501066; Proc. ND2004, September 26–October 1, 2004, Santa Fe, NM, USA, edited by R. C. Haight, M. B. Chadwick, T. Kawano, and P. Talou, (AIP Conf. Proc. **769**, Melville, New York, 2005), pp. 1066–1069.
- [107] J. Taieb *et al.*, Nucl. Phys. **A724** (2003) 413–430.
- [108] M. Bernas *et al.*, Nucl. Phys. **A725** (2003) 213–253.
- [109] N. V. Mokhov *et al.*, Radiation Protection Dosimetry **116** (2005) 99–103; E-print: nucl-th/0404084.
- [110] K. K. Gudima *et al.*, JINR Preprint JINR-E2-83-101, Dubna (1983); H. Schulz *et al.*, Phys. Lett. B **124** (1983) 458–460.
- [111] J. I. Kapusta, Phys. Rev. C **21** (1980) 1301–1310.
- [112] V. Blideanu *et al.*, Phys. Rev. C **70** (2004) 014607.
- [113] V. V. Abramov *et al.*, *Yad. Fiz.* **41** (1985) 357–370 [*Sov. J. Nucl. Phys.* **41** (1985) 227–236]; *Yad. Fiz.* **45** (1987) 1362–1372 [*Sov. J. Nucl. Phys.* **45** (1987) 845–851].
- [114] R. E. Prael, LANL Research Note XCI-RN 98-10 (U), January 14, 1998; LA-UR-00-2116; LANL Report LA-UR-01-1655, Los Alamos, 2001.
- [115] T. Ericson, Adv. in Physics **9** (1960) 425–511.
- [116] F. C. Williams Jr., Phys. Lett. B **31** (1970) 184–186.
- [117] F. C. Williams Jr., Nucl. Phys. **A161** (1971) 231–240.
- [118] I. Ribansky, P. Oblozinsky, and E. Betak, Nucl. Phys. **A205** (1973) 545–560.
- [119] K. Kikuchi and M. Kawai, *Nuclear Matter and Nuclear Reactions*, North-Holland, Amsterdam (1968).
- [120] N. Metropolis *et al.*, Phys. Rev. **110** (1958) 185–203.
- [121] E. Betak, Acta Phys. Slov. **26** (1976) 21–24.
- [122] J. R. Wu and C. C. Chang, Phys. Rev. C **17** (1978) 1540–1549.
- [123] G. Mantzouranis, H. A. Weidenmüller, and D. Agassi, Z. Phys. A **276** (1976) 145–154.
- [124] C. Kalbach, Phys. Rev. C **37** (1988) 2350–2370.

- [125] V. F. Weisskopf and D. H. Ewing, Phys. Rev. **57** (1940) 472–483.
- [126] N. Bohr and J. A. Wheeler, Phys. Rev. **56** (1939) 426–450.
- [127] A. V. Ignatyuk, G. N. Smirenkin, and A. S. Tishin, Yad. Fiz. **21** (1975) 485–490 [Sov. J. Nucl. Phys. **21** (1975) 255–257]; A. V. Ignatyuk *et al.*, Yad. Fiz. **21** (1975) 1185–1205 [Sov. J. Nucl. Phys. **21** (1975) 612–621].
- [128] A. S. Iljinov, *et al.*, Nucl. Phys. **A543** (1992) 517–557.
- [129] P. Möller *et al.*, Atomic Data and Nuclear Data Tables, **59** (1995) 185–381.
- [130] P. Möller, J. R. Nix, and K.-L. Kratz, Atomic Data and Nuclear Data Tables, **66** (1997) 131–343.
- [131] R. E. Prael and H. Lichtenstein, LANL Report LA-UR-89-3014, Los Alamos (1989).
- [132] A. Ferrari *et al.*, Z. Phys. C **70** (1996) 413–426; these proceedings.
- [133] M. Veselský, Nucl Phys. **A705** (2002) 193–222; M. Veselský *et al.*, Z. Phys. A **356** (1997) 403–410.
- [134] M. Böhning, Nucl. Phys. **A152** (1970) 529–546.
- [135] A. Guertin, *et al.*, Eur. Phys. J. **A23** (2005) 49–60.
- [136] A. A. Cowley *et al.*, Phys. Rev. C **54** (1996) 778–783.
- [137] R. E. L. Green and R. G. Korteling, Phys. Rev. C **18** (1978) 311–316.
- [138] J. Franz *et al.*, Nucl. Phys. **A510** (1999) 774–802.
- [139] R. C. Haight, LANL Report LA-UR-04-4010, Los Alamos (2004).
- [140] E. Raeymackers *et al.*, Phys. Rev. C **68** (2003) 024604.
- [141] I. Leya *et al.*, Nucl. Instrum. Meth. **B229** (2005) 1–23.
- [142] P. Talou *et al.*, Nucl. Instrum. Meth. **A562** (2006) 823–826.
- [143] A. V. Ignatyuk *et al.*, Nucl. Sci. Eng. **136** (2000) 340–356.
- [144] S. Furihata, Nucl. Instr. Meth. B **171** (2000) 252–258; Proc. MC2000, Lisbon, Portugal, 2000, edited by A. Kling, F. J. C. Barão, M. Nakagawa, L. Távora, and P. Vaz, Springer, Berlin, (2001), pp. 1045–1050; *The Gem Code Version 2 Users Manual*, Mitsubishi Research Institute, Inc., Tokyo, Japan (November 8, 2001).
- [145] S. Furihata *et al.*, JAERI-Data/Code 2001-015, JAERI, Tokai-mura, Naka-gam, Ibaraki-ken, Japan (2001).
- [146] S. Furihata, Ph.D. thesis, Tohoku University, March, 2003; S. Furihata and T. Nakamura, J. Nucl. Sci. Technol. Suppl. **2** (2002) 758–761.
- [147] I. Dostrovsky, Z. Frankel, and G. Friedlander, Phys. Rev. **116** (1959) 683–702.
- [148] F. Atchison, in Proc. Meeting on Targets for Neutron Beam Spallation Source, Julich, June 11–12, 1979, pp. 17–46, G. S. Bauer, Ed., Jul-Conf-34, Kernforschungsanlage Julich GmbH, Germany (1980).
- [149] F. Atchison, pp. 199–218 in [10].
- [150] F. Atchison, Nucl. Instrum. Methods B **259** (2007) 909–932.
- [151] G. Audi and A. H. Wapstra, Nucl. Phys. **A595** (1995) 409–480.
- [152] P. E. Haustein, Atomic Data and Nuclear Data Tables **39** (1988) 185–393.

- [153] A. G. W. Cameron, Can. J. Phys. **35** (1957) 1021–1032.
- [154] T. Matsuse, A. Arima, and S. M. Lee, Phys. Rev. C **26** (1982) 2338–2341.
- [155] A. S. Botvina *et al.*, Nucl. Phys. **A475** (1987) 663–686.
- [156] A. Gilbert and A. G. W. Cameron, Can. J. Phys. **43** (1965) 1446–1496.
- [157] J. L. Cook, H. Ferguson, and A. R. del Musgrove, Australian Journal of Physics **20** (1967) 477–487.
- [158] W. A. Friedman and W. G. Lynch, Phys. Rev. C **28** (1983) 16–23.
- [159] The Evaluated Nuclear Structure Data File (ENSDF) maintained by the National Nuclear Data Center (NNDC), Brookhaven National Laboratory, <http://www.nndc.bnl.gov/>.
- [160] S. G. Mashnik *et al.*, in Proc. TRAMU@GSI, Darmstadt, Germany, 2003, Eds. A. Kelic and K.-H. Schmidt, ISBN 3-00-012276-1, <http://ww-wnt.gsi.de/tramu>; E-print: nucl-th/0404018.
- [161] F. Rejmund *et al.*, Nucl. Phys. **A683** (2001) 540–565; J. Benlliure, *et al.*, Nucl. Phys. **A683** (2001) 513–539.
- [162] C. Villagrasa-Canton, PhD Thesis, Universite de Paris XI Orsay, December 5, 2003, <http://www-w2k.gsi.de/charms/theses.htm>; private communication from Dr. Villagrasa to SGM, March 11, 2004; C. Villagrasa-Canton, *et al.*, Phys. Rev. C **75** (2007) 044603.
- [163] P. Napolitani, PhD Thesis, University Paris XI Orsay, IPNO-T-04-14, September 24, 2004; P. Napolitani *et al.*, Phys. Rev. C **70** (2004) 054607.
- [164] S. G. Mashnik *et al.*, LANL Report LA-UR-98-6000 (1998); Eprint: nucl-th/9812071; Proc. SARE-4, Knoxville, TN, September 13-16, 1998, edited by T. A. Gabriel, ORNL, 1999, pp. 151–162.
- [165] C.-M. Herbach *et al.*, Nucl. Phys. **A765** (2006) 426–463.
- [166] H. Machner *et al.*, Phys. Rev. C **73** (2006) 044606.
- [167] R. Vandenbosch and J. R. Huizenga, *Nuclear Fission*, Academic Press, New York (1973).
- [168] E. F. Neuzil and A. W. Fairhall, Phys. Rev. **129** (1963) 2705–2710.
- [169] A. Ya. Rusanov *et al.*, Yad. Fiz. **60** (1997) 773–803 [Phys. At. Nucl. **60** (1997) 683–712]; M. G. Itkis *et al.*, Yad. Fiz. **58** (1995) 2140–2165 [Phys. At. Nucl. **58** (1995) 2026–2051].
- [170] W. D. Myers and W. J. Swiatecki, Phys. Rev. C **60** (1999) 014606.
- [171] M. G. Itkis, *et al.*, Ya. Fiz. **52** (1990) 23–35 [Sov. J. Nucl. Phys. **52** (1990) 15–22].
- [172] F. Atchison, Paul Scherrer Insitutut Report No. 98-12, Villigen PSI, Switzerland (1998).
- [173] H. W. Bertini, Phys. Rev. **131** (1963) 1801–1871; Phys. Rev. **188** (1969) 1711–1730.
- [174] Y. Yariv and Z. Frankel, Phys. Rev. C **20** (1979) 2227–2243; *ibid.* **24** (1981) 488–494; Y. Yariv, these proceeding.
- [175] A. V. Prokofiev, Nucl. Instr. Meth. A **463** (2001) 557–575; A. V. Prokofiev, S. G. Mashnik, and W. B. Wilson, LANL Report LA-UR-02-5837, Los Alamos (2002); E-print: nucl-th/0210071.
- [176] V. P. Eismont *et al.*, Proc. ISINN-13, Dubna, Russia, May 25-28, 2005; LANL Report LA-UR-05-3757, Los Alamos (2005); E-print: nucl-ex/0507013.
- [177] E. Jacobs *et al.*, Phys. Rev. C **19** (1979) 422–432; *ibid.* **21** (1980) 237–245.

- [178] T. Enqvist *et al.*, Nucl. Phys. **A703** (2002) 435–465.
- [179] S. G. Mashnik *et al.*, Proc. 10th Int. Conf. on Nuclear Reaction Mechanisms, Varenna, Italy, June 9–13, 2003, edited by Ettore Gadioli, pp. 569–578; E-print: nucl-th/0308043.
- [180] E. Fermi, Prog. Theor. Phys. **5** (1950) 570–583.
- [181] G. I. Kopylov, *Principles of Resonance Kinematics*, Moscow, Nauka (1970) [in Russian].
- [182] K. Ishibashi *et al.*, J. Nucl. Sci. Techn. **34** (1997) 529–537.
- [183] W. B. Amian *et al.*, Nucl. Sci. Eng. **115** (1993) 1.
- [184] W. B. Amian *et al.*, Nucl. Sci. Eng. **112** (1992) 78–86.
- [185] M. L. Brooks, Ph.D. thesis, U. of New Mexico, (LA-12210-T, UC-910, Oct., 1991, Los Alamos); M. L. Brooks, *et al.*, Phys. Rev. C **45** (1992) 2343–2354.
- [186] T. Nakamoto *et al.*, J. Nucl. Sci. and Techn. **34** (1997) 860–862.
- [187] R. A. Schumacher *et al.*, Phys. Rev. C **25** (1982) 2269–2277.
- [188] K. Sakamoto, J. Nucl. Radiochem. Sci. **4** (2003) A9–A31.
- [189] K. A. Van Riper, S. G. Mashnik, and W. B. Wilson. LANL Report LA-UR-98-5379, Los Alamos (1998), a 684 page detailed report with 37 tables and 264 color figures available on the Web at: <http://t2.lanl.gov/publications/publications.html>.
- [190] Yu. E. Titarenko *et al.*, LANL Report LA-UR-07-2659, Los Alamos (2007); Proc. of the 2007 International Conference on Nuclear Data for Science and Technology (ND2007), Nice, France, April 22–27, 2007; E-print: arXiv:0705.1020.
- [191] Yu. E. Titarenko *et al.*, LANL Report LA-UR-08-2219, Los Alamos (2008); E-print: arXiv:0804.1260v1 [nucl-ex]; to be published in Phys. Rev. C.
- [192] K. Ammon *et al.*, Nucl. Instr. Meth. B **266** (2008) 2–12.
- [193] A. J. Koning, S. Hilaire, and M. C. Duijvestijn, Proc. ND2004, September 26–October 1, 2004, Santa Fe, NM, USA, edited by R. C. Haight, M. B. Chadwick, T. Kawano, and P. Talou, (AIP Conf. Proc. **769**, Melville, New York, 2005), pp. 1154–1159.
- [194] A. Yu. Konobeyev and Yu. A. Korovin, Nucl. Instr. Meth. B **82** (1993) 103–115.
- [195] A. R. Junghans *et al.*, Nucl. Phys. **A629** (1998) 635–655.
- [196] M. I. Baznat *et al.*, Proc. ND2004, September 26–October 1, 2004, Santa Fe, NM, USA, edited by R. C. Haight, M. B. Chadwick, T. Kawano, and P. Talou, (AIP Conf. Proc. **769**, Melville, New York, 2005), pp. 1245–1248; E-print: nucl-th/0501075, v2, November 2, 2005.
- [197] J. P. Bondorf *et al.*, Phys. Rep. **257** (1995) 133–221.
- [198] A. S. Botvina *et al.*, Yad. Fiz. **57** (1994) 667–674 [Phys. At. Nucl. **57** (1994) 628–635].
- [199] A. S. Botvina, A. S. Iljinov, and I. N. Mishustin, Nucl. Phys. **A507** (1990) 649–674.
- [200] A. S. Botvina, A. S. Iljinov, and I. N. Mishustin, Yad. Fiz. **42** (1985) 1127–1137 [Sov. J. Nucl. Phys. **42** (1985) 712–718].
- [201] A. Botvina, ICTP Lecture Note 1930-3 (2008), viewgraphs of the invited lectures presented at the Joint ICTP-IAEA Advanced Workshop on Model Codes for Spallation Reactions, February 4–8, 2008, Trieste, Italy, [http://cdsagenda5.ictp.it/full\\_display.php?ida=a07139](http://cdsagenda5.ictp.it/full_display.php?ida=a07139), and these proceedings.

- [202] L. G. Sobotka *et al.*, Phys. Rev. Lett. **53** (1984) 2004–2007.
- [203] R. J. Charity *et al.*, Nucl. Phys. **A483** (1988) 371–405.
- [204] R. J. Charity *et al.*, Nucl. Phys. **A476** (1988) 516–544.
- [205] R. J. Charity, Phys. Rev. C **58** (1988) 1073–1077.
- [206] R. J. Charity *et al.*, Phys. Rev. C **63** (2001) 024611; <http://www.chemistry.wustl.edu/~rc/gemini/>.
- [207] R. J. Charity, ICTP Lecture Note 1930-15 (2008), viewgraphs of the invited lectures presented at the Joint ICTP-IAEA Advanced Workshop on Model Codes for Spallation Reactions, February 4–8, 2008, Trieste, Italy, [http://cdsagenda5.ictp.it/full\\_display.php?ida=a07139](http://cdsagenda5.ictp.it/full_display.php?ida=a07139), and these proceedings.
- [208] L. G. Moretto, Nucl. Phys. **A247** (1975) 211–230.
- [209] E. Le Gentil *et al.*, Phys. Rev. Lett. **100** (2008) 022701.
- [210] S. Leray, Presentation (viewgraphs) of the invited talk at the *International Conference on Nuclear Fragmentation (NUFRA2007)* Kemer (Antalya), Turkey, September 24 – October 1, 2007, <http://fias.uni-frankfurt.de/nufra2007/>.
- [211] P. Napolitani *et al.*, Phys. Rev. C **76** (2007) 064609.
- [212] S. Mashnik, Presentation (viewgraphs) of the invited talk at the *International Conference on Nuclear Fragmentation (NUFRA2007)* Kemer (Antalya), Turkey, September 24 – October 1, 2007, LANL Report LA-UR-07-5348, Los Alamos (2007); <http://fias.uni-frankfurt.de/nufra2007/>.
- [213] T. Enqvist *et al.*, Nucl. Phys. **A686** (2001) 481–524.
- [214] I. C. Gomez, private communication to SGM on results of simulations of a 400 MeV/nucleon Uranium Beam on a 0.2-cm Thick Lithium Target with MCNPX and PHITS, 2007.
- [215] H. Iwase, K. Niita, and T. Nakamura, J. Nucl. Sci. Technol. **39** (2002) 1142–1151; K. Niita *et al.*, AIP Conf. Proc. **896** (2007) 61–70; these proceedings.
- [216] H. G. Hughes, *et al.*, LANL Report LA-UR-08-1065, Los Alamos, 2008; to be published in Proc. Workshop on Uncertainty Assessment in Computational Dosimetry, Bologna, Italy, October 8–10, 2007.